JPRS L/9656

10 April 1981

USSR Report

PHYSICS AND MATHEMATICS

(FOUO 3/81)

FBIS FOREIGN BROADCAST INFORMATION SERVICE

NOTE

JPRS publications contain information primarily from foreign newspapers, periodicals and books, but also from news agency transmissions and broadcasts. Materials from foreign-language sources are translated; those from English-language sources are transcribed or reprinted, with the original phrasing and other characteristics retained.

Headlines, editorial reports, and material enclosed in brackets [] are supplied by JPRS. Processing indicators such as [Text] or [Excerpt] in the first line of each item, or following the last line of a brief, indicate how the original information was processed. Where no processing indicator is given, the information was summarized or extracted.

Unfamiliar names rendered phonetically or transliterated are enclosed in parentheses. Words or names preceded by a question mark and enclosed in parentheses were not clear in the original but have been supplied as appropriate in context. Other unattributed parenthetical notes within the body of an item originate with the source. Times within items are as given by source.

The contents of this publication in no way represent the policies, views or attitudes of the U.S. Government.

APPROVED FOR RELEASE: 2007/02/08: CIA-RDP82-00850R000300100019-7

JPRS L/9656

10 April 1981

USSR REPORT

PHYSICS AND MATHEMATICS

(FOUO 3/81)

CONTENTS

CRYSTALS AND SEMICONDUCTORS

UDC 537.311.33

ELECTRON-HOLE LIQUID IN SEMICONDUCTORS IN STRONG MAGNETIC FIELDS

Moscow TRUDY ORDENA LENINA FIZICHESKOGO INSTITUTA IMENI P. N. LEBEDEVA: ELEKTRONNO-DYROCHNAYA ZHIDKOST' V POLUPROVODNIKAKH V SIL'NYKH MAGNITNYKH POLYAKH in Russian Vol 123, 1980 (signed to press 23 May 80) pp 2, 118-119

[Annotation and abstracts from book "Works of the Order of Lenin Physics Institute imeni P. N. Lebedev: Electron-Hole liquid in Semiconductors in Strong Magnetic Fields", edited by N. G. Basov, Izdatel'stvo "Nauka", 1450 copies, 119 pages]

[Text] The book is dedicated to theoretical and experimental studies of the behavior of an electron-hole liquid in strong magnetic fields. L. V. Keldysh et al. analyze the change in bonding energy and other parameters of electron-hole drops in indirect semiconductors in quantizing magnetic fields and predict some new phenomena, in particular the magnetic oscillations of carrier density in electron-hole drops. In other papers these effects are experimentally investigated by studying the spectral form and intensity of germanium photoluminescence in the fundamental absorption region, and also by methods of long-wave infrared spectroscopy. Oscillations in the intensity of plasma absorption have been observed in the resonant absorption spectra of an electron-hole liquid in the far infrared in a magnetic field with a period corresponding to sequential passage of Landau levels through the Fermi level of electrons with minimum effective mass. Investigation of the kinetics of photoluminescence in pure germanium has revealed oscillations of the carrier lifetime in an electron-hole liquid, which gives unambiguous confirmation of the effect of oscillations of density and other parameters of the electron-hole liquid in a magnetic field. It has been shown that exciton-impurity complexes play an important part in processes of magnetic oscillations in doped n-germanium.

The collection is intended for physicists and engineers involved in solid-state research.

UDC 537.311.33

ELECTRON-HOLE LIQUID IN SEMICONDUCTORS IN A MAGNETIC FIELD

[Abstract of paper by L. V. Keldysh and A. P. Silin]

[Text] Known results for the energy of an electron-hole liquid in semiconductors without a magnetic field are used to get estimates of the additional oscillating component in the energy and equilibrium density of an electron-hole liquid in a

magnetic field. It is shown that these additions may explain the fluctuations of integrated intensity of recombination radiation of an electron-hole liquid in germanium in a magnetic field. References 13.

UDC 537.311.33

ELECTRON-HOLE LIQUID IN A SUPERSTRONG MAGNETIC FIELD

[Abstract of paper by T. A. Onishchenko]

[Text] A method is presented for calculating the energy of interaction of electron liquids with maximally strong anisotropy that leads to a common law of $E_{corr}/n \sim -n^{\frac{1}{4}}$ and two consequences are considered for strongly anisotropic electron-hole systems: thermodynamics of the gas-liquid transition (for quasi-unidimensional systems), and the semimetal-dielectric transition. Specific calculations are done for systems in a superstrong magnetic field. Figures 2, references 11.

UDC 537.311.33

QUANTUM OSCILLATIONS OF INTENSITY OF PLASMA ABSORPTION IN AN ELECTRON-HOLE DROP IN GERMANIUM

[Abstract of paper by V. A. Zayats, V. L. Kononenko and V. N. Murzin]

[Text] The authors study the intensity dependences of absorption in the plasma resonance region in an electron-hole drop in germanium at 1.5 K in magnetic fields with intensity of up to 40 kOe for all three principal field orientations: $\vec{H} \parallel [100]$, [110], [111]. It is shown that periodic changes of intensity observed in fields of 5-25 kOe are due to quantum oscillations of the thermodynamic characteristics of the electron-hole drop, primarily the equilibrium densities of particles in the electron-hole liquid. It is established that the direct cause of change in the intensity of resonant absorption in the electron-hole drop in a magnetic field is to be found in the changes in overall number of carriers in the condensed phase that are due to fluctuations of carrier lifetime in the electron-hole drop as a result of corresponding antiphase changes of equilibrium density. The monotonic fall-off of intensity of absorption in fields stronger than 17-25 kOe is also due to a reduction of carrier lifetime in the electron-hole drop as a consequence of self-compressibility of the electron-hole liquid in the magnetic field. Figures 4, references 12.

UDC 537.311.3

MAGNETIC OSCILLATIONS OF LUMINESCENCE OF ELECTRON-HOLE DROPS IN PURE GERMANIUM

[Abstract of paper by K. Bettsler, B. G. Zhurkin and A. L. Karuzskiy]

[Text] It is shown that charge carrier density n oscillates in an electron-hole drop when a magnetic field is applied. These density oscillations lead to oscillations of luminescence intensity and lifetime of the line of the electron-hole drop (LA - 709 meV). The properties of the electron-hole drop that depend on density n were studied by investigating these magnetic oscillations. It was found that

quantum efficiency in the electron-hole drop is only 25% in contrast to previously made estimates of this quantity. The principal non-radiative process in the electron-hole drop is Auger recombination, which is intensified by e—e-, e—h- and h—h-correlations. A proof is derived from the differences in oscillatory behavior of TA- and LA-lines that the radiative transition in the electron-hole drop with emission of a TA-phonon is forbidden in the first order. Figures 6, references 21.

UDC 537.311.33

SPECTRAL DEPENDENCE OF MAGNETIC OSCILLATIONS OF LUMINESCENCE INTENSITY OF AN ELECTRON-HOLE DROP IN PURE GERMANIUM

[Abstract of paper by K. Bettsler, P. S. Gladkov, B. G. Zhurkin and A. L. Karuzskiy]

[Text] An investigation is made of oscillations of intensity at different points of the luminescence line (LA - 709 meV) of electron-hole condensate in pure Ge. At short delay times ($t \lesssim 10$ μs) the relative amplitude of oscillations in the center of the line is minimum and increases toward the edges. The resultant spectral pattern of the oscillations is explained within the framework of the drop model. From the oscillations of intensity at three points of the line, the authors calculate the magnetic oscillations of spectral width of the line and the characteristic energies of the electron-hole condensate (oscillations of the chemical potential, and of the kinetic, exchange and correlational energies per particle pair in the electron-hole condensate). Figures 2, references 11.

UDC 537.311.33

MAGNETIC OSCILLATIONS OF THE HALF-WIDTH OF THE LUMINESCENCE LINE OF ELECTRON-HOLE DROPS IN PURE GERMANIUM

[Abstract of paper by B. M. Balter, K. Bettsler, B. G. Zhurkin and A. L. Karuzskiy]

[Text] Magnetic oscillations of the half-width of the radiative recombination line of electron-hole drops in germanium (line LA - 709 meV) were experimentally observed. It is shown that the observed oscillations can be explained by Fermi energy oscillations of charge carriers with density ρ_c in the drops. The ratio between dE_F/E_F and $d\rho_c/\rho_c$ is introduced and used as the basis for calculating the magnetic field dependence of the half-width ΔE of the line with consideration of oscillations of ρ_c. The theoretical curve agrees well with experimental data. Figure 1, references 8.

UDC 537.311.33

MAGNETIC OSCILLATIONS OF LUMINESCENCE OF ELECTRON-HOLE DROPS IN ARSENIC-DOPED GERMANIUM

[Abstract of paper by V. P. Aksenov, K. Bettsler, B. G. Zhurkin and A. L. Karuzskiy]

[Text] Magnetic oscillations of intensities of phononless (NP) and LA-phonon luminescence lines of electron hole drops (EHD) are observed in Ge:As, as well as

oscillations of the intensity ratio $(NP/LA)^{EHD}$. The relative amplitude of oscillations for EHD of the LA-line changes linearly with an increase in delay time t_{del} after the stimulating pulse, whereas the relative amplitude of oscillations of EHD of the NP-line is independent of t_{del}. Figures 2, references 6.

UDC 537.311.33

MAGNETOPLASMA RESONANCE IN ELECTRON-HOLE DROPS IN GERMANIUM

[Abstract of paper by V. I. Gavrilenko, V. L. Kononenko and V. N. Murzin]

[Text] A detailed examination is made of the problems of the theory of magnetoplasma resonance (MPR) in electron-hole drops (EHD) that are small in size compared with a wavelength of electromagnetic radiation, considering both the electro- and magnetodipole mechanisms of absorption. An analysis is made of the principles governing MPR in EHD with many kinds of carriers, and a relation is established between the position of the resonant frequencies of MPR in EHD and the parameters that characterize the carriers in the condensed phase. An in-depth comparison is made between the theory and the overall experimental pattern of MPR in EHD, and it is shown that a quantitative description of experimental data is possible. This comparison is used as a basis for defining and analyzing some important parameters and relations that characterize the electron-hole liquid in an EHD: effective masses of the carriers in drops, variation in density of the EHD in a magnetic field, frequency dependence of damping of plasma fluctuations, and the mechanisms of such damping. The paper points out new possibilities and prospects for further investigation of MPR in EHD. Figures 24, tables 2, references 57.

UDC 537.311.33

SHAPE OF ELECTRON-HOLE DROPS IN A MAGNETIC FIELD

[Abstract of paper by V. L. Kononenko]

[Text] An examination is made of the shape and capillary oscillations of electron-hole drops in a magnetic field with consideration of major influencing factors -- surface tension, interaction with the natural phonon wind, recombination magnetism, and also dia- and paramagnetism of carriers in the drop. It is shown that in an undeformed cubic crystal, fairly small electron-hole drops are always stretched out along the field, and as dimensions increase, the drops are either flattened out along the field (in the case of predominant influence of recombination magnetism), or continue to be stretched out (in the case of phonon wind predominating). The author considers the problem of the critical size of the electron-hole drop in these two cases. Numerical calculations are done on the shape and frequency of capillary oscillations of drops depending on their volume and the magnetic field intensity. The results agree well with experimental data relating to the shape of the electron-hole drop in a magnetic field. Figures 4, table 1, references 26.

[38-6610]

6610
CSO: 1862

LASERS AND MASERS

UDC 614.89:621.373.826

ESTIMATING THE DEGREE OF HAZARD TO HUMAN EYES FROM DIRECTIONAL LASER BEAMS

Moscow KVANTOVAYA ELEKTRONIKA in Russian Vol 7, No 12, Dec 1980 pp 2523-2530

[Article by V. T. Kibovskiy, V. I. Kukhtevich, L. A. Novitskiy, All Union Scientific Research Institute of Opticophysical Measurements, Moscow]

[Text] A study is made of the problems of the quantitative evaluation of the degree of hazard from directional laser beams by the model of interaction of gaussian radiation beams of different divergence with the optical system of the eye. Expressions are obtained for determining the dimensions of the illumination spot on the retina under the conditions of the worst accommodation. Formulas are presented for estimating the degree of hazard as a function of the diameter of the laser beam in the plane of the pupil.

Directional laser beams in the spectral region of 0.5-1.4 microns are highly dangerous to human eyes, inasmuch as when such a beam hits the pupil, the radiation is focused on the retina in a small spot with high radiation intensity in the vicinity of the spot, which can lead to damage to the retina with comparatively low intensity of the radiation on the cornea [1]. Here and hereafter, by radiation intensity we mean the surface density of the power (watts/cm^2) for continuous radiation or the surface density of the energy (joules/cm^2) for pulse radiation. The laser safety norms existing at the present time [2, 3] establish the maximum admissible levels (MAL) of radiation intensity on the cornea with uniform illumination of the entire area of the pupil by a parallel beam of rays for directional beams. Under such irradiation conditions, the degree of hazard of the laser beam for the human eye estimated by its effect on the retina is determined by the ratio of the intensity of the radiation incident on the pupil W_{pupil} to the corresponding value of the MAL on the pupil W_{pupil}^{MAL}. However, under actual conditions the radiation beam incident on the pupil can be essentially nonuniform, converging or diverging, can have a diameter that is less than the pupil diameter -- for such irradiation conditions encountered in practice, it is necessary to more precisely define the criterion for quantitative evaluation of the degree of hazard of the radiation inasmuch as the estimate by the criterion of $W_{pupil}/W_{pupil}^{MAL}$ for the investigated case turns out to be insufficiently reliable.

Let us introduce the hazard coefficient of a directional laser beam for the human eye $R = W_c^{max}/W_c^{MAL}$, where W_c^{max} is the maximum intensity of the radiation at the illumination spot on the retina when a real beam hits the eye; W_c^{MAL} is the maximum

admissible value of the intensity on the retina when illuminating the pupil by a parallel uniform beam having intensity W_{pupil}^{MAL} in the plane of the pupil. At the present time the radiation intensity on the retina is basically considered by the formulas of references [4, 5]. However, the model for converting the laser beam by the optical system of the eye adopted in these papers does not take into account the peculiarities of focusing of a nonuniform beam and it does not consider the conditions of the worst accomodation in the calculation.

Let us express W_c^{max} in terms of the energy and spatial parameters of the incident beam for which we consider the system **for** irradiating the eye (Figure 1) by a gaussian beam, directed along the viewing axis. The beam with gaussian intensity distribution obviously must be considered to be the most dangerous of the ones actually encountered in practice inasmuch as it creates a greater local intensity on the retina at the distribution maximum by comparison with the beam having the same power, divergence and diameter, but more uniform intensity distribution. The gaussian

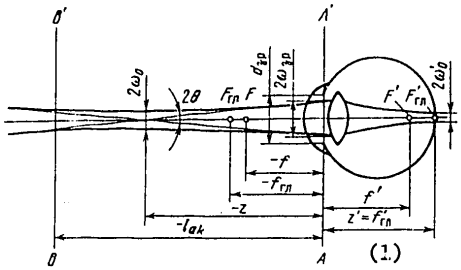

Figure 1. Diagram of irradiation of the eye by a directional laser beam.

Key: 1. principal

radiation beam is characterized by angular divergence θ with respect to the level $1/e^2$, the confocal parameter $R_e = 2\lambda/\pi\theta^2$, and it has constriction $\omega_0 = \lambda/\pi\theta$ [6], which in the general case can be located at any arbitrary distance z from the plane of the pupil. Here the constriction can be located inside the radiator (a laser without a shaping optical system), at the exit surface of the radiator (a laser with collimating optical system) or at a great distance, to several hundreds of meters, from the exit surface of the radiator (laser with focusing optical system). In the investigated model of irradiation the primary spatial parameter influencing W_c^{max} will be the distance z; here the distance from the eye to the exit plane of the radiator has no basic significance. In accordance with the sign rule adopted in the optical system, the distance z is reckoned from the plane of the pupil, and we shall consider it negative if the constriction is to the left of the pupil (the eye is irradiated by a diverging beam), and positive if the constriction is located to the right (the eye is irradiated by a converging beam).

The simplified optical system of the eye (see Figure 1) is a positive lens (the crystalline lens) behind which a substance is located with index of refraction n' = 1.336 (the vitreous body). Let us consider that the front and rear principal planes of the eye are matched with the plane of the pupil AA'. The distance from the principal plane of the eye to the retina is equal to the rear focal length of the

eye with accommodation at rest (accommodation at infinity) $f'_{prin} = 22.365$ mm. On accommodation of the eye to some plane BB' located at a distance ℓ_{ac} from the pupil, the rear focal point f' of the eye is in front of the retina a distance f' from the AA' plane. The numerical values of f'_{prin} and n' are taken from the data for a schematic normal eye according to Gulstrand [7].

The radiation intensity distribution function at the illumination spot on the retina $W_c(\rho)$ can be found knowing the field amplitude distribution $E_c(\rho)$ on the retina. Inasmuch as the illumination spot dimensions are small, the surface of the retina will be considered flat within the limits of the spot. By the irradiation diagram (see Figure 1) we assume that the eye is irradiated by radiation from a coherent source located at the center of the constriction of the incident beam and having dimensions less than the minimum dimension resolvable by the eye at the distance z. Inasmuch as the optical system of the normal eye is isoplanar (the eye aberrations do not influence the structural symmetry of a beam incident on the retina), the space-frequency spectrum of the amplitude distribution $\hat{E}_c(\kappa)$ is the amplitude transfer function of the optical system of the eye $\tilde{k}_{prin}(\kappa)$ [8]. Let us represent the function $\tilde{k}_{prin}(\kappa)$ in the form of the product of the functions $\tilde{k}_D(\kappa)\,\tilde{k}_{ab}(\kappa)$, where $\tilde{k}_D(\kappa)$ is the amplitude transfer function of the aberrationless system describing the diffraction field distribution on the retina which occurs both as a result of limited dimensions of the input gaussian beam and as a result of beam diffraction at the pupil; $k_{ab}(\kappa)$ is the amplitude transfer function of the optical system describing the field distribution caused only by eye aberrations without considering diffraction.

On diffraction of a gaussian beam of radiation on a circular iris (the pupil), the field distribution in the beam after the iris depends on the parameter $\alpha = r_{pupil}/\omega_{pupil}$ [6], where r_{pupil} is the radius of the pupil of the eye; ω_{pupil} is the radius of the incident gaussian beam in the plane of the pupil. From [6] it follows that for $\alpha \geq 2.2$ the field distribution after the iris coincides with the gaussian curve, and the beam can be considered as unlimited, whereas for $\alpha \leq 0.2$ the incident beam can be considered uniform, and the field distribution after the iris can be described by the known Airy formula [8]. For simplification let us replace the Airy distribution by gaussian distribution having the same amplitude at the maximum as the Airy distribution. This substitution does not lead to an error in estimating the degree of danger inasmuch as the intensities at the maximum distributions are equal. For intermediate values of $0.2 < \alpha < 2.2$ the field distribution function after the iris is described analytically by a quite complex expression [6]; therefore we shall also replace this function by the gasussian distribution having the same maximum amplitude as the actual distribution. Thus, for any α the field distribution on the retina without considering aberrations will be described by the gaussian curve with the radius ω_α with respect to the level of decrease in amplitude by e times; then $\tilde{k}_{D\kappa} = e^{-(\pi\kappa\omega_\alpha)^2}$. In order to find the form of the function $\tilde{k}_{ab}(\kappa)$ let us use the data from reference [9] in which graphs of the intensity distribution on the retina are presented for irradiation of the eye by the light of an incoherent source with dimensions less than the minimum dimension resolvable by the eye at the given distance. For large pupil diameter (more

than 5 mm), these curves, when describing both the diffraction and aberration blur of the illumination spot can be completely approximated by gaussian curves with a radius ω_Σ with respect to the level of decrease of intensity by e^2 times. Here the spectrum of the intensity distribution function $e^{-(\pi\kappa\omega_\Sigma)^2/2}$ is the transfer function of the optical system of the eye for incoherent light. Let us represent the transfer function in the form of the product of the function $\tilde{h}_D(\kappa)\tilde{h}_{ab}(\kappa)$, where $\tilde{h}_D(\kappa)$ and $\tilde{h}_{ab}(\kappa)$ are the corresponding transfer functions of the aberrationless and purely aberration system for incoherent radiation. Approximating the actual intensity distribution in the diffraction pattern of the aberrationless system by a gaussian curve with radius ω_D, we obtain

$$\tilde{h}_{a\delta}(\varkappa) = e^{-(\pi\varkappa\omega_{a\delta})^2/2},$$

where $\omega_{ab}^2 = \omega_\Sigma^2 - \omega_D^2$. The function $\tilde{h}_{ab}(\kappa)$ is the Fourier transform of the function $|k_{ab}(\rho)|^2$; consequently,

$$k_{a\delta}(\rho) = e^{-\rho^2/\omega_{a\delta}^2} \text{ and } \tilde{k}_{a\delta}(\varkappa) = e^{-(\pi\varkappa\omega_{a\delta})^2}.$$

Knowing $\tilde{k}_D(\kappa)$ and $\tilde{k}_{ab}(\kappa)$, we find the normalized spectrum of the amplitude distribution of the field on the retina $\tilde{E}_c(\kappa) = \tilde{k}_{prin}(\kappa) = e^{-(\pi\kappa\omega_c)^2}$, where $\omega_c^2 = \omega_\alpha^2 + \omega_{ab}^2$, from which $E_c(\rho) = e^{-\rho^2/\omega_c^2}$. The radiation intensity is equal to the square of the field amplitude; therefore the intensity distribution on the retina is described by the expression

$$W_c(\rho) = W_c^{max}\exp(-2\rho^2/\omega_c^2). \tag{1}$$

For determination of the function $\omega_c(z)$ let us find the dependence of ω_α and ω_{ab} on z. Let us first consider the region z for which $\alpha > 2.2$. In this region, a gaussian beam is formed after the crystalline lens which is characterized by the conformal parameter R_e' and has a new constriction of radius ω_o' located at some distance z' from the plane of the pupil. Applying the well-known formula [6] for determining R_e', considering the index of refraction n', we obtain

$$\omega_0' = \omega_0\left[\left(\frac{n'R_э}{2f'}\right)^2 + \left(\frac{zn'}{f'} + 1\right)^2\right]^{-1/2}. \tag{2}$$

After conversions considering the expressions for ω_0 and R_e, we obtain

$$\omega_0' = 0{,}64\frac{\lambda f'_{гл}}{n'2r_{зр}}\underset{(a)}{\alpha}\underset{(b)}{\beta}; \tag{3}$$

$$\alpha = \frac{r_{зр}}{\theta}\left[\left(\frac{\lambda}{\theta^2\pi}\right)^2 + z^2\right]^{-1/2}; \tag{4}$$

$$\beta = \frac{f'}{f'_{гл}}\left[\frac{(\lambda/\theta^2\pi)^2 + z^2}{(\lambda/\theta^2\pi)^2 + (z + f'/n')^2}\right]^{1/2}. \tag{5}$$

(a) (b)

Key: a. prin b. pupil

Obviously the worst conditions of irradiation of the eye will be those for which the illumination spot size on the retina is minimal. In the case where the constriction of the beam incident on the pupil is to the left of the front focal point of the eye F_{prin}, the least spot size corresponds to the size of the new constriction, that is, we consider that for $\alpha \geq 2.2$ $\omega_\alpha = \omega_0'$. The new constriction is on the retina at a distance ℓ_{ac} which will be called the worst accomodation distance. The focal length f' for the worst accommodation will be found from the known expression for z' [6], which, considering n', assumes the form:

$$z' = f'\left[1 - \frac{n'z/f' + 1}{(n'R_э/2f')^2 + (n'z/f' + 1)^2}\right]. \qquad (6)$$

Inasmuch as the new constriction is located on the retina, let us consider $z' = f'_{prin}$. Then equation (6) reduces to the form

$$x^2(p-1) + x(p^2+q^2-2p) - (q^2+p^2) = 0, \qquad (7)$$

where $x = f'/f'_{prin}$; $q = n'R_e/2f'_{prin}$; $p = n'z/f'_{prin}$. Solving equation (7) for any given distances z, it is possible to define the values of f', β and $\ell_{ac} = f_{prin}x/(x - 1)$.

For $\alpha < 2.2$, the illumination spot begins to "blur" as a result of diffraction, and for $\alpha \leq 0.2$ its size is completely determined by the diffraction on the pupil. Let us assume that for $0.2 < \alpha < 2.2$ the spot size ω_α varies in accordance with the linear law $\omega_\alpha = 0.25\,[3.4 + \alpha\beta]\lambda f'_{prin}/n'2r_{pupil}$ obtained from the condition that $\alpha = 2.2$, $\omega_\alpha = \omega_0'$, and for $\alpha = 0.2$, $\omega_\alpha = 0.9\lambda f'_{prin}/n'2r_{pupil}$ (the last expression is obtained from the condition of equality of the total powers in the Airy distribution and in the gaussian distribution equivalent to it).

In order to find ω_{ab} we use the values of the Strell coefficient ξ for different pupil diameters. Under the approximation conditions assumed previously, the Strell coefficient is equal to the ratio of the maximum intensity in the system with aberrations to the maximum gaussian distribution of the intensity which would occur at the retina in the absence of aberrations. From the condition of equality of the total powers in both distributions we obtain $\omega_{ab} = 0.9\lambda f'_{prin}(\xi^{-1} - 1)^{1/2}/n'2r_{pupil}$.

Substituting the expressions obtained above in the equation for ω_c^2, for the case where the constriction is to the left of F_{prin} we obtain:

$$\omega_c(z) = \frac{\lambda f'_{prin}}{n'2r_{зр}}\left|\gamma^2(z) + 0{,}81\,[\xi^{-1}(z) - 1]\right|^{1/2}, \qquad (8)$$

where

$$\gamma(z) = \begin{cases} 0{,}64\alpha\beta & \text{for } \alpha \geq 2{,}2; \\ 0{,}25\,(3{,}4 + \alpha\beta) & \text{for } 0{,}2 < \alpha < 2{,}2; \\ 0{,}9 & \text{for } \alpha \leq 0{,}2. \end{cases}$$

The graphs of the function $w_c(z)$ are presented in Figure 2 for a pupil of diameter d_{pupil} = 8 mm (the worst case of "night" vision). For the calculations the coefficient ξ was determined by the data from reference [9], where for $\alpha > 1$ a value of $2\omega_{pupil}$ was taken as the pupil diameter. From Figure 2 we see that with increasing distance of the constriction from the front focal point F_{prin} the illumination spot size under the conditions of worst accomodation decreases from a value of $\theta f'_{prin}/n'$ to a minimum value of ω_c^{min}, after which it begins to increase as a result of diffraction and aberration broadening and reaches a value which in practice is completely determined by the aberrations of the eye. At greater distance from the constriction, this value remains constant.

In Figure 2 graphs are also presented for the distance of the worst accommodation ℓ_{ac} as a function of z. For each value of θ there is a least value of ℓ_{ac}^{min} which decreases with an increase in θ. However, ℓ_{ac} cannot be less than the distance to the near point of the eye (~125 mm) [7]. This explains the horizontal segment of the graph for θ = 5 mrad. To the left of the point z_{ℓ}^{min} corresponding to ℓ_{ac}^{min}, the function $\ell_{ac}(z)$ sharply approaches infinity, and to the right of this point it approaches z.

As a result of the investigation above of the process of shaping the illumination spot on the retina of an eye irradiated by a diverging gaussian beam, a result is obtained which is important to estimating the degree of hazard of the radiation: on the beam axis there is a point at a distance from tens of centimeters to several meters (depending on θ) from the initial constriction at which under the conditions of worst accommodation of the eye it is possible to obtain an illumination spot on the retina of minimum size (about 5 microns) which is appreciably less than the illumination spot size obtained on the retina on removal of the eye to infinity (about 20 microns).

For the case where the beam constriction is to the right of the point F_{prin} the worst accommodation conditions will be accommodation at infinity ($f' = f'_{prin}$). Here, for $\alpha \geq 2.2$ a minimum spot will be formed on the retina with radius $\omega'_1 = \theta f'_{prin}/n'$. The general function $\omega_c(z)$ in the case where the constriction is to the right of F_{prin} including for the cases where the eye is irradiated by a converging beam ($z > 0$), will be described by the formula (8), where

$$\gamma(z) = \begin{cases} 2\theta r_{ap}/\lambda & \text{for } \alpha \geqslant 2{,}2; \\ (0{,}2\theta r_{ap}/\lambda)(5\alpha - 1) - 0{,}45(\alpha - 2{,}2) & \text{for } 0{,}2 < \alpha < 2{,}2; \\ 0{,}9 & \text{for } \alpha \leqslant 0{,}2. \end{cases}$$

Key: a. pupil

The graph of the function $\omega_c(z)$ for positive z is presented in Figure 2 for θ = 1 millirad. It is obvious that the illumination spot size in this case will greatly exceed the above-indicated value of ω_c^{min}.

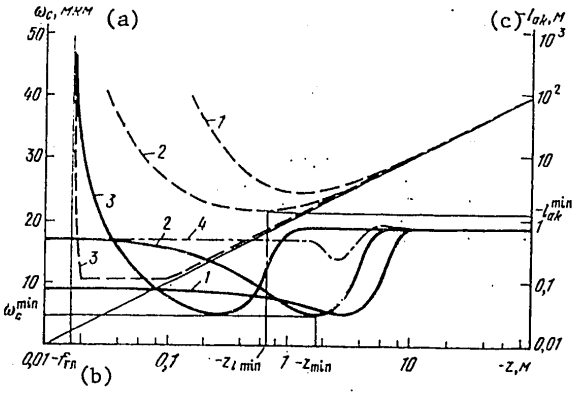

Figure 2. Radius of the illumination spot on the retina ω_c (the solid lines) and the worst accommodation distance ℓ_{ac} (dotted line) as a function of the distance z from the pupil to the beam constriction for $\lambda = 10^{-6}$ m, $d_{pupil} = 8$ mm, $\theta = 0.5$ (1), 1 (2, 4) and 5 milliradians(3); the dash-dot line is ω_c for $f' = f'_{prin}$.

Key: a. microns
b. f_{prin}
c. ℓ_{ac}

The function (8) considering expression (9) also characterizes the spot size on the retina for negative z for accommodation of the eye at infinity. These accomodation conditions are adopted in references [4, 5], which leads to lowering of the degree of hazard of the radiation for small distances from the eye to the constriction if the formulas presented in these papers are used.

During ω_c (z) let us determine $W_c^{max}(z)$ expressing it in terms of the power P of the laser beam measured at some distance from the eye. (All of the arguments presented below are also valid for pulse radiation energy on replacement of the notation P by E_{pulse}.) The power P_{pupil} of the radiation passing through the pupil can be found by the formula $P_{pupil} = P\tau_{medium}[1 - \exp(-2\alpha^2)]$, where τ_{medium} is the radiation transmission coefficient of the medium located between the eye and the point at which the power is measured. From the condition $P_{pupil} = \tau_{prin}\int_0^{2\pi}\int_0^{\infty} W_c(\rho)\rho d\rho d\varphi$, where τ_{prin} is the transmission coefficient of the optical media of the eye at a wavelength λ, we obtain

$$W_c^{max}(z) = \underset{(a)}{\tau_{prin}}\underset{(b)}{\tau_{cp}} P2[1-\exp(-2\alpha^2)]/\pi\omega_c^2(z) = \tau_{prin}\tau_{cp}PH(z), \qquad (10)$$

Key: a. prin
b. medium

where $H(z) = 2[1 - \exp(-2\alpha^2)]/\pi\omega_c^2(z)$ is the recalculation factor for determining the maximum intensity on the retina in terms of the incident radiation power. The graphs of H(z) for $d_{pupil} = 8$ mm are presented in Figure 3. It is obvious that on

removal of the eye from the constriction, the maximum radiation intensity on the retina first increases, reaching the maximum value of H_{max} at some point z_{max}, after which it begins to decrease, where the larger z is, the closer the decreasing law to the function $1/z^2$. Comparing Figures 2 and 3, it is possible to note that the point z_{max} corresponds to the minimum value of ω_c^{min}.

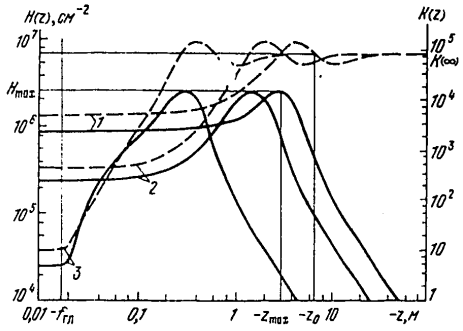

Figure 3. Scaling factors for determining the maximum intensity on the retina in terms of the beam power H(z) (solid lines) and in terms of the maximum value of the intensity on the pupil K(z) (the dotted line) as a function of the distances z to the beam constriction for $\lambda = 10^{-6}$ m, $d_{pupil} = 8$ mm, $\theta = 0.5$ (1), 1 (2) and 5 milliradians (3).

It is convenient to express $W_c^{max}(z)$ in terms of the maximum radiation intensity in the plane of the pupil $W_{pupil}^{max}(z)$, for which it is necessary to substitute $P = W_{pupil}^{max}(z)\pi\omega_{pupil}^2/2\tau_{medium}$ in formula (10). Then we obtain

$$W_c^{max}(z) = \underset{(a)}{\tau_{prin}} \underset{(b)}{W_{зр}^{max}(z)} \frac{r_{зр}^2\left(1-e^{-2\alpha^2}\right)}{\alpha^2\omega_c^2(z)} = \tau_{prin} W_{зр}^{max}(z) K(z), \qquad (11)$$

Key: a. prin b. pupil

where $K(z) = r_{pupil}^2 [1 - \exp(-2\alpha^2)]/\alpha^2\omega_c^2(z)$ is the scaling factor for determining the maximum intensity on the retina in terms of the maximum intensity on the pupil. The graphs of the function K(z) for $\lambda = 10^{-6}$ m, $d_{pupil} = 8$ mm are presented in Figure 3. It is obvious that for large distances z the coefficient K(z) assumes a constant value $K(\infty)$, inasmuch as $\omega_c(z)$ becomes constant with an increase in z.

Knowing $W_c^{max}(z)$, we find the expression for the hazard coefficient of a laser beam R(z) considering the fact that $W_c^{MAL} = \tau_{prin} K(\infty) W_{pupil}^{MAL}$. For the directional beam with power P, we obtain

$$R(z) = \underset{(a)}{\tau_{cp}} PH(z)/K(\infty) \underset{(b)}{W_{зр}^{(c)}}. \qquad (12)$$

Key: a. medium b. pupil c. MAL [maximum allowable level]

Expression (12) can be used as the basis for the calculation methods of laser dosimetry of directional radiation beams, for it permits estimation of the degree of hazard of the radiation at a given point in space and determination of the boundaries of the danger zones, using the nominal values of the radiation power P, the divergence θ and the beam diameter $2\omega_{rad}$ at the radiator output in the calculations.

Let us consider an example of determining the degree of hazard of a laser beam. Let it be required that R be determined at a point located at a distance ℓ = 1 m from the exit opening of the radiator operating in the unimodal continuous radiation regime with λ = 1.06 microns. Let it be known from the certificate data of the radiator that P = 0.1 watt, ω_{rad} = 2 mm, θ = 3 millirads. Let us define the distance from the monitoring point to the constriction by the formula $z = \ell - \theta^{-1}[\omega_{rad}^2 - (\lambda/\pi\theta)^2]^{1/2} = -1.67$ m, $\alpha = 0.8$. By formula (8) we obtain ω_c = 18.6 microns; by formula (10) we obtain $H(z) = 2\cdot10^5$ cm^{-2}. Considering W_{pupil}^{MAL} = 5 milliwatts/cm^2 (according to the data of [3] for radiation duration of 10 sec), τ_{prin} = 0.6 (according to the data of reference [5] for = 1.06 microns), τ_{medium} = 1, $K(\infty) = 90.4\cdot10^3$ (Figure 3), we obtain R = 44. Now let θ = -3 mradians, and the remaining parameters have the same values. Then z = -0.33, R = 575. The second case of irradiation turns out to be more hazardous. It is explained by the closeness of the constriction of the focused beam to the front focal point of the eye.

The value of R(z) at the given point in space can be determined by the results of measuring the radiation power density and the calculations by the formula

$$R(z) = W_{зр(a)}^{max}(z)\,K(z)/K(\infty)\,W_{зр}^{пд(b)}. \qquad (13)$$

Key: a. pupil b. MAL

From formula (13) it follows that for large z when $K(z) = K(\infty)$, R(z) is defined as the ratio $W_{pupil}^{max}/W_{pupil}^{MAL}$. For the sake of definiteness we can assume that this estimate of R(z) is admissible in the region $z > z_0$, where z_0 is the second point of intersection of the graph with the straight line $K(\infty)$ in Figure 3. It is possible to see that z_0 approximately corresponds to α = 1, that is, if the beam diameter at the control point is greater than d_{pupil} = 8 mm, then at the control point it is necessary to measure the largest value of the power density and determine the hazard coefficient as the ratio of the measured value and the corresponding value of MAL. If the beam diameter is less than 8 mm, it is more convenient to measure P at the control point and determine R(z) by formula (12). If the location of the constriction is unknown, it is expedient to use the high value of R(z), setting $H(z) = H_{max} = 3\cdot10^6$ cm^{-2} in formula (12). Then for "narrow" beams ($\omega_{pupil} \leq$ 4 mm), a reliable estimate of the degree of hazard is made by the formula $R = 33.2P/W_{pupil}^{MAL}$, where P is measured in watts, and W_{pupil}^{MAL}, in watts per square centimeter.

The expressions obtained above for estimating the degree of hazard of directional laser beams can be the basis for the development of both calculation methods of laser

dosimetry and the methods of dosimetric control of laser radiation; in particular, from the investigation, a laser dosimeter must measure the power (energy) of the directional radiation beams less than 8 mm in diameter and maximum radiation intensity for beams more than 8 mm in diameter. Here it is expedient to equip the dosimeter with a device for operative estimation of the radiation beam diameter in the range of 2-30 mm.

BIBLIOGRAPHY

1. I. R. Petrov, et al., IZLUCHENIYE LAZEROV, ZASHCHITA I PROFILAKTIKA OT IKH NEBLAGOPRIYATNOGO DEYSTVIYA (Laser Radiation, Protection and Prevention of Harmful Effects from It), Leningrad, LDNTP, 1969.

2. A. I. Kirillov, et al., KVANTOVAYA ELEKTRONIKA (Quantum Electronics), No 3, 1976, p 1394.

3. AMERICAN NATIONAL STANDARD FOR SAFE USE OF LASERS, ANSI, 1973, p 136.1.

4. L. R. Solon, R. Aronson, G. Gould, SCIENCE, No 134, 1961, p 1506.

5. J. Rady, DEYSTVIYE MOSHCHNOGO LAZERNOGO IZLUCHENIYA (Effect of Powerful Laser Radiation), Moscow, Mir, 1974.

6. Yu. M. Klimkov, OSNOVY RASCHETA OPTIKO-ELEKTRONNYKH PRIBOROV S LAZERAMI (Design Principles of Optoelectronic Instruments with Lasers), Moscow, Sov. radio, 1978.

7. V. N. Churilovskiy, TEORIYA OPTICHESKIKH PRIBOROV (Theory of Optical Instruments), Leningrad, Mashinostroyeniye, 1966.

8. M. Born, E. Wolf, OSNOVY OPTIKI (Fundamentals of Optics), Moscow, Nauka, 1973.

9. R. W. Gubisch, J. OPT. SOC. AMER., No 57, 1967, p 407.

Report received 11 March 1980

10845
CSO: 1862

UDC 621.378.335

LIGHT AMPLIFICATION IN HALOGEN ATOM RECOMBINATION REACTIONS

Moscow KVANTOVAYA ELEKTRONIKA in Russian Vol 7, No 12, Dec 1980 pp 2543-2551

[Article by I. A. Izmaylov, V. A. Kochelap, Semiconductors Institute of the Ukrainian SSR Academy of Sciences, Kiev]

[Text] The radiation channel of halogen atom recombination reactions is discussed from experimental data. It is demonstrated that various types of populations of excited electron states formed during recombination exist. The light amplification cross sections are calculated for various transitions. It is demonstrated that for recombining atom concentrations of $1\text{-}5\cdot10^{18}$ cm^{-3} at temperatures not exceeding 600-800 K, light amplification in the near infrared range on the order of 10^{-3} cm^{-1} can be realized.

One of the possibilities for creating a chemical electron phototransition laser is connected with using radiation recombination reactions (see, for example, [1]). A number of problems in recombination lasers have been investigated theoretically: criteria have been defined for obtaining the inverse population, and various methods of creating high concentrations of nonequilibrium recombining particles have been proposed, and so on. For experimental realization of the recombination laser, it is necessary to solve the problem of the working media, that is, find suitable pairs of recombining particles, diluent gases, and investigate the most favorable nonequilibrium recombination conditions for lasing. At the present time there are no experimental data on recombination reactions obtained under nonequilibrium conditions as required for laser emission. Therefore when selecting and discussing the peculiarities of the reactions potentially suitable for a laser it is necessary to use data obtained under other conditions. This type of effort is made in this paper for recombination reactions of various halogen atoms. Previously, the light amplification was estimated for recombination reactions of chlorine and bromine atoms [1-5]. These and other halogen recombination reactions will be investigated in more detail below. The results of experimental studies of chemiluminescence and photoluminescence were analyzed, which made it possible to determine the nature of population of the electron-excited molecular levels of the recombination products under various conditions. The amplification cross sections have been calculated for a number of electron transitions, and the criteria for obtaining inverse population are discussed.

Discussion of the Experimental Data

Chemiuminescence during halogen recombination has been studied in many papers (see the survey [6] and references below). The properties of the chemiluminescence of various reacting pairs turned out to be similar. The chemiluminescence spectra contain a short wave continuous component and a longer-wave band component. The former is characteristic of high temperatures, and the latter is observed under any conditions.

Let us discuss the analysis of the band spectra. The studies of [7-11] performed at room temperatures and pressures not exceeding several millimeters of mercury demonstrated that in the three-particle recombination reaction the $^3\Pi$ multiplet states of the halogen molecules are effectively populated (ground state $X^1\Sigma^+$). The transitions $B^3\Pi_{0^+} \rightarrow X^1\Sigma^+$ and $A^3\Pi_1 \rightarrow X^1\Sigma^+$ are the most allowed. Directly during the course of the three-particle processes all of the vibrational levels of the A-states are populated (and for Cl_2, all of the vibrational levels of the B-state). Subsequent collisions in the gas lead to vibrational relaxation in the excited states.

Among the vibrational levels it is possible to isolate two groups of states. The population of the upper levels corresponds to equilibrium between them and the dissociated states (the recombination and redissociation processes predominate). The kinetics of radiation from this group of levels is of a two-particle nature. The population of the lower levels is below equilibrium, and it increases with an increase in pressure, which causes a red shift of the radiation spectra. The radiation peak is in the range of 1.0 to 1.2 microns. The quenching of the chemiluminescence in an inert or molecular diluent turned out to be weak (the corresponding constants are less than or on the order of 10^{-13} m^3/sec). The quenching of chemiluminescence has not been investigated in detail. With respect to general concepts of nonradiative transitions [12], the variation of the electron state must primarily occur for transitions between states of identical multiplet nature, and an important role is also played by the overlap of the oscillatory functions of the converting states. The validity of these two general principles is confirmed by the experimental data with respect to photoluminescence of the investigated molecules [13-20].

Thus, for Cl_2 small energy distances between the components of the $^3\Pi$ multiplet are characteristic [21]. This leads to significant overlap integrals of the vibrational wave functions of the states with close energy belonging to different components of the multiplet and to strong interaction of these states. Thus, the $^3\Pi_{0^+u}$ levels located above the dissociation limit ($v' \geq 13$) quickly spontaneously and inductively (almost for each collision in the gas) predissociate through other multiplet states [13]. The rapid conversion and subsequent dissociation were also observed for levels located below the dissociation limit (thus, for the levels $v' = 9$-12 the redissociation constant exceeds 10^{-10} cm^3/sec [14]). Rapid self-quenching for the remaining levels ($k_2 = 5 \cdot 10^{-12}$ cm^3/sec [15]) can also be categorized as conversion between the multiplet states. The high probability of electron conversion can also be used to explain the significant magnitude of the recombination constant of the unexcited atoms $^2P_{3/2}$ to the $^3\Pi_{0^+u}$ state not correlating with the $^2P_{3/2}$ atoms (this constant is no less than the recombination constants to the $^3\Pi_{1u}$ Br_2 and

$^3\Pi_0$ + BrCl states, although in the latter cases variation of the electron state is not required [10]). Finally, let us note that the mixing of the $^3\Pi_{0+u}$ and $^3\Pi_{2u}$ states was observed in [16] with respect to the nature of the radiation polarization.

In contrast to what has been discussed, the conversion from the $^3\Pi$-states to the ground state is complicated not only by the selection rules, but also by the small overlap of the vibrational wave functions (thus, for example, the level v' = 0 of the state B corresponds to ground state levels with similar energy and v" = 50, the overlap integral turns out to be negligible in this case). This is confirmed by experiments under the conditions of an inert matrix [16], where it is demonstrated that during photopumping of the B state the excitation decays with radiation time of the lowest state of the $^3\Pi$-multiplet -- the $^3\Pi_{2u}$ state. The molecules get to this state as a result of effective conversion within the multiplet and rapid vibrational relaxation. In the gas phase the quenching of the $^3\Pi$-multiplet is small; it corresponds to the above-presented estimate of the chemiluminescence quenching constant. Actually, during recombination all of the low states of the multiplet are populated, fast exchange between them does not lead to loss of electron excitation. The decrease in glow can be explained either by conversion to the ground state or vibrational relaxation to the lower and less luminescent states.

For Br_2, ICl, I_2 and certain other halogen molecules, another situation occurs: splitting within the $^3\Pi$ multiplet is large, the vibrational wave functions overlap little not only with the vibrational functions of the ground state, but also within the multiplet. Therefore electron exchange both with the ground state and between multiplet states is difficult. Thus, for Br_2 strong predissociation of levels v' $\geq$ 5, $^3\Pi_{0^+_u}$ is known [17], which is connected with the intersections between $^3\Pi_{0+u}$ and the repulsive terms. The levels v' $\leq$ 5, $^3\Pi_{0+u}$ located above the dissociation limit but below these intersections can interact only with the $^3\Pi$-states and, as the experiment shows, they do not decay. On recombination the same levels are populated only through the levels v' > 5, which requires activation energy [9]. The same thing occurs for the B-state of the ICl molecule; in this case the levels v' > 2 predissociate easily and are populated on recombination [18]. Under the conditions of an inert matrix the radiationless transition of the states of the $^3\Pi$-multiplet to the ground state is not observed, and the $^3\Pi$-states decay only in the radiation times where the molecules on the lowest level v' = 0 radiate [19, 20]. For Br_2, under the matrix conditions, only the B state was observed; the other states could not be detected. For ICl, the states A and B were observed, and their decay took place independently. In the gas phase during the Br-Br, I-Cl recombination, primarily the A state is populated [7, 8, 11]. Thus, for this series of halogen molecules the electron conversion has little significance.

Classification of Various Cases of the Population of Excited States

What has been discussed above permits the following diagram of the population and excited state relaxation processes of the Cl_2 molecules during recombination to be adopted:

$$Cl+Cl+M \rightleftarrows Cl_2(^3\Pi)+M; \quad (1)$$

$$Cl_2(^3\Pi_i)+M \rightleftarrows Cl_2(^3\Pi_j)+M; \quad (2)$$

$$Cl_2(^3\Pi, v')+M \rightleftarrows Cl_2(^3\Pi, v'+\Delta v')+M; \quad (3)$$

$$Cl_2(^3\Pi)+M \rightarrow Cl_2(^1\Sigma_g^+)+M; \quad (4)$$

$$Cl_2(^3\Pi_i) \rightarrow Cl_2(^1\Sigma_g^+)+\hbar\omega. \quad (5)$$

Here (1) is recombination to the bound states of the $^3\Pi$-multiplet and the inverse process of dissociation from these states; (2) is the conversion between the multiplet components; (3) is the vibrational relaxation in the excited states; (4) is the conversion to the ground state; (5) are the radiation transitions. The recombination constant to the $^3\Pi_{0+u}$-state is known [10]: $k_1(^3\Pi_{0+u}) = 5\cdot10^{-34}$ cm^6/sec. Under rapid conversion conditions (the corresponding estimate was presented above), it is necessary to define the complete recombination constant to the $^3\Pi$-multiplet k_1. Considering that recombination takes place to all of the bound states except $^3\Pi_{0+u}$ without a change in the electron state, we obtain the estimate $k_1 \geq 6k_1(^3\Pi_{0+u})$. The vibrational relaxation rate constant k_3 can be estimated from the fact that at a pressure of 1-3 mm Hg a red shift of the chemiluminescence spectrum is still observed [9, 10], that is, the vibrational relaxation rate is comparable to the radiation loss rate. As a result, we find $k_3 = (1-3)\cdot10^{-13}$ cm^3/sec, T = 300 K. The calculation of k_3 by the empirical formulas of [22] (see also [23]) leads to a value of $4\cdot10^{-13}$ cm^3/sec, that is, for T = 300 K the vibrational relaxation rate does not exceed the quenching rate by much. With an increase in T, the inequality $k_3 > k_4$ will become stronger. Thus, for T = 450 K the estimate by formulas [22] gives $k_3 = 10^{-12}$ cm^3/sec, that is, for pressures exceeding several millimeters of mercury, it will be possible to establish the vibrational equilibrium in the excited states.

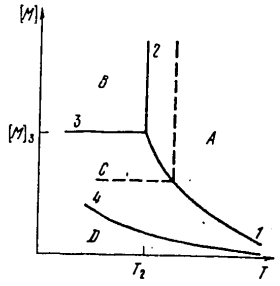

It is important to compare the role of the individual processes (1)-(5) as a function of the experimental conditions: density [M], composition [X]/[M] and temperature T([X] is the concentration of X atoms). For this purpose the set of parameters [M], [X]/[M], T is broken down into regions in each of which one process of deactivation of the electron-excited states or another predominates. The convenience of the breakdown into the limiting regions consists in the following. Simple expressions for the populations of the excited states are obtained in each of the regions which permit analysis of their concentration and temperature functions. It is possible to isolate the regions of greatest interest in laser respects. This subdivision permits estimation of the populations of the states in the individual regions in the absence of complete information about the deactivation processes.

Let us begin with the case of high dilution: $[X]/[M] \ll 1$. The figure illustrates the breakdown of the plane of significant parameters [M], T into the regions A, B, C in which the inverse process (1) and processes (4), (5), respectively predominate. The processes of internal conversion are considered to be the fastest. Curve 1 is defined by the condition $[M] = (\Sigma k_{5i}/K_i)/(\Sigma k_{1'i}/K_i)$, where summation is carried out with respect to the electron states, between which effective exchange takes place. K_i are the chemical equilibrium constants of these states with the dissociated states. The line 2 is found from the condition $\Sigma k_{4i}/K_i = \Sigma k_{1'i}/K_i$, line 3, from $[M] = (\Sigma k_{5i}/K_i)/(\Sigma k_{4i}/K_i)$, curve 4 -- $[M] = \sum_i \frac{k_{si}}{K_i k_s} \sum_j K_j$ -- bounds the region of parameters below, in which vibration equilibrium can be established in the excited states. In region A the recombination and dissociation processes (1) predominate, therefore the population of each of the states can be calculated using the equiliqrium constants:

$$[XY]_i = [X][Y]/K_i \tag{6}$$

(for generality the atom concentrations [X] and [Y] are introduced). In region B the recombination (1) and quenching (4) processes predominate, population and radiation have an apparent two-particle nature:

$$[XY]_i = (\Sigma k_{1j}/K_i \Sigma k_{4j}/K_j)[X][Y]. \tag{7}$$

In region C the recombination (1) and radiative emission (5) processes are the most important, population and radiation are of a three-particle nature:

$$[XY]_i = (\Sigma k_{1j}/K_i \Sigma k_{5j}/K_j)[X][Y][M]. \tag{8}$$

From (6)-(8) it follows that for the investigated case of a highly dilute mixture with fixed [X], [Y], the highest concentrations of excited particles are realized in the region of parameters B.

Using the kinetic parameters of the reactions (1)-(5) discussed above and the equilibrium constants of the electron states of the $^3\Pi$-multiplet of Cl_2, it is easy to calculate curves 1-3 of the figure. Here let us present only the characteristic values $[M]_3 = 1.3 \cdot 10^{17}$ cm^{-3}, $T_2 = 450$ K. Formulas (6)-(8) are used below to calculate the light amplification.

Above, we discussed the processes of quenching in a molecular or inert gas. With an increase in the halogen atom concentration, a violet shift of the radiation spectra and a decrease in the glow [7, 8], which was interpreted as strong quenching of the radiation luminescence on the atoms, were detected. However, as is obvious from [7], this quenching depends on the type of diluent. It is also known that additives of the molecules, for example, HCl (the ground state $^1\Sigma^+$) also lead to the violet shift and quenching of the radiation. Considering this fact and the above discussed arguments about conversion of electron states in halogens, it is possible to present another explanation for the observed effects: an increase in the atom concentration leads to acceleration of the vibrational relaxation inside the multiplet $^3\Pi$ in the

atomic states $Cl(^2P_{3/2})$, to variation of the distribution function with respect to vibrational levels, which causes a violet shift of the spectra; part of the molecules are converted to the lower and less glowing levels. (The vibrational relaxation rate on the atoms is discussed, for example, in [24].)

If the quenching in the atoms differs significantly from quenching in the molecules, then it is necessary to make the following substitution in the above-discussed results: $k_4 \to k_4^{(M)} + k_4^{(X)}[X]/[M]$. This leads to expansion of the region B in which the quenching is significant, and to constriction of the regions A and C (see the dotted line on the curve). We shall assume that the quenching constant in the atoms $k_4^{Cl} = 10^{-11}$ cm^3/sec [7, 8]. Then for $[X]/[M] = 0.1$, it turns out that $[M]_3 = 10^{16}$ cm^{-3}, $T_2 = 600$ K. In the absence of a diluent, the subdivision of the plane of the parameters requires only the two regions A and B. The temperature at which the change in nature of the population takes place is $T_2 = 800$ K.

Inasmuch as for the Br_2, ICl and I_2 molecules the conversion between states of the multiplet is appreciably weaker, for the corresponding reactions the system (1)-(5) is simplified: the process (2) can be omitted, and each of the states must be considered independently. In the above-presented formulas it is necessary to consider only one term in the sums. Applying these formulas, for example, for the state $A^3\Pi_{1u}Br_2$, we find $[M]_3 = 10^{17}$ cm^{-3}, $T_2 = 400$ K. The calculation of k_3 by the formulas [22] shows that under these conditions, vibrational equilibrium can be established in state A of the Br_2 molecule. In the case of the absence of dilution with quenching constant on the atoms $k_4^{(Br)} = 10^{-11}$ cm^3/sec, we find the temperature bounding the region A and B, $T_2 = 600$ K. Analogous estimates have also been obtained for other halogens.

Criteria for Obtaining Inverse Population and Amplification Coefficients

Let us discuss the inversion radiation criteria and the magnitude of the amplification in halogen recombination reactions. The amplification (absorption) coefficient is conveniently represented in the form $\alpha = \alpha^+ - \alpha^-$, where α^+ corresponds to the radiation of quanta, α^- corresponds to absorption. The amplification condition $\alpha > 0$ assumes the simplest form if the following two conditions are satisfied: equilibrium exists between the bound states of the electron-excited molecule and the dissociated states, and equilibrium can be established in the vibrational subsystem of the electron ground state. The complete equilibrium, of course, must be absent. The region of parameters where the first condition is satisfied has already been discussed above (region A). For the ground state in a number of cases vibrational relaxation times are known. Thus, for Cl_2 at $T = 500$ K, according to [22], $p\tau_v = 10^{-6}$ sec-atm; for Br_2 - $p\tau_v = 3 \cdot 10^{-7}$ sec-atm. For $[X]/[M] \approx 0.1$, $[M] \approx 10^{19}$ cm^{-3} these values are an order less than the characteristic recombination times. Let us note that in the presence of atoms the vibrational relaxation is accelerated [24]. Thus, for $T \sim 500$K the equilibrium in the vibrational subsystem of the ground state must be able to be established. On satisfaction of the two above-indicated conditions the inversion criterion assumes the form [1, 25]

$$[X][Y] \geqslant K(T) e^{\hbar\omega/kT} [XY], \tag{9}$$

where K(T) is the equilibrium constant of the entire process X + Y = XY, ω is the phototransition frequency.

If the condition of equilibrium with dissociated states is not satisfied, but equilibrium exists in the vibrational subsystems of the ground and excited states (regions B and C), then the inversion criterion can be written in the form

$$[XY]_i > (Z_i/Z_0)[XY]_0 e^{-(\Delta E_{i0} - \hbar\omega)/kT}, \quad \Delta E_{i0} = E_{iv'l'} - E_{0v''l''}, \tag{10}$$

where Z_i and Z_0 are the statistical sums of the excited (i) and ground (0) states; $E_{iv'\ell'}$, $E_{0v''\ell''}$ are the energies of the vibrational-rotational levels of the electron states i and 0.

The criteria (9), (10) make it possible to find the operating temperature ranges of the recombination laser. For concreteness, let us consider the region A. As is obvious, the criterion (9) for fixed ω essentially depends on T and depends slightly on the concentrations. For the estimates it is convenient to set [X] = [Y] = [XY] and define the "limiting" temperature T_{lim} [26], below which ($T < T_{lim}$) condition (1) is satisfied. For Cl_2, setting [Cl] = 10^{18} cm^{-3}, we find the following: for λ = 1170 nm, T_{lim} = 1070 K; for λ = 738 nm, T_{lim} = 600 K. For Br_2, setting [Br] = 10^{18} cm^{-3}, at λ = 1200 nm we find T_{lim} = 800 K; for λ = 1400 nm, T_{lim} = 950 K. Analogous estimates are also obtained for other pairs of recombining atoms.

If the criteria (9), (10) are satisfied with reserve, then for calculating the light amplification coefficient it is sufficient to calculate α^+. For the transitions between the iv'ℓ', 0v"ℓ" levels of the XY molecule, α^+ is defined by the amplification cross section $\sigma^{iv'\ell'}_{0v''\ell''}$ and the population of the state iv'ℓ' - $[XY]_{iv'\ell'}$: $\alpha^+ = \sigma^{iv'\ell'}_{0v''\ell''} [XY]_{iv'\ell'}$. For the amplification cross section at the maximum of the doppler-broadened line, the following expression is valid

$$\sigma^{iv'l'}_{0v''l''} = \frac{4\pi^2}{3\hbar} \frac{|R^i_0|^2 q_{v'v''} S_{l'l''}}{(2\pi kT/m_{XY})^{1/2}(2l'+1)}, \tag{11}$$

where R^i_0 is the electron matrix element; $q_{v'v''}$ and $S_{\ell'\ell''}$ are the Franck-Condon and Hanle-London factors; m_{XY} is the mass of the XY molecule. If equilibrium is realized in the subsystem of vibrational-rotational levels of the state i (the regions A, B and C), then instead of (7) it is convenient to use the cross section σ_i in the calculation for the complete population of the state i $[XY]_i$:

$$\alpha^{(+)} = \sigma_i [XY]_i, \quad \sigma_i = \sigma^{iv'l'}_{0v''l''} (2l'+1) e^{-E_{iv'l'}/kT}/Z_i(T). \tag{12}$$

For the fixed band in the radiation spectrum v' → v" the maximum of $\alpha^{(+)}$ corresponds to transitions with rotational levels with $\ell' \approx \ell_m \equiv \sqrt{kT/2B_{v'}}$, $B_{v'}$ is the rotational

constant of the state i, v'. The generalization of (11) to the case of impact broadening is realized using the known Voigt formula. However, the impact broadening cross sections, as a rule, are not known; therefore here we shall present the formula for calculating α^+ suitable for such large pressures where the rotational structure disappears in the radiation spectrum:

$$\alpha^+(\lambda) = \sigma^i_{v'v''}(\lambda)[XY]_i,$$

$$\sigma^i_{v'v''}(\lambda) = \frac{8\pi^3 |R^i_0|^2 q_{v'v''} B_{v'} \hbar\omega_{v'}}{3\lambda (kT)^2 |B_{v'} - B_{v''}|} \exp\left[-\frac{B_{v'}(\lambda - \lambda_{v'v''})}{(B_{v'} - B_{v''})\lambda^2_{v'v''} kT}\right]. \quad (13)$$

Here $\lambda_{v'v''}$ is the wavelength of the light for the transition iv' → v". Expression (13) gives the spectral distribution of the value of $\alpha^+(\lambda)$ in the given radiation band iv'-0v". For arbitrary pressures, it is possible to use (13) as the estimate for the lower bound of the interval of variation of α^+.

Light amplification coefficient

X+X+M	Type of transition	b^*_λ, 10^{-42} см⁶	T_λ, K	λ, nm	v'−v"
Cl + Cl + M	$^3\Pi_{0^+u} \leftrightarrow {}^1\Sigma^+_g$	1	2250	740	3—9
		2	3400	1060	0—16
		2 (0,08)	3400	1170	0—18
Br + Br + M	$^3\Pi_{1u} \leftrightarrow {}^1\Sigma^+_g$	1,3 (0,06)	3150	1200 1240 1280	0—18 0—19 0—20
		0,9	3150	1430	0—23
Br + Cl + M	$^3\Pi_{0^+} \leftrightarrow {}^1\Sigma^+$	4	1800	800 865	0—10 0—12
J + Cl + M	$^3\Pi_{0^+} \leftrightarrow {}^1\Sigma^+$	40	0	720—755	0—9 to 11
J + Cl + M	$^3\Pi_1 \leftrightarrow {}^1\Sigma^+$	5	5300	1200	0—13
J + J + M	$^3\Pi_{0^+u} \leftrightarrow {}^1\Sigma^+_g$	7	4400	1220—1920	0—22 to 38
J + J + M	$^3\Pi_{1u} \leftrightarrow {}^1\Sigma^+_g$	1	2100	1300—1500	0—18 to 20

*The "broadened" values are presented.

Let us proceed to the calculation of the amplification for specific systems. For the Cl_2 molecule it is necessary to consider that the transition $B^3\Pi_{0^+u} \rightarrow X^1\Sigma^+_g$ has the same structure as the transition $^1\Sigma^+_g \rightarrow {}^1\Sigma^+_g$ for the b-type Hund bond [27]: the

P and R branches are intense, and the Q-branch is absent. The nuclear spin of the ^{34}Cl and ^{37}Cl isotopes is 3/2; therefore transitions from the even rotational levels of the upper state predominate. The spectroscopic parameters of Cl_2 were taken from [28], the matrix element from [14], the factors $q_{v'v''}$ from [29]. Let us present the results for the transition from the level v' = 0. Inasmuch as for the transitions $0 \to 17$, $0 \to 18$, $0 \to 19$ the values of $q_{v'v''}$ are close and approximately equal to 0.1, we find $\sigma_i = 8.3 \cdot 10^{-19} \cdot (1000\ K/T)^2\ cm^2$ for them at the transitions from the rotational levels $\ell' \approx \ell_m$ for both P and R-branches. The oscillatory statistical sum was calculated at the classical limit, $\sigma^i_{0v''} = 3 \cdot 10^{-20}\ (1000\ K/T)^2\ cm^2$; v" = 17, 18, 19.

An analogous calculation was made for the more forbidden transitions: $A^3\Pi_{1u} \to X^1\Sigma^+_g$: $\sigma_i = 5 \cdot 10^{-21} (1000\ K/T)^2\ cm^2$, λ in the vicinity of 1200 nm; $^3\Pi_{2u} \to X^1\Sigma^+_g$: $\sigma_i = 8 \cdot 10^{-22}$ $(1000\ K/T)^2\ cm^2$ λ in the vicinity of 1300 nm.

In region A (see the figure) the value of α^+ is represented in the following form by using the above-presented cross section for the B → X transition and the expression for the population of the B-state (6)

$$\alpha^+(\lambda, T) = a(\lambda, T)[X][Y],\ a(\lambda, T) \equiv b_\lambda (1000K/T)^{3,2} e T_\lambda / T. \qquad (14)$$

The parameters of formula (14) for Cl_2 with doppler broadening are presented in the table for a series of transitions. The parameters are presented there for the value of $a(\lambda, T)$ calculated using (13) for the case of high pressure, for $\lambda = \lambda_{v'v''}$, $T \gtrsim 800$ K.

In region B for Cl_2 the value of α^+ does not have such simple form (see formula (7)). The values of α^+ will be presented only for a few cases. In the absence of dilution at T = 450 K we find $\alpha^+ = 7 \cdot 10^{-41}\ cm^5 \times [Cl]^2$ for λ = 1060-1200 nm. At the same temperature [Cl]/[M] = 0.1 and $[Cl] = 10^{18}\ cm^{-3}$, impact broadening is felt in the value of α^+; therefore we shall present the upper and lower bounds of the interval of variation of α^+: $5 \cdot 10^{-40}\ cm^5 \times [Cl]^2 > \alpha^+ > 2 \cdot 10^{-41}\ cm^5 \times [Cl]^2$, the last value was found using the "broadened" cross section (13). For [Cl]/[M] = 0.01 and T = 450K, which corresponds to the boundary of the regions A and B, we shall present only the lower bound for α^+: $4 \cdot 10^{-40}\ cm^5 \times [Cl]^2$. It is obvious that in order to obtain the amplification coefficient 10^{-4} to $10^{-3}\ cm^{-1}$ it is necessary to create $[Cl] \approx 3 \cdot 10^{18}\ cm^{-3}$.

For the Br_2 molecule the $A^3\Pi_{1u}$ state has the type of bond close to case C. For the transitions $A^3\Pi_{1u} - X^1\Sigma^+_g$, the selection rules and the structure of the transitions are valid just as for $^1\Pi_{1u} - ^1\Sigma^+_g$ for the a-type bond [30]. The spectroscopic parameters are presented in [28]. The matrix element R^0_i for the A → X transition can be calculated by the splitting of the $^3\Pi$-multiplet and using the matrix element R' of the transition $^1\Pi_{1u} - ^1\Sigma^+_g$ [20] (see also the survey [31]). According to [32] for the

equilibrium position of the bromine nuclei in the A-state, R_e = 0.26 nm, $|R_i^0|^2$ = 0.17 $|R'|^2$. The values of $q_{v'v''}$ for the A-X system are presented in [33]. The calculation for the amplification cross sections at the transitions 0 → 18-20 gave: $\sigma_{i_2} = 1.3 \cdot 10^{-18}$ (1000 K/T)^2 cm^2, the broadened value of $\sigma^i_{0v''}$ is $2 \cdot 10^{-20}$ (1000 K/T)^2 cm^2. For the parameters for which the type A population is realized (see the figure), the values determining the amplification by formula (14) are presented in the table. The broadened value of $a(\lambda, T)$ is presented there also. In the region B for T = 400 K in the absence of a diluent, we find $\alpha^{(+)} = 5 \cdot 10^{-40}$ cm$^5 \times$ [Br]^2, λ = 1200-1300 nm. For dilution of [Br]/[M] = 0.1, let us present the bounds of the region of variation of $\alpha^{(+)}$: $3 \cdot 10^{-39}$ cm$^5 \times$ [Br]$^2 > \alpha^{(+)} > 5 \cdot 10^{-41}$ cm$^5 \times$ [Br]^2. For the dilution [Br]/[M] = 0.01 (the boundary of the regions A and B), we find the lower bound $\alpha^{(+)}$: $2.5 \cdot 10^{-40}$ cm$^5 \times$ [Br]^2. In order to obtain amplification in the range of 10^{-4} to 10^{-3} cm^{-1}, the following concentrations are necessary: [Br] = 10^{18} cm^{-3}.

The results of calculating $a(\lambda)$ for other recombination reactions of the group VII atoms are presented in the table for the case where the population of the bound states is in equilibrium with the dissociated states (region A).

Let us briefly repeat the basic conclusions obtained above. Using experimental data, the radiation channel of the recombination reactions, the role of various electron states, and the processes of vibrational relaxation are discussed. It is demonstrated that there are various types of populations of excited electron states. The regions of the parameters are estimated: density, temperature, dilution, for which one type of population or another is realized. Various methods of creating an inverse population in a reacting gas will correspond to various types of population. Thus, on initiation of the recombination reactions by a shock wave, during photolysis of a slightly diluted gas, case A must be realized. During photolysis of a highly diluted gas in the heating-cooling method case B will be realized, and so on. An estimate was presented of the conditions under which population inversion occurred. The light amplification cross sections were calculated for various electron transitions. The light amplification coefficient was calculated for the regions of parameters with different types of population. It is obvious that for concentrations of the recombining atoms $(1-5) \cdot 10^{18}$ cm^{-3} and temperatures not exceeding 600-800 K, for the halogen atom recombination reactions, light amplification on the order of 10^{-3} cm^{-1} can be realized in the near infrared range. The indicated conditions are realized in the heating-cooling method (see, for example, [1, 34]) and for excitation of radiation recombination during photolysis [35].

BIBLIOGRAPHY

1. A. S. Bashkin, V. I. Igoshin, A. N. Nikitin, A. N. Orayevskiy, KHIMICHESKIYE LAZERY (Chemical Lasers), Moscow, VINITI, 1975.

2. V. A. Kochelan, Yu. A. Kukibnyy, S. I. Pekar, KVANTOVAYA ELEKTRONIKA (Quantum Electronics), No 1, 1974, p 279.

3. B.Fonten, B. Forest'ye, KVANTOVAYA ELEKTRONIKA, No 3, 1976, p 897.

4. I. A. Izmaylov, V. A. Kochelap, Yu. A. Kukibnyy, UKR. FIZ. ZHURNAL (Ukrainian Physics Journal), No 21, 1976, p 508.

5. A. S. Bashkin, A. N. Orayevskiy, KVANTOVAYA ELEKTRONIKA, No 3, 1976, p 29.

6. B. A. Thrush, R. Golde, REP. PROGR. PHYS., No 36, 1973, p 1285.

7. M. A. A. Cline, D. H. Stedman, TRANS. FARADAY SOC., No 64, 1968, p 1816.

8. R. J. Browne, E. A. Ogryslo, J. CHEM. PHYS., No 52, 1970, p 5774.

9. M. A. A. Cline, J. A. Coxon, A. R. Woon-Fat, TRANS. FARADAY SOC., No 67, 1971, p 3155.

10. M. A. A. Cline, D. J. Smith, J. CHEM. SOC. FARAD. TR., part II, No 75, 1979, p 67.

11. M. A. A. Cline, J. A. Coxon, PROC. ROY. SOC. LONDON, No 298A, 1967, p 430.

12. B. Genri, M. Kasha, UFN (Progress in the Physical Sciences), No 108, 1972, p 113.

13. R. E. Huie, N. J. T. Long, CHEM. PHYS. LETTS, No 44, 1976, p 608.

14. M. A. A. Cline, J. S. McDermid, J. CHEM. SOC. FARAD. TR., part II, No 74, 1978, p 1935.

15. M. A. A. Cline, J. S. McDermid, J. CHEM. SOC. FARAD. TR., part II, No 75, 1979, p 1313.

16. V. E. Bondybey, C. Fletcher, J. CHEM. PHYS., No 61, 1975, p 3615.

17. G. Capelle, K. Sakurai, H. P. Broida, J. CHEM. PHYS., No 54, 1971, p 1728.

18. R. D. Gordon, K. K. Innes, J. CHEM. PHYS., No 71, 1979, p 2824.

19. V. E. Bondybey, S. S. Barder, C. Fletcher, J. CHEM. PHYS., No 64, 1976, p 5242.

20. V. E. Bondybey, L. E. Brus, J. CHEM. PHYS., No 64, 1976, p 3248.

21. R. S. Mulliken, PHYS. REV., No 36, 1930, p 1140; No 46, 1934, p 529; No 57, 1940, p 500.

22. R. C. Millikan, D. R. White, J. CHEM. PHYS., No 39, 1963, p 3209.

23. B. F. Myers, E. R. Bartle, J. CHEM. PHYS., No 48, 1968, p 3935.

24. Ye. Ye. Nikitin, GAZODINAMICHESKIYE LAZERY I LAZERNAYA FOTOKHIMIYA (Gas Dynamic Lasers and Laser Photochemistry), Moscow, MGU, 1978, p 126.

25. S. I. Pekar, V. A. Kochelan, DAN SSSR (Reports of the USSR Academy of Sciences), No 196, 1971, p 808.

26. V. L. Tal'roze, Ye. B. Gordon, Yu. L. Moskvin, A. P. Kharitonov, DAN SSSR, No 214, 1974, p 864.

27. M. A. A. Cline, J. A. Coxon, J. MOL. SPECTROSC., No 33, 1970, p 381.

28. TERMODINAMICHESKIYE SVOYSTVA INDIVIDUAL'NYKH VESHCHESTV (Thermodynamic Properties of Individual Substances), Edited by V. P. Glushko, Moscow, Izd-vo AN SSSR, Vol 1, 1962.

29. J. A. Coxon, J. QUANTUM SPECTROSC. RAD. TRANSFER, No 11, 1971, p 443.

30. J. A. Coxon, J. MOL. SPECTR. No 33, 1971, p 443.

31. J. A. Coxon, MOL. SPECTR., No 1, 1973, p 177.

32. R. J. LeRoy, R. G. MacDonald, G. Burns, J. CHEM. PHYS., No 65, 1976, p 1485.

33. J. A. Coxon, J. MOL. SPECTROSC. No 41, 1972, p 566.

34. V. A. Kochelap, Yu. A. Kukibnyy, KVANTOVAYA ELEKTRONIKA, No 2, 1975, p 1471.

35. I. A. Izmaylov, V. A. Kochelap, KVANTOVAYA ELEKTRONIKA, No 6, 1979, p 2349.

Report received 4 April 1980

10845
CSO: 1862

UDC 621.373.826.038.826

EFFECT OF GAS DENSITY DISTURBANCES ON THE LIMITING CHARACTERISTICS OF REPETITIVELY PULSED ULTRAVIOLET PREIONIZATION LASERS

Moscow KVANTOVAYA ELEKTRONIKA in Russian Vol 7, No 12, Dec 80 received 20 May 80 pp 2589-2593

[Article by V. Yu. Baranov, D. D. Malyuta, V. S. Mezhevov, A. P. Napartovich, Nuclear Power Institute imeni I. V. Kurchatov, Moscow]

[Text] Experimental results are presented from a study of the effect of small (~1%) gas density disturbances on the average power of a repetitively pulsed laser with the application of an electrode system with ultraviolet preionization.

1. Introduction

When building efficient periodically pulsed lasers (PPL) researchers have encountered the phenomenon of decreasing maximum energy contribution in an individual current pulse with an increase in the pulse repetition frequency f. The energy contribution in the discharge decreases noticeably for frequencies appreciably less than the gas exchange frequency in the interelectrode gap $f_0=v/b_0$ (v is the gas flow velocity in the interelectrode region; b_0 is the electrode width). The restriction of the energy contribution per pulse is connected with pinching of the discharge. The basic known causes of pinching for $f<f_0$ reduce to the appearance of density nonuniformities of the gas or the composition of the gas environment in the discharge zone. The behavior of the gas density disturbances has been investigated in a number of papers (heating of the gas by shock waves [1], the development of a temperature boundary layer [2], resonance sound waves [3], expansion of the heated portion of the gas [4]). However, the quantitative criteria of the influence of the enumerated effects on the maximum energy contribution are in practice absent.

In this paper results are presented from direct measurements of the sensitivity of the electrode system with ultraviolet preionization to gas density disturbances in the discharge zone, and a number of causes leading to the appearance of such density nonuniformities are analyzed.

2. Experimental Results

The experiments were performed on the "Dyatel" unit [5]. An electrode system with ultraviolet illumination and discharge region size 2.5×5×60 cm was used.

The capacitance of the working capacitor was 0.2 microfarads, and the experiments were performed with a mixture of CO_2:N_2:He=1:2:5 at a pressure of 0.5-0.6 absolute atmospheres and a flow velocity in the electrode gap of ~30 m/sec.

The volumetric density disturbances were created using a heated coil 10 cm long installed at a distance of 7 cm upstream from the electrodes. A thermocouple was used to measure the spatial temperature distribution created by the heated element in the electrode gap in the gas flow as a function of the power fed to the element. Then the thermocouple was removed from the discharge gap and the maximum power contributed to the discharge per pulse $\mathcal{E}_0$, as a function of the temperature of the disturbed section averaged over the electrode gap was recorded under conditions with low pulse repetition frequency ($f \leq 10$ hertz). This relation is presented in Figure 1.

In addition, a study was made of the effect of the gas density disturbances caused by heating of the electrodes on the maximum energy contribution per pulse. Usually during operation of the PPL, the electrodes are heated up and begin to heat the gas. The thickness of the heated layer of gas at the upstream edge of the electrode is 0, and at the downstream edge $\delta_T \approx 0.59\ Pr^{1/2}\delta \approx 0.1$ cm (δ is the thickness of the velocity boundary layer, Pr is the Prandtl number). The gas temperature averaged over the electrode gap at the input to the discharge and at the output from it can differ by an amount on the order of 1% which, as Figure 1 shows, has a significant influence on the maximum energy contribution. In the experiment, the electrode temperature was varied by using an external heating element. The relation obtained for the maximum energy contribution is presented in Figure 2. Comparing Figures 1 and 2, it is possible to see that the decrease in the energy contribution in both cases is determined by the average temperature or density disturbance of the gas with respect to the electrode gap. In the general case it is necessary to sum the gas density disturbances caused both by the volumetric effects and by heating (or cooling) of the gas from the surface. It was found experimentally on the "Dyatel" unit that the electrode temperature depends on the average discharge power $\mathcal{E}f$ by the law $\Delta T(K) = \mathcal{E}f/2\mathcal{E}_0$, where $\mathcal{E}$ is the energy contributed per discharge in one pulse.

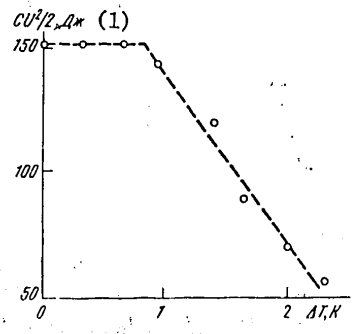

Figure 1. Maximum energy contributed to discharge as a function of the average temperature of the disturbed section over the electrode gap

Key: 1. joules

In accordance with the detected influence of the electrode temperature on the maximum energy contribution per pulse, the maximum average power of the laser as a function of f turns out to be different when working for short periods of time (on the order of seconds) and long periods (the solid curves 1 and 2 in Figure 3). When the electrodes are heated for long times (curve 2), the PPL power drops.

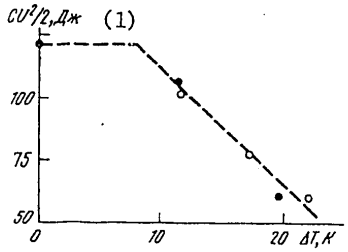

Figure 2. Maximum energy contributed to the discharge as a function of the electrode temperature with discharge heating of the electrode (circles on the graph) and with an external heating element (solid dots)

Key:
1. joules

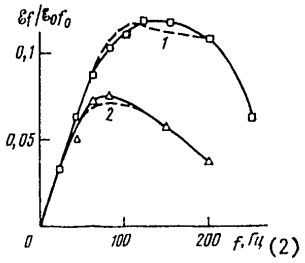

Figure 3. Output power of the laser as a function of the pulse repetition frequency, gas mixture replacement rates in the loop 100 ℓ/min:
1 -- measurement time for the entire characteristic ~1 minute;
2 -- measurement time for each point ~10 minutes

Key:
1. hertz

3. Discussion of the Results

The experimentally determined sensitivity of the discharge with ultraviolet illumination and continuous electrodes permits estimation of the effect of an entire series of factors on the discharge stability and, consequently, average

power of the PPL. As is obvious from Figure 1, the maximum energy contribution in practice does not change on heating to $\Delta T \lesssim 0.7$ K. This means that the temperature fluctuations of this level already exist and can be caused, in particular, by incomplete thermalization of the gas flow (by the difference in wall temperature of the channel or the electrodes as a function of the gas temperature). A sharp decrease in the energy contribution with a further increase in Δt can be explained, assuming that the maximum contribution in the discharge is connected with the achievement of local energy contribution of critical magnitude. In the isolated pinch with dimensions much greater than diffusion and much less than the electrode dimensions, the gas density fluctuation $\delta\rho<0$ leads to a sharp relative increase in the local energy contribution as a result of the high ionization amplification in the discharge and its sensitivity to the parameter E/N (N is the density of the number of gas particles). The requirement of limiting the local energy contribution leads to a decrease in the specific energy contribution in the rest of the discharge and, consequently, to a decrease in the total energy contribution:

$$\frac{\delta\mathcal{E}}{\mathcal{E}_0} \approx \frac{\delta\rho}{\rho} \frac{d \ln \nu_i}{d \ln E} \ln \frac{n_m}{n_0} \qquad (1)$$

(ν_i is the ionization frequency of the gas; E is the electric field intensity; n_m is the plasma density at maximum current; n_0 is the photoplasma density; ρ is the gas density; $\Delta\rho/\rho \sim -\Delta T/T$). Since $d\ln\nu_i/d\ln E \sim 10$-15, $\ln(n_m/n_0) \sim 10$-15, the density fluctuations $\Delta\rho/\rho \sim 10^{-2}$ must lead to a reduction in the maximum energy contribution $\delta\mathcal{E}/\mathcal{E} \sim 1$. The coefficient defined by the slope of the experimental function $\mathcal{E} = f(\Delta T)$ for $\Delta\rho/\rho$ in formula (1) turned out to be equal to 10^2, which agrees well with the presented estimates. The value of $\mathcal{E}$ as a function of the electrode temperature agrees with this same estimate.
The heating of the gas by shock waves [1], estimation of which shows that this effect has no significant influence on the operation of the PPL, leads to a gas density and temperature gradient in the discharge zone. The development of the thermal boundary layer in the incomplete thermalization load or as a result of heating of the electrode can lead to a reduction in power (which was observed experimentally) if the gas and wall temperature difference exceeds 10 K. Even in an isothermal flow there are gas density fluctuations connected with the flow velocity pulsations $\Delta T/T \sim M^2 \Delta v/v$ (here M is the Mach number of the flow; $\Delta v/v$ is the relative velocity pulsation). If $\Delta v/v \sim 0.1$, these fluctuations can influence the laser power at $M \gtrsim 0.2$. Under our experimental conditions the role of these density fluctuations is also small.

As was demonstrated in [3, 6], during the operation of PPL in the gas dynamic channel, an entire set of acoustic waves occurs. The Q-factor of the acoustic resonator formed by the channel walls in our case is small for sound propagated across the flow. The time for establishment of the acoustic vibrations for the waves moving along the flow is comparable to the pulse repetition period; therefore the superheating-acoustic instability observed in [6] was absent in our case. The characteristic frequency of the strongest sound vibrations in the channel during operation of the laser (ω) and their damping rate (decrement γ) were measured experimentally by oscillograms with the signals from a piezopickup in the channel near the discharge zone (Figure 4). This made it possible to relate the gas density gradient along the flow on the electrode width to the energy contribution per pulse and the pulse repetition period f:

$$\frac{\Delta\rho}{\rho} \approx \frac{2b_0\omega}{\pi c_s \varkappa}\left(\frac{\Delta p}{p}\right)_0 \frac{\mathcal{E}}{\mathcal{E}_0} e^{-\nu/f}, \qquad (2)$$

where c_s is the speed of sound; $\varkappa$ is the adiabatic exponent; $(\Delta p/p)_0$ is the initial oscillation amplitude of the pressure for $\mathcal{E}=\mathcal{E}_0$. Since calculation of $(\Delta p/p)_0$ by the known energy contribution is complicated as a result of complexity of the spectrum of excited oscillations and the complexity of the acoustic resonator, $(\Delta p/p)_0$ was estimated by oscillograms of the signals from the piezopickup (Figure 4). Assuming that the lasing efficiency in an individual pulse depends slightly on the energy contribution, it is possible by using (2) and the experimental function in Figure 1 to recalculate the decrease in the power of the laser pulse emission with an increase in f and to construct the dimensionless average power of the PPL $\mathcal{E}f/\mathcal{E}_0 f_0$ as a function of f. The relation obtained in this way for $(\Delta p/p)_0=0.15$ is shown in Figure 3 (the dotted curve 1). As is obvious from Figure 3, quite good agreement is observed between the calculation and the experimental data.

Figure 4. Oscillogram of acoustic vibrations in a gas dynamic channel near (~20 cm) the discharge zone

The effect of the electrode heating and the gas density gradient connected with this under the same assumptions as above, can also be calculated using the experimental functions $\mathcal{E}(\Delta T_{el})$ (see Figure 2 and ΔT_{el} ($\mathcal{E}$, f). Here it is natural to assume that the gas density pulsations in the sound wave and as a result of heating of the electrodes are additive. Accordingly, it is possible to obtain the dimensionless average power $\mathcal{E}f/\mathcal{E}_0 f_0$ shown in Figure 3 (curve 2).

4. Conclusions

Thus, the experimentally obtained relations for the maximum energy contribution as a function of the gas density gradients in the discharge zone (Figures 1 and 2) make it possible to calculate the average power of the PPL as a function of frequency, agreeing reasonably with the experimental data. The experimentally measured sensitivity of the discharge system with ultraviolet illumination and continuous electrodes indicates the necessity for sustaining uniformity of the temperature field in the flow with high accuracy (the difference in the gas and wall temperatures must not exceed $\pm$5-10 K) and elimination of the acoustic oscillations in the channel. In particular, the results obtained explain the lack of success in creating such a discharge system in a supersonic flow attempted by the authors when writing reference [7]. It must be noted that the critical nature of the discharge with respect to the gas density pulsations decreases sharply on sectioning the electrodes as a result of negative feedback through the ballast resistances. The conversion to independent discharge also eliminates the criticalness of the discharge with respect to the gas density gradients and permits achievement close to the maximum pulse recurrence rate [8].

In conclusion the authors express their appreciation to A. I. Starodubtsev and M. Yu. Orlov for their assistance in performing the experiments.

BIBLIOGRAPHY

1. Baranov, V. Yu.; Breyev, V. V., et al. KVANTOVAYA ELEKTRONIKA [Quantum Electronics], No 4, 1977, p 1861.

2. Baranov, V. Yu., et al. TVT, No 15, 1977, p 872.

3. Baranov, V. Yu.; Lyubimov, B. Ya.; Niz'yev, V. G.; Pigul'skiy, S. V. KVANTOVAYA ELEKTRONIKA, No 6, 1979, p 184.

4. Dzakowic, G.; Witzke, S. J. APPL. PHYS., No 44, 1973, p 5061.

5. Baranov, V. Yu.; Velikhov, Ye. P.; Kazakov, S. A., et al. KVANTOVAYA ELEKTRONIKA, No 6, 1979, p 811.

6. Baranov, V. Yu.; Malyuta, D. D.; Mezhevov, V. S.; Napartovich, A. P. FIZIKA PLAZMY [Plasma Physics], No 6, 1980, p 785.

7. Baranov, V. Yu.; Malyuta, D. D.; Mezhevov, V. S.; Napartovich, A. P. KVANTOVAYA ELEKTRONIKA, No 3, 1976, p 149.

8. Golubev, S. A.; Kovalev, A. S., et al. DAN SSSR [Reports of the USSR Academy of Sciences], No 225, 1975, p 1300.

10845
CSO: 1862

UDC 621.373.826-038.823

STUDY OF THE QUASI-STEADY INTERACTION OF CO_2-LASER RADIATION WITH A GRAPHITE TARGET IN THE AIR

Moscow KVANTOVAYA ELEKTRONIKA in Russian Vol 7, No 12, Dec 80 received 6 Jun 80 pp 2594-2598

[Article by A. V. Bondarenko, Ye. V. Dan'shchikov, V. A. Dymshakov, F. V. Lebedev, A. V. Ryazanov, Nuclear Power Institute imeni I. V. Kurchatov, Moscow]

[Text] The spectroscopic, interferometric and photometric methods of diagnosis were used to study a quasi-steady laser flame initiated by the emission of a CO_2-laser with power density of 0.1-2 Mwatts/cm^2 in graphite in the air. It is demonstrated that the flame is a carbon vapor jet transparent to the laser radiation and propagated in the air in the vicinity of the target without noticeable heating of it by the laser radiation. The problems of gas dynamics and thermophysics of the flame, which are of interest for the problems of laser processing of materials and the creation of a laser jet engine are discussed.

On irradiation of the surface of an absorbing condensed medium by laser radiation of sufficiently high intensity, a laser flame is formed -- a jet of evaporated material escaping into the surrounding gas. The study of the properties of the laser flame is required to describe the processes of interaction of the laser radiation with the material in many areas of laser application, both developing and just proposed. The problem of the effectiveness of the interaction of the laser emission with the laser flame formed is one of the basic problems, for example, when creating a laser jet engine and for laser working of materials. This interaction is determined by the parameters of the laser flame plasma and can lead to significant heating and the occurrence of various types of laser emission absorption waves. The occurrence and the propagation of such "laser combustion waves" or "light-detonation waves" introduces qualitatively new effects into the process of laser energy transmission to the radiated surface [1], and it has great significance for the laser working of material. The absorption of the laser emission in the flame is important also for the laser jet engine, for as a result of the occurrence of heating of the laser flame here, it is possible to realize the possibilities of the laser jet engine which, as is assumed, offer advantages over traditional propulsion systems [2].

The number of experimental studies of the interaction of radiation with the laser flame and quantitative measurements of the laser flame plasma parameters is highly limited. Let us briefly discuss the ones of them in which, just as in our paper, the effect of the laser emission of medium power density on graphite was studied. In reference [3] it was discovered that the carbon vapor jet remains transparent and is not heated by the Nd-laser emission initiating it with an intensity S to 3 Mwatts/cm^2. On irradiation of graphite by the pulsed radiation of a CO_2-laser, S~1-5 Mwatts/cm^2, the occurrence of optical breakdown absorbing the laser emission was observed [4] in the time $\tau \lesssim 10^{-6}$ from hot ($T \gtrsim 1$ ev) plasma. In [4], noticeable heating of the laser flame in the graphite by the radiation of the CO_2-laser was not observed until S~10-50 Mwatts/cm^2. The contradictoriness of these results obviously is connected with indeterminacy of the experimental conditions. The optical breakdown in [4] could be initiated by the initial power peak which is typical of electrical ionization CO_2-lasers and later is only supported by the emission with S~1-5 Megawatts/cm^2. The values of S presented in [5] appear to be high inasmuch as they are based on a rough estimate of the lower bound of the diameter of the focal point. It is necessary to note that the indeterminacy of the experimental conditions connected with variation of the radiation power with time and not knowing the power density distribution at the target, is characteristic of many experiments performed with pulsed lasers. This complicates the interpretation of the obtained results.

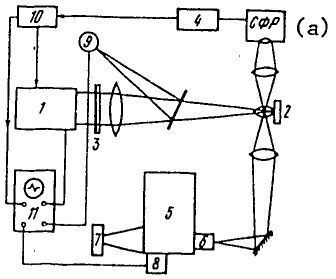

Figure 1. Experimental setup:
1 -- laser; 2 -- target; 3 -- attenuator; 4 -- high-speed photographic recorder panel; 5 -- monochromator; 6 -- light guide; 7 -- camera; 8 -- photoelectric attachment; 9 -- radiation receiver; 10 -- synchronization unit; 11 -- oscillograph

Key:
a. SFR high-speed photographic recorder

In this paper the results are presented from studies of the quasi-steady effect of a CO_2-laser on a graphite target in the air. The electric discharge CO_2-laser gave a square emission pulse with duration $\tau_0 \sim 1$ millisecond with known power density distribution in the focusing plane. The quasi-steady-state nature of the processes taking place made it possible to perform simple and, at the same time, reliable spectroscopic measurements of the laser flame plasma parameters with spatial resolution. The interest in graphite used in the given paper as the irradiated target arises from the fact that it appears to be one of the prospective

working media for a laser jet engine [2], and the coatings based on it can be used for laser working of materials to increase the absorption of the infrared radiation by metals.

Experimental Setup

The experimental setup is presented in Figure 1. The distribution S(r) in the focusing plane was recorded by evaporation of a thin teflon film. The effective radius of the focusing spot $r_0=(2\int S(r)rdr/S_0)^{1/2}$ (S_0 is the power density at the center of the spot) turned out to be 0.25 and 0.45 mm for the two lenses used in the experiments with focal lengths of 40 and 150 cm, respectively. The value of S_0 was varied in the experiment by using attenuators from 0.1 to 0.6 Mwatts/cm^2 for a long focal length lens and to 2 Mwatts/cm^2 for a short focal length lens.

Selected molecular bands and segments of the continuum in the spectrum of the laser flame were photoelectrically recorded, and the time-integrated spectrum was photographed in the wavelength range of 410-430 nm where one of the band systems of the CN molecule is located. The laser flame temperature was measured by the relative intensity of five bands of the system with unresolved rotational structure [6]. The detailed description of the procedure and substantiation of its applicability under the conditions of our experiment are discussed in a separate article.[1]

The target surface temperature was measured by the intensity of the surface emission in the isolated spectral interval [7]. The dynamics of the integral luminosity of the laser flame was investigated using a high-speed recorder (SFR). Interferometric studies of the gas region were made near the irradiated section of the target. The interferometric and photometric diagnostic diagrams are not shown in Figure 1. They are described in references [7, 8].

Experimental Results

According to the high-speed photographic recording data, the laser flame occurs on the target surface after the delay time τ_* following the beginning of the radiation of the target which quickly decreases with an increase in S0, and for $S_0>0.3$ Mwatts/cm^2 it becomes much less than the pulse duration τ_0 (Figure 2). The time of appearance of the laser flame luminescence is connected with the target temperature. The laser flame occurs when the temperature $T_*\approx 4000\pm 200$ K is reached at the center of the spot.

After the occurrence of the laser flame, it is propagated normally from the target surface independently of its orientation with respect to the incident radiation (see Figure 3). The propagation rate of the laser flame v decreases slowly on going away from the target. At distances from the target of $x\geq 10r_0$, the velocity v in practice does not depend on r_0 and is determined by the power of the incident radiation, increasing from 10 to 100 m/sec with an increase in the radiation power of the laser from 0.5 to 3 kilowatts.

---

[1]Sent to the Journal of Applied Spectroscopy.

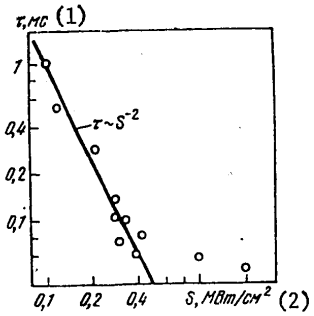

Figure 2. Delay time for the occurrence of the laser flame as a function of the power density of the incident radiation
Key:
1. milliseconds
2. Megawatt/cm^2

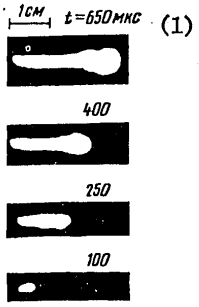

Figure 3. High-speed photographic recording frames for the process of laser flame propagation (S_0≈0.3 Mwatt/cm^2, r_0≈0.5 mm)
Key:
1. t=650 microseconds

The radiation intensity of the molecular bands and the continuum from the selected cross section of the laser flame reached a constant level soon after the appearance of glow in this cross section and then it varied only slightly. The temperature of the laser flame was determined by the radial intensity distributions I(r) of the CN bands, and it varied slightly within the boundaries of the glow region of radius r_1(I(r_1)~(1/3I(0)). For example, for x≈5 mm, S_0≈0.2 Mwatt/cm^2, r_0≈0.45 mm, r_1≈0.6 mm, and T(r_1)-T(0)≈300 K.

The average temperature distributions in the glow region $\overline{T}$ with respect to length of the laser flame are presented in Figure 4 where $\overline{T}$ does not depend on the target orientation with respect to the direction of the incidence of the radiation, and in each cross section it increases slightly with an increase in S_0. The transverse dimensions of the zone occupied by the heated air and the products of destruction of the target obtained from the interferograms is close to the length of the laser flame and greatly exceeds the size of the glow region r_1.

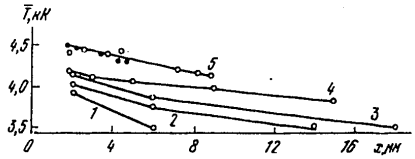

Figure 4. Flame temperature as a function of the distance to the target for r_0=0.45 (1-4) and 0.25 (5), S_0≈0.1 (1), 0.2 (2), 0.4 (3), 0.6 (4) and 2 Mwatt/cm^2 (5) for normal (the circles) and oblique (the dots) incidence of the radiation on the target

Discussion of the Experimental Results

The presented experimental data indicate that the investigated laser flame is a jet of carbon vapor escaping into the atmosphere and cooled on expansion and mixing with the air. The jet escape of the vapor occurs with an increase in saturated vapor pressure of the target material p_s to the external pressure. In our experiments, this occurs at a target surface temperature T_* coinciding with the boiling point of graphite T_k=4100 [3]-4200 K [9]. The recorded delay time for the formation of the laser flame τ_* is determined by the time required to reach T_k. Since the surface temperature $T_\pi(t) \sim S_0\sqrt{t}$ [10], then $\tau_* \sim S_0^{-2}$. This agrees well with the experimental data until τ_* becomes comparable with the time of establishment of the laser radiation power of $\tau_1 \approx$50-100 microseconds (see Figure 2).

The jet temperature at the target surface is close to T_π. The basic proportion of the radiation energy absorbed by the target is used for evaporation. Using the function presented in [3] $P_s(T_\pi)$, it is possible to show that with an increase in S_0 from 0.1 to 1-2 Mwatts/cm^2 T_π must increase from T_k to T$\approx$4400-4600 K. This corresponds to the increase in the measured temperature of the laser flame and target surface (see Figure 4).

On going away from the target, the vapor is mixed with the surrounding gas, it heats the gas and forces the gas out of the region of propagation of the jet. Thus, the jet is propagated inside the relatively large region of heating gas. This also agrees with the data from the interferometric studies and with the experimentally obtained small temperature gradients both along and across the laser flame.

The experimentally measured velocity v is appreciably less than the escape of the vapor u which can be estimated, neglecting the thermal conductivity removal of energy to the target, as $u \sim S_0 (1-R)/n_0\varepsilon_0$, where R is the reflection coefficient of the laser radiation from the target; n_0 is the vapor pressure close to atmospheric for a subsonic jet; ε_0 is the energy of evaporation. For example, for $S_0 \sim 1$ Mwatt/cm^2 the escape velocity $u \sim 10^3$ m/sec turns out to be close to the speed of sound, whereas v does not exceed 100 m/sec. This is explained by the fact that the propagation rate of the leading edge of the glow of the laser flame is determined by the heating rate of the cold gas forced out of a zone significantly greater than the glow region of the laser flame.

The energy release Q_+ occurring in each laser flame cross section as a result of the inflow of a hotter gas from the target and heat release in the direction of Q_- can be estimated using the data of [11] on the flow dynamics of the turbulent jet and the measured values of the temperature gradients with respect to length and radius of the laser flame. Inasmuch as $Q_-/Q_+ \sim \alpha|\nabla_r T|/|\nabla_x T|$, where $\alpha = dr_c/dx \sim 0.2$ [11] (r_c is the jet radius), using the experimental values of $|\nabla_x T|$ and $|\nabla_r T|$, we obtain $Q_+ \sim Q_-$. For example, for $S_0 \approx 0.3$ Mwatt/cm^2 and at a distance of $x \approx 5$ mm from the target $|\nabla_x T| \approx 700$ K/cm, $|\nabla_r T| \approx$3-5 kK/cm and $Q_+ \sim Q_- \sim c_p n_0 u(x)|\nabla_x T| \sim$1-2 kwatts/cm^3. Thus, the energy balance of the investigated laser flame is possible without calling on any other volumetric sources of energy release.

From the experimental data (see Figure 4) it follows that with an accuracy to the measurement errors ($\delta T \simeq 150$ K) the temperature of the laser flame does not depend on whether the jet escapes in the laser beam or outside it. This permits estimation of the upper bound of the absorption coefficient K of the CO_2-laser radiation by the laser flame plasma. For maximum experimental values of $S_0 \simeq 2$ Mwatts/cm^2 and $T \simeq 4500$ K we obtain $KS_0(1+R) < 1$ kilowatts/cm^3 and $K < 3 \cdot 10^{-4}$ cm^{-1}.

Thus, the investigated laser flame is transparent for the CO_2-laser radiation. As applied to the laser working of materials this means that in the case of steady irradiation with power densities of at least 2 Mwatts/cm^2 it is possible to realize the evaporation conditions of interaction with the graphite without shielding the target by the laser flame plasma.

For effective operation of a laser jet engine, heating of the escaping vapor jet by the laser radiation is required. For realization of a graphite laser jet engine with irradiation by a CO_2-laser either higher power densities of the steady irradiation ($S \geq 3$ Mwatts/cm^2) or initiation of the laser combustion wave by short-term irradiation with higher power density ($S \sim 10$-100 Mwatts/^{2} and further maintenance of it in a weak ($S \leq 1$ Mwatt/cm^2) steady beam is necessary. It is possible that the required heating of the escaping vapor in full scale laser jet engines can be insured by increasing the region of one-dimensional discharge.

Summing up the results of this work, it is possible to say that under the quasi-steady effect of CO_2-laser emission with power densities of $S \sim 0.1$-2 Mwatts/cm^2 on the surface of the graphite target in the air, optical breakdown is not observed for dimensions of irradiated zone to ~1 mm. When the boiling point of the graphite T_k is reached on the surface of the target, developed evaporation conditions are realized. The laser flame that arises is a jet of carbon vapor escaping into the atmosphere and cooled on expansion and mixing with the surrounding gas. The vapor jet is not heated by the laser radiation and has no effect on its transmission to the target surface. The results obtained are of interest when studying the prospects for using laser working of materials and the creation of laser jet engines and also when solving other problems connected with the interaction of laser radiation with matter.

BIBLIOGRAPHY

1. Pirri, A. N.; Root, R. G.; Wu, P. K. S. AIAA PAPER No 77-658 (AIAA 10th FLUID AND PLASMADYNAMICS CONF. ALBUQUERQUE, USA, 1977).

2. Bunkin, F. V.; Prokhorov, A. M. UFN [Progress in Physical Sciences], No 119, 1976, p 425.

3. Covington, M. A.; Liu, G. N.; Lincoln, K. A. AIAA PAPER No 76-22 (AIAA 14th AEROSPACE SCIENCES MEETING, Washington, USA, 1976).

4. Bakeyev, A. A.; Vasil'yev, L. A.; Nikolashina, L. I.; Prokopenko, N. V.; Churilov, A. S.; Yakovlev, V. I. KVANTOVAYA ELEKTRONIKA [Quantum Electronics], No 2, 1975, p 1278.

5. Pirri, A. N.; Monsler, M. J.; Nebolsine, P. E. AIAA J., No 12, 1974, p 1254. Translation: RAKETNAYA TEKHNIKA I KOSMONAVTIKA [Rocket Engineering and Cosmonautics], Vol 12, No 9, 1974, p 112.

6. Kitayeva, V. F.; Alyamovskiy, V. N. OPTICHESKAYA PIROMETRIYA PLAZMY [Optical Plasma Pyrometry], edited by Prof N. N. Sobolev, Moscow, IL, 1960, p 328.

7. Bondarenko, A. V.; Golubev, V. S.; Dan'shchikov, Ye. V.; Lebedev, F. V.; Nastoyashchiy, A. F.; Ryazanov, A. V. PIS'MA V ZHTF [Letters to the Technical Physics Journal], No 5, 1979, p 221.

8. Bondarenko, A. V.; Voronina, V. P.; Gorodnicheva, I. I.; Dan'shchikov, Ye. V.; Zakharchenko, A. I.; Lebedev, F. V.; Ryazanov, A. V.; Smakotin, M. M. KVANTOVAYA ELEKTRONIKA, No 7, 1980, p 420.

9. SVOYSTVA ELEMENTOV, Ch. 1., FIZICHESKIYE SVOYSTVA [Properties of Elements. Part 1. Physical Properties], Moscow, Metallurgiya, 1976.

10. Rady, J. DEYSTVIYE MOSHCHNOGO LAZERNOGO IZLUCHENIYA [Effect of Powerful Laser Radiation], Moscow, Mir, 1974.

11. Abramovich, G. N. PRIKLADNAYA GAZOVAYA DINAMIKA [Applied Gas Dynamics], Ch. VII, "Turbulent Jets," Moscow, Nauka, 1969.

10845
CSO: 1862

UDC 621.373.826.038.823

EXPERIMENTAL STUDY OF INTERNAL LOSSES IN IODINE LASERS PUMPED BY OPEN HIGH-CURRENT DISCHARGE ULTRAVIOLET RADIATION

Moscow KVANTOVAYA ELEKTRONIKA in Russian Vol 7, No 12, Dec 80 received 9 Jul 80 pp 2604-2613

[Article by V. S. Zuyev, K. S. Korol'kov, O. Yu. Nosach, Ye. P. Orlov, Physics Institute imeni P. N. Lebedev, USSR Academy of Sciences, Moscow]

[Text] An experimental study was made of the internal losses in iodine photodissociation lasers. It was demonstrated that the predominant role is played by refraction losses: in the investigated laser the refraction loss factor is $(2-6).10^{-4}$ cm^{-1}, and the loss factor arising from the volumetric absorption of the laser radiation in the active region does not exceed 10^{-4} cm^{-1}. The possibilities of decreasing the internal losses in iodine lasers are discussed.

1. Introduction

The simplicity of controlling the parameters of the active medium of an iodine photodissociation laser and powerful sources of ultraviolet radiation (for example, open high-current discharge) used for pumping permits the energy of the lasers to be increased by increasing the volume of the active medium. In reference [1] a laser is described with a discharge length of 140 cm and light diameter of 34 cm with energy in the free lasing pulse of 1.7 kilojoules. A further increase in the laser diameter leads to an inefficient increase in cost of the optical system and also to the necessity for suppressing the spurious emission in the transverse direction. At the same time the radiation intensity of the output of the existing lasers is 1-2 orders less than the radiation strength of glass; therefore a further increase in power should be realized by increasing the length of the laser. The internal loss factor estimated in [2] at $(1.5-2)\times10^{-3}$ cm^{-1} limits the laser length to a few meters. However, up to now there are no direct experimental data indicating the presence of particles in the active medium of an iodine laser the absorption or scattering on which can cause the losses on the indicated level. At the same time theoretical [3] and experimental [4] studies of the process of formation of the angular radiation spectrum of iodine lasers have led to the concept of a refraction mechanism of the internal losses in these lasers [5]. Estimation of the refraction loss factor gave approximately 10^{-3} cm^{-1} [5]; therefore it was proposed that the refraction losses themselves are the basic form of losses in the investigated lasers.

The purpose of our work is experimental study of the nature of the internal losses in iodine photodissociation lasers (PDL) and also measurement of both the refraction losses and the losses caused by volumetric absorption of the laser radiation in the active region.

2. Mechanism of Refraction Losses and Statement of the Experiment

The PDL are pumped by the ultraviolet radiation of a powerful electric discharge which is initiated directly in the working gas medium along the axis of the cylindrical discharge chamber using electric explosion of tungsten wires [6]. The discharge channel is a plasma column of right cylindrical shape which expands at a rate of 1-2 km/sec and generates a shock wave. The discharge ultraviolet radiation passes through the interlayer of shock-compressed gas and goes to the active region of the laser -- a layer several centimeters thick in the form of a hollow cylinder. The internal boundary of the active region and the lasing coincide with the shock wave front. The transverse cross section of the laser is represented schematically in Figure 1.

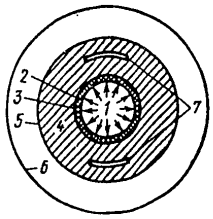

Figure 1. Diagram of the transverse cross section of an iodine laser: 1 -- discharge channel; 2 -- interlayer of shock-compressed gas; 3 -- shock wave front; 4 -- lasing zone; 5 -- outer boundary lasing zone; 6 -- chamber walls: 7 -- regions projected on the curvilinear diaphragms

As a result of absorption of the pumping radiation and the secondary photochemical reactions in the region ahead of the shock wave, an increment in the refraction coefficient Δn arises. This increment is nonuniform in the radial direction: it reaches the maximum ($\sim 10^{-6}$) near the shock wave front and decreases on going away from the shock wave by a law close to exponential with the characteristic constant $\gamma_n \sim 1\text{-}2$ cm^{-1}; γ_n^{-1} will be called the transverse size of the optical nonuniformity. This distribution of the refraction coefficient in the lasing zone leads to discrimination of the types of oscillations with respect to the transverse index [3, 4]. Lasing takes place on several higher modes of the medium with nonuniform distribution of the index of refraction. The wave front of the laser emission was well formed; the local value of the dispersion of the directions of the wave vectors $\Delta u \leq 5 \cdot 10^{-5}$ radians [4]. Here the angle u between the laser axis and the normal to the wave front, considering the fact that the discharge does not completely fill the resonator with respect to length, is related to Δn by the expression [3, 7]

$$u = \sqrt{2\Delta n l / L}, \qquad (1)$$

where l is the length of the active region; L is the length of the resonator.

Since as a result of axial symmetry Δn and u depend only on the radius r, the wave front of the laser radiation turns out to be bent in the form of a funnel which has been recorded experimentally in [4]. The maximum value of u(r) is reached on the inside boundary of the lasing zone where $r=r_н$ is the radius of the shock wave front. A typical value of $u(r_н)$ for the investigated laser is 1-3 milliradians. The shape of the wave front is neither planar nor spherical and $2u(r_н)$ is recorded as the divergence of the laser beam during measurements of it with respect to the spot diameter at the focal point of the lens.

The funnel-shaped wave front of the stimulated emission leads to the fact that part of the radiation is incident on the inside boundary of the lasing zone This radiation is partially absorbed in the interlayer of shock-compressed gas, it is partially scattered at a greater angle than $u(r_н)$, not participating any further in the lasing process. By the estimates of [3, 4, 8] in practice all of the radiation incident on the internal boundary of the lasing zone is lost. Thus, there is an uncompensated radiation flux to the internal boundary of the lasing zone which leads to internal resonator losses which are called refraction losses in [5]. An analysis of the mechanism of refraction losses in [5] made it possible to develop a procedure for measuring them simultaneously with measuring the losses caused by the volumetric absorption of the radiation in the active region and determination of the relative contribution of these types of losses. In accordance with [5], the refraction loss factor is defined by the expression

$$\Gamma=2\pi r_н I_{л}^{(1)}(r_н)\, u^{(2)}(r_н)/W_л, \qquad (2)$$

Key: 1. laser; 2. pumping

where $I_{laser}(r_{pumping})$ is the radiation intensity at the laser output near the inside boundary of the lasing zone; W_{laser} is the radiation power at the laser output. Thus, for experimental determination of Γ it is necessary to measure the laser radiation power, its intensity near the inside boundary of the generation zone, the radius of shock wave front $r_н$ and $\Delta n(r_н)$, by the use of which according to formula (1) it is possible to calculate $u(r_н)$.

In order to determine the intra-cavity losses caused by volumetric absorption in the active region, experiments were run for each pressure of the working medium with different exit mirrors (R=93 and 65%). The remaining parameters in each pair of experiments were kept constant. The instantaneous values of the loss factors were measured for times close to the time the maximum lasing power was reached when the pumping and the lasing power could be considered steady-state. For calculation of the volumetric losses the equation for the power budget inside the resonator was used:

$$W_{н}^{(1)}=W_{в}^{(2)}+W_{п}^{(3)} \qquad (3)$$

Key: 1. pumping; 2. output; 3. losses

where $W_н$ is the pumping power; W_{output} is the power output from the working volume of the laser; $W_п$ is the power lost inside the working volume. Let us

more specifically define the terms in the righthand side of the equation. The power W_{output} can be represented in the form

$$W_{\text{в}}=W^{-}(0)(1-R_1)+W^{+}(L)(1-R_2). \tag{4}$$

Here $\overset{+}{W}(z)$ are the powers of the laser radiation propagated inside the resonator in the positive and negative directions of the laser axis Z. The points of intersection of the surfaces of the opaque (R_1) and the output (R_2) mirrors of the resonator with the laser axis have the coordinates z=0 and z=L, respectively. In order to express W_{output} in terms of the experimentally measured power W_{laser}, let us use the obvious expressions

$$W_{\text{л}}=W^{+}(L)T_2;\quad W^{-}(L)=W^{+}(L)R_2;\quad W^{+}(0)=W^{-}(0)\,R_1, \tag{5}$$

where T_2 is the transmission of the output mirror and also the condition of constancy of the radiation power with respect to length of the resonator

$$W^{+}(z)+W^{-}(z)=W=\text{const}. \tag{6}$$

For R_1, $R_2>0.6$, the last condition is satisfied with accuracy of 3% [9]. Substituting (5) and (6) in (4), we obtain

$$W_{\text{в}}=2(1-R_1R_2)W_{\text{л}}/T_2(1+R_1). \tag{7}$$

The expression for $W_{\text{п}}$ is written in the form

$$W_{\text{п}}=W\Gamma L+W\Gamma_{\text{п}}L, \tag{8}$$

where $\Gamma_{\text{п}}$ is the loss factor caused by volumetric absorption in the working volume. Using (1), (2), (5) and (6) and the analogous equalities for the intensity, we obtain

$$W_{\text{п}}=I_{\text{л}}(r_{\text{в}})\frac{1+R_2}{T_2}2\pi r_{\text{в}}\sqrt{2\Delta n(r_{\text{в}})\,l/L}\;L+W_{\text{л}}\frac{1+R_2}{T_2}\Gamma_{\text{п}}L. \tag{9}$$

Substituting (7) and (9) in (3), we obtain the expression for the pumping power $W_{\text{н}}$ in terms of the parameters measured experimentally:

$$W_{\text{н}}^{(i)}=W_{\text{л}}^{(i)}2\left(1-R_1^{(i)}R_2^{(i)}\right)/\left(T_2^{(i)}\left(1+R_1^{(i)}\right)\right)+I_{\text{л}}^{(i)}\left(r_{\text{в}}^{(i)}\right)\frac{1+R_2^{(i)}}{T_2^{(i)}}2\pi r_{\text{в}}^{(i)}\times$$
$$\times\sqrt{2\Delta n^{(i)}\left(r_{\text{в}}^{(i)}\right)l/L}\;L+W_{\text{л}}^{(i)}\frac{1+R_2^{(i)}}{T_2^{(i)}}\Gamma_{\text{п}}L \tag{10}$$

(i=1,2 are the run numbers in each pair of experiments). Since in each pair of experiments we varied only the Q-factor of the resonator, it is natural to assume that the pumping powers at the corresponding points in time are

$$W_{\text{н}}^{(1)}(t)=W_{\text{н}}^{(2)}(t)=W_{\text{н}}(t). \tag{11}$$

Thus, for the pair of experiments we obtained a system of two equations (10) for instantaneous values of the unknowns W_H and Γ_π which permits determination of the volumetric loss factor. Let us note that if R_1, R_2<0.6, then it is expedient to use the system of equations of [5] in which the variation of W along the laser was taken into account to determine Γ_π.

When performing the experiments, special attention was given to the elimination of possible sources of errors. The radiation losses in the replaceable glass windows covering the ends of the laser cell were included in the losses in the resonator mirrors. The adjustment system provided for parallelness of the resonator mirrors and the cell openings of no worse than 10^{-5} radian.

The symmetry of the energy distribution of the laser beam with respect to the optical axis of the resonator was specially monitored.

3. Experimental Setup

The diagram of the experimental setup is presented in Figure 2. A study was made of an iodine laser, the design of which is similar to that described in [2]. The cylindrical laser cell 13 with light diameter 13.5 cm on the axis of which high-current discharge 14, 55 cm long, was initiated, was covered on the ends with plane-parallel K8 glass plates 15 and placed in a resonator formed by plane dielectric mirrors 12. The optical length of the resonator was 220 cm. The plates 15 were adjusted parallel to the resonator mirrors. A capacitor bank feeding the discharge was charged to a voltage of 50 kv and stored an energy of 45 kjoules. Experiments were performed with the working media CF_3I and $n\text{-}C_3F_7I$. The conditions of performing the experiments and the results are presented in the table.

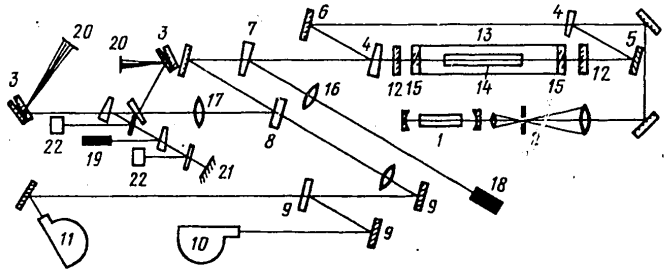

Figure 2. Diagram of the experiment setup:
1 -- ruby laser; 2 -- telescope with diaphragm in the focal plane of the objectives; 3 -- mirror wedges; 4 -9 -- mirrors and light dividing plates; 10, 11 -- high-speed photorecorders; 12 -- iodine laser resonator mirror; 13 -- discharge chamber; 14 -- discharge channel; 15 -- chamber openings; 16, 17 -- lenses; 18, 19 -- photodiodes; 20, 21 -- exposed and developed photographic paper; 22 -- calorimeters.

The following parameters were recorded in the experiments: the discharge current as a function of time, the energy and power of the lasing pulse, intensity of the laser radiation on the inside boundary of the lasing zone energy distribution with respect to angle in the far zone and also variation of the index of refraction Δn in the lasing zone. The discharge current was measured by a Rogowski loop. The shape of the current was identical in all of the experiments (Figure 3, a).

The lasing pulse energy was recorded by two calorimeters 22, at the entrance openings of which the image of the output mirror of the laser was constructed by using the lens 17.

The emission power was measured by the photodiode 19, type 9E-111. The structural design of the case of the photodiodes 18, 19 provided for independence of the signal with respect to the angle of incidence of the beam and location of the point of incidence of the beam on the entrance opening of the photodiode. The characteristic form of the power as a function of time is presented in Figure 3, b.

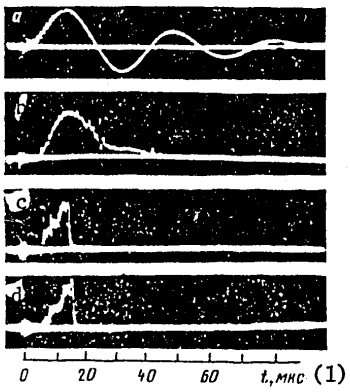

Figure 3. Discharge current (a), emission power (b), radiation power passing through the upper curvilinear diaphragm (c) and lower curvilinear diaphragm (d) as functions of time (experiment No 6)

Key:
1. microseconds

For measuring the intensity of the radiation on the inside boundary of the lasing zone part of the radiation was tapped by a light dividing wedge 7. Using the lens 16 in the plane of the entrance openings of the two photodiodes 18 the image of the plane passing through the front end of the discharge was constructed on a 1:1 scale on the wave length of the laser radiation. In the entrance openings of the photodiodes curvilinear slotted diaphragms were installed cutting two segments of an annular zone 0.3 mm wide out of the overall image (see Figure 1). The diameter of the annular zone was 34 (experiments Nos 1 and 2) and 30 mm (experiments Nos 3-6). When the diameter of the shock wave front reached the diameter of the slotted diaphragms, which corresponded

approximately to the maximum emission power with respect to time, the signal reached the maximum value, giving the magnitude of the radiation intensity of the inside boundary of the lasing zone, and then it broke off sharply (Figure 3, d, e).

The divergence of the laser radiation was determined by the spot sizes obtained at the focal length of the lens 17 on reflection from the mirror wedges 3 [10]. The spots were burned out on the exposed and developed photographic paper 20. The angular energy distribution of the radiation is presented in Figure 4. The image of the plane lying in the near zone of the laser was projected on the same photographic paper 21 by the lens 17. The axial symmetry of the burn indicated the symmetry of the energy distribution in the transverse cross section of the laser.

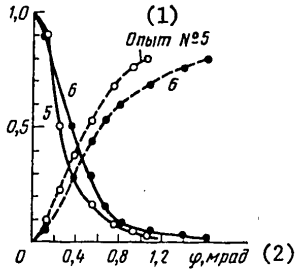

Figure 4. Characteristics of laser radiation in the far zone: angular distribution of the energy density (solid lines) and ratio of the radiation energy propagated within the limits of the cone with an angle ϕ between the axis and the generatrix to the total energy (dotted line)

Key:
1. Experiment No 5
2. mradians

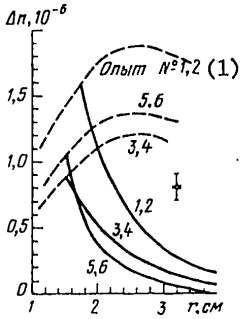

Figure 5. Δn near the shock wave as a function of its radius (dotted line) and instantaneous profiles Δn (solid lines)

Key:
1. Experiment Nos 1, 2

Part of the laser radiation going through the dielectric mirror 8 (transmission T=1.2%) using the mirrors 9 was directed at the high-speed photorecorder SFR-2, 10, operating in the scanning mode. In the plane of the slit of the SFR-2 oriented vertically an image of the plane passing through the front end of the discharge was constructed. The laser axis was oriented toward the center of the slit. The pictures taken provided information about the uniformity of the time distribution of the intensity of the laser emission with respect to the vertical diameter. From these pictures, the time was determined between the beginning of lasing and the time when the shock wave diameter reached the diameter of the cylindrical electrodes located on the axis of the chamber which made it possible to reduce the data on Δn to a united time scale.

The value of Δn was measured by the interferometric method using a ruby laser 1 by the procedure described in [2, 6]. The Mach-Zehnder interferometer formed by the elements 4-6 was used. The interferometer was tuned so that the localization plane of the bands would be located in the front end of the discharge. The dependence of Δn at the inside boundary of the lasing zone on the radius of the zone and the distribution of Δn as a function of the distance to the shock wave are presented in Figure 5.

The absolute accuracy of measuring the energy, power and intensity of the laser radiation was 15%. The reproducibility of the results was no worse than 5%.

In order to consider absorption in the interchangeable glass windows of different thickness covering the ends of the laser cell, before performing the experiments, the parameters of the equivalent mirrors of the resonator R_k and T_k (k=1,2) were determined, each of which consisted of its own dielectric mirror and glass opening. It was established in advance that for the given lot of K8 glass the absorption γ on a wave length λ=1.315 microns was $(8\pm0.5)\cdot10^{-3}$ cm^{-1}. The reflection and transmission of the windows were calculated considering multiple reflection from their faces by the formulas

$$R_0=r_0[1+(1-2r_0)e^{-2\gamma d_0}]/(1-r_0^2e^{-2\gamma d_0}); \quad T_0=(1-r_0)^2e^{-\gamma d_0}/(1-r_0^2e^{-2\gamma d_0}), \tag{12}$$

where r_0=0.04 is the Fresnel reflection coefficient; d_0 is the window thickness. The parameters of the equivalent mirrors were also calculated considering multiple reflections:

$$R_k=R_{0k}+R_{3k}T_{0k}^2/(1-R_{3k}R_{0k}); \quad T_k=T_{3k}T_{0k}/(1-R_{3k}R_{0k}), \tag{13}$$

where R_{3k} and T_{3k} are the reflection and transmission coefficients of the dielectric mirrors of the resonator, respectively. In order to improve the reliability of the results the parameters T_{0k} and T_k were measured before each experiment on a specially assembled device and they were compared with the results calculated by formulas (12) and (13). Within the limits of error being 0.5%, the measured transmission values coincided with the calculated values. The parameters of the equivalent mirrors required to calculate the losses are presented in the table.

Experiment No	1	2	3	4	5	6
P, atm	0,06 (CF_4)+0,44 (SF_6)		0,035 (CF_4)+0,465 (SF_6)		0,05 (n-C_4F_{10})+0,45 (SF_6)	
R_1	0,938	0,941	0,944	0,936	0,934	0,937
R_2	0,880	0,624	0,889	0,626	0,878	0,626
T_2	0,0588	0,320	0,0592	0,321	0,0588	0,321
r_H, cm	1,76±0,06	1,76±0,06	1,53±0,06	1,58±0,06	1,55±0,06	1,55±0,06
E, J	21	61	33	92	27	93
$W_л$, 10^6 W	1,36±0,08	4,01±0,23	2,09±0,12	5,17±0,30	1,69±0,10	5,11±0,30
$I_л$, 10^4 W·cm^{-2}	5,86±0,34	23,4±1,4	7,68±0,44	24,8±1,4	7,83±0,45	30,9±1,8
Δn, 10^{-6}	1,59±0,10	1,53±0,10	0,88±0,10	0,85±0,10	1,05±0,10	1,05±0,10
γ_n, cm^{-1}	1,25		1,10		2,00	
Γ, 10^{-4} cm^{-1} (experiment)	4,27±0,38	5,69±0,53	2,36±0,26	3,12±0,36	3,29±0,34	4,30±0,44
$\Gamma_п$, 10^{-4} cm^{-1}	−0,78±1,4		−0,66±1,1		0,03±1,2	
$\sigma_0 N_0$, cm^{-1}	0,866		0,505		0,950	
$\Gamma_т$, 10^{-4} cm^{-1} (theory)	7,64		3,32		6,87	
$\sigma_H N_0/\gamma_n$	0,69		0,46		0,475	
β/g	1,28	0,449	0,916	0,293	1,61	0,593
Γ, 10^{-4} cm^{-1} (theory)	5,13	6,05	2,26	2,86	4,18	5,10
W_H, 10^6 Bt	7,48±0,50		8,29±0,64		9,24±0,67	

4. Discussion of the Results

Results are presented in the table which were obtained upon substituting the experimental data in system (10). As the errors, the doubled standard deviation are presented which correspond to the confidence coefficient of 0.95. Comparison of the values obtained for Γ and Γ_π indicates that the losses in the investigated laser are caused primarily by the refraction mechanism. The achieved accuracy of the procedure does not permit determination of the magnitude of the losses caused by the volumetric absorption, but it is clear that Γ_π does not exceed 10^{-4} cm $^{-1}$. Consequently, a decrease in the refraction losses themselves permits a significant increase in the length of the laser without decreasing its efficiency.

Let us consider the experimental values of the refraction loss coefficients Γ as a function of the conditions of performing the experiments. As is obvious from the table, in each pair of experiments the increase in R_2 from ~0.63 to ~0.88 leads to a decrease in Γ by approximately 1.3 times. This is connected with variation of the distribution of the laser radiation intensity in the transverse cross section of the laser as a result of nonuniformity of the distribution of the refraction losses in the active zone. Although the radiation is lost on the inside boundary of the generation zone, it is easy to understand that the refraction losses are of a quasivolumetric nature. Let us isolate a cylindrical region with thickness Δr in the lasing zone at an arbitrary distance r from the shock wave. As a result of the presence of a gradient of the angle u, the radiation flux entering through the outer boundary of the isolated region (a distance $r+\Delta r$ from the shock wave) is less than the flux departing through the internal boundary where the angle u is larger. In this sense, the losses have a quasivolumetric nature. They are maximal at the shock wave boundary and minimal at the outer boundary of the lasing zone: therefore increasing the Q factor of the resonator has a weak influence on the intensity of the laser radiation in the region separated from the shock wave, and it leads to a stronger decrease in

the intensity of the output emission as a result of the shock wave where the losses are greater. The ratio $I_{laser}(r_H)/W_{laser}$ and, in accordance with (2), Γ decreased. The presence of this effect is confirmed by the results of measuring the angular distribution of the intensity of the laser radiation in the far zone. Figure 4 shows the integral angular distribution of the energy density and the energy of the laser radiation with respect to time in the experiments with $n\text{-}C_3F_7I$. It is obvious that increasing the Q-factor of the resonator leads to constriction of the angular spectrum of the laser emission, that is, the contribution to the total power of the radiation which with maximum deviation of $u(r_H)$ leaves the region close to the shock wave, decreases. Quantitatively this effect can be described by using the equations obtained in reference [11] for the stimulated radiation field in the lasers with refraction losses.

During analysis of these equations we considered that under the conditions of performing the experiments, the variation in the increment of the index of refraction on going away from the shock wave, as is obvious from Figure 5, is approximated well by an exponential function

$$\Delta n\,(r)=\Delta n\,(r_{\text{н}})\,e^{-\gamma_n (r-r_{\text{н}})}, \tag{14}$$

and the rate of expansion of the pumping source v_H is appreciably greater than the velocity of the photochemical decomposition wave v_ϕ [12]. Here the pumping rate F (the density of the dissociated particles per unit time) also is approximated well by an exponential function on going away from the shock wave [13]. Considering the axial symmetry

$$F\,(r)=F\,(r_{\text{н}})\,(r_{\text{н}}/r)\,e^{-\gamma_F (r-r_{\text{н}})}. \tag{15}$$

Without discussing the intermediate calculations, let us present the final result which is the coefficient of refraction losses as a function of the Q-factor of the resonator:

$$\Gamma=\Gamma_0\frac{(g/\beta)^{2\gamma_F/\gamma_n+1}e^{g/\beta}\Gamma\,(-2\gamma_F/\gamma_n,\,g/\beta)}{1-(2\gamma_F/\gamma_n)\,(g/\beta)^{2\gamma_F/\gamma_n}e^{g/\beta}\Gamma\,(-2\gamma_F/\gamma_n,\,g/\beta)}, \tag{16}$$

where

$$\Gamma_0=\lim_{\beta/g\to 0}\Gamma=\gamma_F\sqrt{2\Delta n\,(r_{\text{н}})\,l/L};\quad \beta={}^1/_2\gamma_n\sqrt{2\Delta n\,(r_{\text{н}})\,l/L};$$

under the conditions of our experiment

$$g=\frac{1}{2L}\left(\frac{1-R_1}{\sqrt{R_1}}+\frac{1-R_2}{\sqrt{R_2}}\right)\text{ при }{}^1/_2\,\Gamma_0 L\ll 1;$$

$$\Gamma\,(-2\gamma_F/\gamma_n,\,g/\beta)=\int_{g/\beta}^{\infty}e^{-t}\,t^{-(2\gamma_F/\gamma_n+1)}dt$$

is the incomplete gamma function [14].

In order to see that formula (16) correctly reflects the dependence of Γ on the Q-factor of the resonator we compared the values of Γ calculated by this formula for each experiment with the experimental values. Here γ_F was considered

equal to $\sigma_H N_0$ [12], where σ_H is the absorption cross section of the pumping radiation by the molecules of working medium with initial concentration N_0; $\sigma_H N_0$ was taken from reference [15]. The values of γ_n and $\Delta n(r_H)$ were measured experimentally, and in each experiment g was given by the resonator parameters. The values of Γ calculated by (16) are presented in the table from which it is obvious that the theoretical and experimental values of Γ agree well with each other.

Thus, within the framework of the model of refraction losses the dependence of the losses on the Q-factor of the resonator will obtain a natural explanation and at the same time serve as confirmation of the predominant role of the refraction mechanism of the losses in the given type of lasers. The experimentally obtained values of Γ under the various operating conditions of the iodine PDL permit us to see that the estimated ratio for Γ obtained in [5] actually agrees well with the experiment if $\beta/g<1$. This expression coincides with the expression for Γ_0 (see formula (16)) for $\gamma_F=\sigma_H N_0$.

Having found the basic mechanism of the intracavity losses, it is possible to indicate ways of decreasing them. From the relation $\Gamma\approx\sigma_H N_0\sqrt{2\Delta n(r_H)\ell/L}$ it follows that with an increase in the characteristic transverse dimension of the pumping energy release zone $\gamma_F^{-1}\sim(\sigma_F N_0)^{-1}$ as a result of reducing the pressure of the working medium the magnitude of the refraction losses must decrease. In the experiments with a reduction in pressure from 0.06 to 0.035 atm, the losses diminish by approximately 1.7 times. The reduction in pressure has led both to an increase in γ_F^{-1} and to a decrease in Δn.

A more radical means of decreasing the refraction losses must be the transition to operating in the amplifier mode, to the input of which a signal is fed with plane wave front perpendicular to the amplifier axis. At the amplifier input the refraction losses are absent. They will gradually increase together with an increase in the bending of the wave front as the signal passes through the optically nonuniform amplifying medium. In addition, the length of the amplifier can be doubled without decreasing its efficiency, feeding a signal to the input with the wave front which will be converted to a plane wave in the middle cross section of the amplifier.

From the results obtained it is understandable that the problem of describing the effect of the refraction losses on the energy characteristics of the lasers has a number of peculiarities and does not reduce to an analogous problem in lasers with volumetric losses. Therefore for estimation of the prospects for increasing the energy of iodine PDL as a result of increasing their length, it is required that a detailed analysis be made of the effect of the refraction losses on the energy characteristics of the lasers operating both in the lasing and in the amplifier modes.

Now let us compare some data obtained in our work with the results of reference [2]. The increment of the index of refraction measured experimentally in [2] decreases on going away from the shock wave front faster than the calculated density of the dissociated particles. The results of this paper confirm these conclusions. Actually, since the experimental measured values of Γ are close to the theoretical values calculated under the assumption that $\gamma_F\approx\sigma_H N_0$, this means that $\gamma_F/\gamma_n\approx\sigma_H N/0\gamma_n\sim 0.5$-$0.7$ (see the table), that is, on going away from the shock wave Δn decreases approximately twice as fast as the density of the dissociated particle, which agrees well with the results of reference [2].

In addition, it is interesting to compare the pumping power obtained in our experiments with the results of reference [2] where studies were also made of the emitting characteristics of high-current discharge and transparency of the shock wave surrounding the discharge. The recalculation of the data from reference [2] (for the working medium $n\text{-}C_3F_7I$) for our experimental conditions gives $W_H=7.8\cdot10^6$ watts, which also is in good agreement with our results obtained from the power budget equation in the resonator.

It must be noted that the predominant role of the refraction mechanism in the intracavity losses is not a specific characteristic of only the given type of laser. In lasers, the active medium of which is optically nonuniform, the refraction losses can make a significant contribution to the total losses. In addition, the lasers with resonator mirrors out of adjustment or deformed under defined conditions can also be described within the framework of the refraction loss model. Consideration of the refraction losses can turn out to be especially significant when starting new lasers with small amplification.

5. Conclusion

In the present paper, an experimental study is made of the nature of the internal losses in iodine photodissociation lasers with pumping by high-current discharge open ultraviolet radiation. The procedure has been developed for simultaneous measurement of the total and refraction losses caused by optical nonuniformity of the active medium of the laser.

It has been demonstrated that in the investigated lasers the predominant role is played by the refraction losses. A relation has been established for the coefficient of refraction losses as a function of the partial pressure of the working gas and the Q-factor of the resonator. The coefficient of refraction losses in the investigated laser is $(2.4\text{-}5.7)\cdot10^{-4}$ cm^{-1}.

The losses caused by volumetric absorption of laser radiation in the active medium have not been detected in general. The accuracy of the experimental procedure permits confirmation that the coefficient of volumetric losses on the wave length 1.315 microns during lasing does not exceed 10^{-4} cm^{-1}. The possibility of decreasing the refraction losses both by decreasing the partial pressure of the working gas and by going over to operation in the amplifier mode where refraction losses must be less than in the laser is discussed.

B BIBLIOGRAPHY

1. Basov, N. G.; Zuyev, V. S.; Katulin, V. A.; Lyubchenko, A. Yu.; Nosach, V. Yu.; Petrov, A. L. KVANTOVAYA ELEKTRONIKA [Quantum Electronics], No 6, 1979, p 311.

2. Borovich, B. L.; Zuyev, V. S.; Katulin, V. A.; Nosach, V. Yu.; Nosach, O. Yu.; Startsev, A. V.; Stoylov, Yu. Yu. KVANTOVAYA ELEKTRONIKA, No 2, 1975, p 1282.

3. Nosach, O. Yu.; Orlov, Ye. P. KVANTOVAYA ELEKTRONIKA, No 3, 1976, p 1423.

4. Zuyev, V. S.; Korol'kov, K. S.; Netemin, V. N.; Nosach, O. Yu.; Orlov, Ye. P. KVANTOVAYA ELEKTRONIKA, No 3, 1976, p 2434.

5. Nosach, O. Yu.; Orlov, Ye. P. PREPRINT FIAN [Preprint of the Physics Institute of the USSR Academy of Sciences], Moscow, No 7, 1979.

6. Borovich, B. L.; Zuyev, V. S.; Katulin, V. A.; Mikheyev, L. D.; Nikolayev, F. A.; Nosach, O. Yu.; Rozanov, V. B. ITOGI NAUKI I TEKHNIKI. SER. RADIOTEKHNIKA [Results of Science and Engineering. Radio Engineering Series], Vol 15, 1978, p 189.

7. Kirillov, G. A.; Kormer, S. B.; Kochemasov, G. G.; Kulikov, S. M.; Murugov, V. M.; Nikolayev, V. D.; Sukharev, S. A.; Urlin, V. D. KVANTOVAYA ELEKTRONIKA, No 2, 1975, p 666.

8. Zuyev, V. S.; Nosach, O. Yu.; Orlov, Ye. P. PREPRINT FIAN, Moscow, No 94, 1980.

9. Meytlend, A.; Dann, M. VVEDENIYE V FIZIKU LAZEROV [Introduction to Laser Physics], Moscow, Nauka, 1978, p 201.

10. Ragul'skiy, V. V.; Fayzullov, F. S. OPTIKA I SPEKTROSKOPIYA [Optics and Spectroscopy], No 27, 1969, p 707.

11. Nosach, O. Yu.; Orlov, Ye. P. PREPRINT FIAN, Moscow, No 19, 1980.

12. Borovich, B. L.; Zuyev, V. S.; Krokhin, O. N. ZHETF [Journal of Experimental and Theoretical Physics], No 64, 1973, p 1184.

13. Borovich, B. L.; Zuyev, V. S.; Katulin, V. A.; Nosach, O. Yu.; Tyurin, Ye. L.; Shcheglov, V. A. KVANTOVAYA ELEKTRONIKA, No 2(8), 1972, p 88.

14. Gradshteyn, I. S.; Ryzhik, I. M. TABLITSY INTEGRALOV, SUMM, RYADOV I PROIZVEDENIY [Tables of Integrals, Sums, Series and Products], Moscow, Nauka, 1971, p 954.

15. Davis, C. C.; Pirkle, R. J.; McFarlane, R. A.; Wolga, G. J. IEEE J. QE-12, 1976, p 334.

10845
CSO: 1862

UDC 535.373.5

STIMULATED LIGHT SCATTERING IN A THERMODYNAMICALLY NONEQUILIBRIUM MEDIUM WITH EXCITATION OF COLLECTIVE MOTIONS AS A RESULT OF LIGHT-INITIATED CHEMICAL REACTION

Moscow KVANTOVAYA ELEKTRONIKA in Russian Vol 7, No 12, Dec 80 received 11 Jun 80 pp 2614-2620

[Article by N. G. Basov, V. S. Zuyev, O. Yu. Nosach, Ye. P. Orlov, Physics Institute imeni P. N. Lebedev of the USSR Academy of Sciences, Moscow]

[Text] It is demonstrated that in thermodynamically nonequilibrium media, during the course of light-initiated exothermal reactions, a new type of stimulated scattering of light on ultrasonic vibrations excited as a result of nonuniform heat release caused by nonuniform distribution of the light intensity can occur. The primary characteristics of this type of scattering are analzyed, and estimates are made of the amplification coefficient of the scattered light wave.

1. Introduction

In [1] it was discovered that during lasing small-scale optical nonuniformities with transverse dimension ~0.01 to 0.04 cm occur in the active region of iodine photodissociation lasers under defined conditions. In [2] and then in [3] it was demonstrated that the occurrence of this phenomenon can be explained as follows. Under the effect of the ultraviolet pumping radiation the molecules of the gaseous working medium RI (for example, CF_3I or $n\text{-}C_3F_7I$) decompose into excited iodine atoms I^* and radicals R. In the active region exothermal reactions can take place, the fastest of which are [4]

$$R + I \rightarrow RI; \quad (1)$$
$$R + R \rightarrow R_2. \quad (2)$$

The reactions $R+I^* \rightarrow RI$ and $I+I \rightarrow I_2$, and so on, are slow by comparison with (1) and (2), and it is possible to neglect their contribution to the effects discussed below.

Even with uniform pumping with respect to volume in the region where the intensity of the laser radiation increases, the concentration of the I atoms also increases, and the reaction (1) is accelerated, which means the heat release in this region increases. As a result, the gas temperature and pressure in it

increase. The nonuniform temperature distribution and gas dynamic disturbances occurring as a result of nonuniform increase in pressure lead to modulation of the index of refraction of the gas which, in turn, has an effect on the laser field, scattering it. Thus, the nonlinear self-stressing of the light occurs which is realized as a result of a closed chain: light-chemical reaction-temperature and gas dynamic disturbances-light.

The purpose of this paper was to demonstrate that the nonlinear relation between the field and the medium is realized in such a way that the gas dynamic disturbances of the medium are fed as a result of heat release during the chemical reactions (1) and (2) initiated by the laser radiation, as a result of which amplification of the scattered light field takes place. In addition, an estimate will be made of the amplification coefficient of the given type of scattering, and a comparison made with the amplification coefficient of VRMB.*

The difference of the described type of scattering from the known types of stimulated scattering [5, 6] consists primarily in the fact that the energy causing disturbance of the medium is extracted not from the light field, but from the thermodynamically nonequilibrium medium itself. The light in the given case is only the controlling element initiating the chemical reactions. In addition, amplification of the light takes place with resonance (single-photon) transition $I^* \to I$.

2. Basic Equations

Just as during stimulated thermal scattering of light [6-8], the effect of the electromagnetic waves on the substance is manifested in heating of the nonlinear medium. However, the mechanism of the relation of the heat release and the field is theoretically different here. The quantity of heat released per unit volume per unit time as a result of the occurrence of the chemical reactions (1) and (2) initiated by light

$$\dot{Q} = q_1 \varkappa_1 [I][R] + q_2 \varkappa_2 [R]^2, \tag{3}$$

where [I], [R] are the concentrations of the unexcited iodine atoms and radicals; $\varkappa_1$ and $\varkappa_2$ are the reaction constants for (1) and (2) [4]; q_1, $2q_2$ are the energy released during recombination of the iodine atom with the radical and recombination of two radicals, respectively.

In order to find the relation between $\dot{Q}$ given using (3) and the electromagnetic field, we shall begin with the equations describing the balance of particles at a given point of the active region:

$$\begin{aligned}
&\frac{\partial [R]}{\partial t} + \nabla ([R]\,w) = F - \varkappa_1 [R][I] - \varkappa_2 [R]^2;\\
&\frac{\partial [I]}{\partial t} + \nabla ([I]\,w) = \sigma_y \left([I^*] - \frac{g_2}{g_1}[I]\right)\frac{n^2 c E^2}{4\pi\hbar\omega_0} - \varkappa_1 [R][I];\\
&\frac{\partial [I^*]}{\partial t} + \nabla ([I^*]\,w) = F - \sigma_y \left([I^*] - \frac{g_2}{g_1}[I]\right)\frac{n^2 c E^2}{4\pi\hbar\omega_0},
\end{aligned} \tag{4}$$

where w is the mass velocity of the gas; F is the pumping velocity to the upper laser levels of the iodine atom [9]; σ is the amplification cross section of the laser transition; $[I^*]$ is the concentration of the excited iodine atoms;

* Mandelstamm-Brillouin stimulated scattering.

g_2/g_1 is the ratio of the statistical weights of the upper and lower laser levels; E is the total field of the exciting E_0 and scattered E_1 waves; c is the speed of light in the medium with index of refraction n; $\hbar\omega_0$ is the quantum energy of the electromagnetic field.

The difference of the equations (4) from the kinetic equations of [10] frequently used in the literature consists in the addition of terms describing the variation of the number of particles as a result of inflow (outflow) of the particles during gas dynamic displacements of the medium. In addition, we have neglected the slow reactions and loss of molecules of the working medium.

It does not appear possible to obtain the solution to the system (4) in analytical form in the general case. However, it can be linearized, assuming that the intensity of the stimulated scattering $\sim|E_1|$ is appreciably less than the intensity of the exciting light $\sim|E_0|$. After linearization, the system (4) assumes the form

$$\frac{\partial [R]_1}{\partial t}+(\varkappa_1[I]_0+2\varkappa_2[R]_0)[R]_1+\varkappa_1[R]_0[I]_1=[R]_0\frac{\partial u}{\partial t};$$

$$\frac{\partial [I]_1}{\partial t}+\left(\varkappa_1[R]_0+\frac{g_2}{g_1}\sigma_y I_0\right)[I]_1+\varkappa_1[I]_0[R]_1-\sigma_y I_0[I^*]_1=[I]_0\frac{\partial u}{\partial t}+\sigma_y\Delta_0 I_1;$$

$$\frac{\partial [I^*]_1}{\partial t}+\sigma_y I_0[I^*]_1-\frac{g_2}{g_1}\sigma_y I_0[I]_1=[I^*]_0\frac{\partial u}{dt}-\sigma_y\Delta_0 I_1, \qquad (5)$$

where $[I]_0$, $[I^*]_0$, $[R]_0$ are the particle concentrations in the absence of the scattered field ($E_1\equiv 0$); $[I]_1$, $[I^*]_1$, $[R]_1$ is the deviation of the particle concentrations from $[I]_0$, $[I^*]_0$, $[R]_0$; $\Delta_0=[I^*]_0-[I]_0 g_2/g_1$; $I_0=n^2cE_0^2/4\pi\hbar\omega_0$ is the intensity of the exciting waves; $I_1=2n^2c(E_0, E_1)/4\pi\hbar\omega_0$ is the deviation of the intensity of the total field from I_0; $u=\rho_1/\rho$; ρ_1 is the deviation of the density of the medium from its equilibrium value ρ. On derivation of (5), the continuity equation for u was used

$$\frac{\partial u}{\partial t}+\operatorname{div} w=0. \qquad (6)$$

For solution of the problem of scattering of the exciting radiation in the investigated case we shall begin with the equations (3), (5) and the system of nonlinear Maxwell equations, hydrodynamics and thermal diffusivity:

$$\frac{\partial^2 u}{\partial t^2}=\nabla^2\left\{\frac{1}{\rho\beta_T}(u+\sigma T_1)+\Gamma\frac{\partial u}{\partial t}-\frac{Y}{8\pi\rho}E^2\right\}; \qquad (7)$$

$$\frac{\partial T_1}{\partial t}-\gamma\chi\nabla^2 T_1-\frac{\gamma-1}{\sigma}\frac{\partial u}{\partial t}=\frac{1}{\rho c_V}\dot{Q}; \qquad (8)$$

$$\frac{1}{c^2}\frac{\partial^2 E}{\partial t^2}-\nabla^2 E=-\frac{1}{n^2c^2}\frac{\partial^2}{\partial t^2}\left\{YEu+\left(\frac{\partial\varepsilon}{\partial T}\right)_\rho ET_1\right\}, \qquad (9)$$

where $\beta_T=1/\rho v_T^2$; β_T and v_T are the isothermal compressibility and speed of sound; σ is the thermal coefficient of volumetric expansion; $\Gamma=(4\eta/3+\eta')/\rho$; η, η' are the shearing and volumetric viscosity coefficients; $Y=(\rho\partial\varepsilon/\partial\rho)_T$; $\varepsilon=n^2$ is the dielectric constant of the medium; T_1 is the deviation of the temperature of the medium from its equilibrium value T_0; χ is the coefficient of thermal diffusivity; $\gamma=c_p/c_v$.

For the solution of the stated problem, the system of equations (7)-(9) also must be linearized, which is possible if $|E_0|>>|E_1|$. The linearization procedure is well known [5, 8], and we shall not discuss it. The system of equations (3), (5), (7)-(9) is the complete closed system of equations sufficient for the solution of the problem of the scattering of the exciting wave. Here we shall limit ourselves only to the case of a monochromatic exciting field and we shall consider only the steady-state theory.

The steady-state theory is applicable if the duration of the exciting pulse $t_0>>\tau_\phi$, τ_T, where $\tau_\phi=1/2\alpha v$, $\tau_T=1/2\chi q^2$ is the lifetime of the acoustic phonons and the time for establishment of the thermal equilibrium in the "temperature wave" [8]; $q=k_0-k_1$; k_0, k_1 are the wave vectors of the exciting and scattered light waves; α, v are the amplitude coefficient of absorption and the speed of sound.

Let the total field E consist of linearly polarized exciting E_0 and scattered E_1 light waves. Then E is represented in the form

$$E=\tfrac{1}{2}E_0\exp\{i(\omega_0 t-k_0 r)\}+\tfrac{1}{2}E_1\exp\{i(\omega_1 t-k_1 r)\}+\text{complex conjugate}, \tag{10}$$

where ω_0, ω_1 are the frequencies of the exciting and scattered light waves. Here the intensity $I_0=n^2cE_0^2/8\pi\hbar\omega_0$, $I_1=\tilde{I}\exp[i(\Omega t-qr)]+$ complex conjugate, where $\tilde{I}=n^2cE_0E_1^*/8\pi\hbar\omega_0$; $\Omega=\omega_0-\omega_1$.

First let us find the relation of $[R]_1$, $[I]_1$ to I_1 and u. For this purpose let us represent $[R]_1$, $[I]_1$, $[I^*]_1$, u in the form

$$\begin{aligned}
[R]_1&=[\tilde{R}]\exp[i(\Omega t-qr)]+\text{complex conjugate};\\
[I]_1&=[\tilde{I}]\exp[i(\Omega t-qr)]+\text{complex conjugate};\\
[I^*]_1&=[\tilde{I}^*]\exp[i(\Omega t-qr)]+\text{complex conjugate};\\
u&=\tilde{u}\exp[i(\Omega t-qr)]+\text{complex conjugate}
\end{aligned} \tag{11}$$

and substituting them in equations (5) together with I_1, we obtain the algebraic system of equations relating $[\tilde{R}]$, $[\tilde{I}]$, $[\tilde{I}^*]$ to $\tilde{I}$, u:

$$\begin{aligned}
&(\varkappa_1[I]_0+2\varkappa_2[R]_0+i\Omega)[\tilde{R}]+\varkappa_1[R]_0[\tilde{I}]=i\Omega[R]_0\tilde{u};\\
&\varkappa_1[I]_0[\tilde{R}]+(\varkappa_1[R]_0+\sigma_y I_0 g_2/g_1+i\Omega)[\tilde{I}]-\sigma_y I_0[\tilde{I}^*]=i\Omega[I]_0\tilde{u}+\sigma_y\Delta_0\tilde{I};\\
&-\sigma_y I_0[\tilde{I}]g_2/g_1+(\sigma_y I_0+i\Omega)[\tilde{I}^*]=i\Omega[I^*]_0\tilde{u}-\sigma_y\Delta_0\tilde{I}.
\end{aligned} \tag{12}$$

The study of this system of equations in general form leads to very awkward expressions; therefore let us consider one of the special cases which is realized in practice.

3. Scattering on Ultrasonic Vibrations of the Medium

If the lifetime of the iodine atoms in the excited state and the characteristic times of the chemical reactions are greater than the period of the ultrasonic vibrations, the inequalities $\Omega \gg \sigma_y I_0$ and $\Omega \gg \varkappa_1 [I]_0, \varkappa_1 [R]_0, \varkappa_2 [R]_0$ are valid. These conditions are actually satisfied in iodine lasers. In reality, the characteristic scattering angle (the angle between k_0 and k_1) $\theta \sim 1$-10 mradians [2]. For $\theta \sim 1$ mradian $\Omega \sim \Omega_{MB} = 2|k_0| v \sin \theta/2 > 10^6$ sec^{-1} (here $|k_0| \sim 5 \cdot 10^4$ cm^{-1}, $v \sim 2.5 \cdot 10^4$ cm/sec for gases usually used as buffer gases -- CO_2, SF_6, and so on), at the same time as the probabilities of recombinations of the iodine atoms and the radicals $\varkappa_1 [I]_0, \varkappa_1 [R]_0, \varkappa_2 [R]_0$ under standard conditions are appreciably less than 10^6 cm^{-1}. The probability of induced transitions $\sigma_y I_0$ to the intensities $\hbar \omega_0 I_0 \sim 10^5$ watts/cm^2 is also appreciably less than Ω_{MB} ($\sigma_y \sim 5 \cdot 10^{-19}$ cm^2 [10]).

Under these conditions the expressions for $[\tilde{R}]$, $[\tilde{I}]$ obtained from the system of equations (12) are simplified significantly, and the heat release (3) can be represented in the form

$$\dot{Q} = \dot{Q}_0 + \left\{ -iq_1 \frac{\varkappa_1 [R]_0}{\Omega} \sigma_y \Delta_0 \tilde{I} \exp(i\Omega t - i\mathbf{qr}) + 2\dot{Q}_0 \tilde{u} \exp(i\Omega t - i\mathbf{qr}) + \right.$$
$$\left. + \text{complex conjugate} \right\}, \qquad (13)$$

where $\dot{Q}_0 = q_1 \varkappa_1 [I]_0 [R]_0 + q_2 \varkappa_2 [R]_0^2$ is the uniform heat release in the absence of a scattered field.

Substituting T_1 in (7) in the form of $T_1 = T_1^0 + (\tilde{T} \exp\{i(\Omega t - \mathbf{qr})\} +$ complex conjugate), where T_1^0 is the deviation of the temperature from the equilibrium value of T_0 in the absence of the scattered field, and substituting (11), (13) in (8), we discover that in the investigated case $2\dot{Q}_0/\rho c_p \ll \Omega(\gamma-1)/\sigma$, and the second term in (13) can be neglected. In addition, assuming that the relative variation of the amplitudes is small at distances on the order of the wave length, in (9) we keep only the first spatial derivative of the amplitude, and in (7), (8) we in general neglect the derivatives of the amplitudes inasmuch as the absorption of the ultrasonic and the temperature waves α and α_T is greater than their amplification in the process of stimulated scattering. Abstracting from the process of amplification of electromagnetic waves and the active medium of the laser, we assume that $|E_0(r)|^2 \sim$ const.

Considering the assumptions made, we obtain exponential growth of the scattered radiation in the region of nonlinear interaction:

$$|E_1(\zeta)|^2 = |E_1(\zeta=0)|^2 \exp\{g(\Omega)\zeta\}, \qquad (14)$$

where ζ is the coordinate in the direction k_1, and $g(\Omega)$ is the steady-state amplification coefficient:

$$g(\Omega) = \frac{|k_1| q^2 Y}{4\pi n^2 \rho} \operatorname{Re} \frac{A_1}{A_2} |E_0|^2; \qquad (15)$$

$$A_1 = \frac{\sigma}{\rho c_p \beta_s} \frac{n^2 c \frac{q_1}{2\hbar\omega_0} \frac{\varkappa_1 [R]_0}{\Omega} \sigma_y \Delta_0}{i\Omega + \gamma\chi q^2} - \frac{1}{4} iY;$$
$$A_2 = \Omega^2 - \frac{q^2}{\rho\beta_T} - i\Omega q^2 \Gamma - \frac{iq^2(\gamma-1)\Omega}{\rho\beta_T (i\Omega + \gamma\chi q^2)}.$$

For scattering on an ultrasonic wave $\Omega^2 \sim \Omega_{МБ}^2 = q^2/\rho\beta_s \gg (\chi q^2)^2$.

Neglecting the small terms in (15), we find the expression for the amplification coefficient:

$$g(\Omega) = \frac{|k_1| Y^2 \Omega_{МБ} \beta_s}{32\pi n^2} \frac{\delta\Omega_{МБ}}{(\Omega-\Omega_{МБ})^2+(\delta\Omega_{МБ})^2} |E_0|^2 + \frac{|k_1| Y\sigma}{8\pi\rho c_p} \frac{cq_1 \mathcal{H}_1 [R]_0 \sigma_y \Delta_0}{2\hbar\omega_0} \times$$
$$\times \frac{1}{\Omega_{МБ}} \frac{\delta\Omega_{МБ}}{(\Omega-\Omega_{МБ})^2+(\delta\Omega_{МБ})^2} |E_0|^2 + \frac{|k_1| Y\sigma}{8\pi\rho c_p} \frac{cq_1 \mathcal{H}_1 [R]_0 \sigma_y \Delta_0}{2\hbar\omega_0} \frac{\chi\gamma}{v^2} \times \qquad (16)$$
$$\times \frac{\Omega-\Omega_{МБ}}{(\Omega-\Omega_{МБ})^2+(\delta\Omega_{МБ})^2} |E_0|^2,$$

where $2\delta\Omega_{МБ}=\Gamma q^2$ is the halfwidth of the thermal Mandelstamm-Brillouin scattering [11].

The first term in (16) is caused by electrostriction and describes the Mandelstamm-Brillouin scattering spectrum. The second and third terms describe the scattering spectrum on ultrasonic waves excited by chemical reactions. On the basis of the fact that the electromagnetic field influences the medium through heat release, the scattering spectrum (just as from the scattering effect of stimulated thermal scattering on VRMB [8]) contains symmetric and antisymmetric parts with respect to $\Omega_{МБ}$.

Let us denote the first term in (16) by $g_{МБ}(\Omega)$, and the second by $g_x(\Omega)$, and the third by $g'_x(\Omega)$. The values of $g_{МБ}(\Omega)$ and $g_x(\Omega)$ reach the maximum value where $\Omega=\Omega_{МБ}$. Here they are equal to

$$g_{МБ} = \frac{|k_1| Y'\beta_s}{32\pi n^2} \frac{\Omega_{МБ}}{\delta\Omega_{МБ}} |E_0|^2; \qquad (17)$$

$$g_x = \frac{|k_1| Y\sigma}{8\pi\rho c_p} \frac{cq_1 \mathcal{H}_1 [R]_0 \sigma_y \Delta_0}{2\hbar\omega_0} \frac{1}{\Omega_{МБ}\delta\Omega_{МБ}} |E_0|^2. \qquad (18)$$

The value of $g'_x(\Omega)$ reaches the maximum value when $\Omega=\Omega_{МБ}+\delta\Omega_{МБ}$:

$$g'_x = \frac{|k_1| Y\sigma}{8\pi\rho c_p} \frac{cq_1 \mathcal{H}_1 [R]_0 \sigma_y \Delta_0}{2\hbar\omega_0} \frac{\chi\gamma}{2v^2} \frac{1}{\delta\Omega_{МБ}} |E_0|^2. \qquad (19)$$

Comparing g_x and g'_x, we see that the ratio $g'_x/g_x=\gamma\chi\Omega_{МБ}/2v^2=\gamma\chi|q|/2v$ reaches the maximum value for backscattering ($\theta=\pi$). However, even in this case, as a rule, it is much less than one. For example, for CO_2, $g'_x/g_x \sim 0.2$. For angles $\theta<\pi$, this ratio is still less; therefore g'_x in the majority of cases makes a small contribution to the total amplification coefficient and can be neglected for the estimates of $g(\Omega)$.

Now let us compare g_x and $g_{МБ}$. Their ratio will be represented in the form

$$\frac{g_x}{g_{МБ}} = \frac{2\sigma n^2 v^2 c}{\rho c_p (\partial\varepsilon/\partial\rho)_T} \frac{q_1}{\hbar\omega_0} \mathcal{H}_1 [R]_0 \sigma_y \Delta_0 \Omega_{МБ}^{-2}. \qquad (20)$$

We shall substitute the characteristic values for the standard gas mixture (the pressure of the working gas n-C_3F_7I was 0.03 atmospheres, the buffered gas CO_2 was 0.47 atmospheres): $v \sim 2.5 \cdot 10^4$ cm/sec, $\rho \sim 10^{-3}$ g/cm^3, $c_p \sim 0.2$ cal/g-deg, $\Upsilon \sim 9 \cdot 10^{-4}$, $q_1 = 3.8 \times 10^{-19}$ joule, $\hbar\omega_0 = 1.5 \cdot 10^{-19}$ joules, $\varkappa_1 [R]_0 \sim 10^5$ sec^{-1}, $\sigma_y \Delta_0 \sim 10^{-1}$ cm^{-1} (the unsaturated amplification coefficient). As a result, we obtain $g_x/g_{MB} \sim 4.2 \cdot 10^{17} \Omega_{MB}^{-2}$. During backscattering ($\theta = \pi$) $\Omega_{MB} \sim 2.5 \cdot 10^9$ sec^{-1}, the ratio $g_x/g_{MB} \sim 7 \cdot 10^{-2}$ and the primary contribution to $g(\Omega)$ is made by the Mandelstalm-Brillouin scattering. On the contrary, for forward scattering ($\theta \sim 1$-10 mradians) $\Omega_{MB} \sim 10^6$ to 10^7 sec^{-1}, and the ratio $g_x/g_{MB} \sim 4 \cdot 10^5$ to $4 \cdot 10^3$. Consequently, in this case the scattering on the ultrasonic vibrations of the medium caused by chemical reactions is many times more effective than the Mandelstamm-Brillouin scattering. Let us estimate what amplification coefficients can be achieved here. Let us denote by G_x the ratio $g_x/\hbar\omega_0 I_0$:

$$G_x = \frac{|k_1| Y \sigma}{2n^2 \rho c_p} \frac{q_1}{\hbar\omega_0} \varkappa_1 [R]_0 \sigma_y \Delta_0 \frac{1}{\Omega_{MB} \delta\omega_{MB}}. \qquad (21)$$

If we take $\theta = 10^{-2}$ radians, then $\Omega_{MB} = 1.25 \cdot 10^7$ sec^{-1}, and $\delta\Omega_{MB} = 2.13 \cdot 10^4$ sec^{-1}. Here $G_x \sim 10$ cm/Mwatt, which is approximately 10^2 to 10^3 times larger than the amplification coefficient for stimulated Mandelstamm-Brillouin scattering in compressed gas [12] and liquids [13]. This value of G_x was obtained under the assumption that the width of the spectrum of the exciting radiation $\delta\omega_0 \ll \delta\Omega_{MB}$. In reality, this condition, as a rule, is not satisfied. However, in references [12, 14-16] it is demonstrated that on excitation by steady-state pumping with a wide spectrum, the threshold of the stimulated Raman scattering and the Mandelstamm-Brillouin scattering is in practice the same as for the narrow-band spectrum even when $\delta\omega_0 \gg \delta\Omega_{MB}$ if the length of the scattering medium $\ell \lesssim 2\pi c/\delta\omega_0$. On satisfaction of this condition obviously also in the investigated form of scattering the value of G_x for wide-band pumping is maintained at a level of ~10 cm/Mwatt.

Let us note another peculiarity of the well-investigated scattering. It is connected with saturation of the amplification coefficient of the laser transition $\kappa_0 = \sigma_y \Delta_0$. Actually, in the case of uniform saturation of the luminescence line as is known, $\kappa_0 = \sigma_y F \tau_1 / [1 + (1 + g_2/g_1) \sigma_y \tau_1 I_0]$. In iodine lasers $\tau_1 \sim 10^{-4}$ sec, and the intensity $\hbar\omega_0 I_{sat} = \hbar\omega_0 / (1 + g_2/g_1) \times \sigma_y \tau_1 \sim 10^3$-$10^4$ watts/cm^2. If $I_0 \gg I_{sat}$, then $\kappa_0 \simeq F/I_0$ and g_x assumes the form

$$g_x = \frac{|k_1| Y \sigma}{2n^2 \rho c_p} q_1 \varkappa_1 [R]_0 F \frac{1}{\Omega_{MB} \delta\Omega_{MB}}, \qquad (22)$$

that is, g_x is proportional to the pumping rate to the upper laser levels of atomic iodine. This agrees with the experimental data which indicate that the occurrence of small-scale optical nonuniformities begins with defined pumping levels [1, 2]. Let us note that the relation (22) was obtained under the assumption that $I_{sat} \ll I_0 \ll \Omega_{MB}/\sigma_y$. The behavior of g_x with further increase in I_0 requires separate investigation.

Let us also note that the relation of the electromagnetic field to the nonlinear medium realized through heat release must also lead to scattering of the type of stimulated thermal scattering. However, the investigation of this phenomenon requires a more detailed analysis of the equations (12).

In conclusion, the authors express their appreciation to I. I. Sobel'man, V. A. Alekseyev and V. N. Netemin for useful discussion and valuable remarks.

BIBLIOGRAPHY

1. Borovich, B. L.; Zuyev, V. S.; Katulin, V. A.; Nosach, V. Yu.; Nosach, O. Yu.; Startsev, A. V.; Stoylov, Yu. Yu. KVANTOVAYA ELEKTRONIKA [Quantum Electronics], No 2, 1975, p 1282.

2. Zuyev, V. S.; Netemin, V. N.; Nosach, O. Yu. KVANTOVAYA ELEKTRONIKA, No 6, 1979, p 875.

3. Alekhin, B. V.; Borovkov, V. V.; Lazhintsev, B. V.; Nor-Arevyan, V. A.; Sukhanov, L. V.; Ustinenko, V. A. KVANTOVAYA ELEKTRONIKA, No 6, 1979, p 1948.

4. Kuznetsova, S. V.; Maslov, A. I. KVANTOVAYA ELEKTRONIKA, No 5, 1978, p 1587.

5. Starunov, V. S.; Fabelinskiy, I. L. UFN [Progress in the Physical Sciences], No 98, 1969, p 441.

6. Shubert, M.; Vil'gel'mi, B. KVANTOVAYA ELEKTRONIKA, No 1, 1974, p 1056.

7. Zaytsev, G. I.; Kyzylasov, Yu. I.; Starunov, V. S.; Fabelinskiy, I. L. PIS'MA V ZHETF [Letters to the Journal of Experimental and Theoretical Physics], No 6, 1967, p 802.

8. Starunov, V. S. ZHETF [Journal of Experimental and Theoretical Physics], No 57, 1969, p 1012.

9. Zuyev, V. S.; Katulin, V. A.; Nosach, V. Yu. Nosach, O. Yu. ZHETF, No 62, 1972, p 1673.

10. Borovich, B. L.; Zuyev, V. S.; Katulin, V. A.; Mikheyev, L. D.; Nikolayev, F. A.; Nosach, O. Yu.; Rozanov, V. B. ITOGI NAUKI I TEKHNIKI. SER. RADIOTEKHNIKA [Results of Science and Engineering. Radio Engineering Series], Moscow, Izd-vo VINITI, Vol 15, 1978, pp 157, 158.

11. Landau, L. D.; Lifshits, Ye. M. ELEKTRODINAMIKA SPLOSHNYKH SRED. [Electrodynamics of Continuous Media], Moscow, GIFML, 1959, p 501.

12. Ragul'skiy, V. V. TRUDY FIAN [Works of the Physics Institute of the USSR Academy of Sciences], No 85, 1976, p 3.

13. Gangardt, M. G.; Grasyuk, A. Z.; Zubarev, I. G. KVANTOVAYA ELEKTRONIKA, No 6, 1971, p 118.

14. Bocharov, V. V.; Grasyuk, A. Z.; Zubarev, I. G.; Mulikov, V. F. ZHETF, No 56, 1969, p 430.

15. D'yakov, Yu. Ye. PIS'MA V ZHETF, No 11, 1970, p 362.

16. Zubarev, I. G.; Mikhaylov, S. I. KVANTOVAYA ELEKTRONIKA, No 5, 1978, p 2383.

10845
CSO: 1862

UDC 621.375.82+533.601

CO_2 GAS DYNAMIC LASER USING THE COMBUSTION PRODUCTS OF C_2H_2-CO-N_2O-N_2 MIXTURES

Moscow KVANTOVAYA ELEKTRONIKA in Russian Vol 7, No 12, Dec 80 received 13 May 80 pp 2635-2637

[Article by N. V. Yevtyukhin, Institute of Chemical Physics of the USSR Academy of Sciences, Chernogolovka]

[Text] The amplification coefficients K_0 were measured in a CO_2 gas dynamic laser using the combustion products of C_2H_2-pCO-$(5+n)N_2O$-mN_2 mixtures. For $T_0 \approx 1600$-2000 K values of $K_0 \approx 1$ m^{-1} were obtained. The possibility of using fuel versions of the type of C_2H_2-$3N_2O$-mN_2 in gas dynamic laser systems with selective excitation of the working gas was indicated.

For high operating efficiency in the CO_2-gas dynamic lasers it is necessary that the working medium contain a large quantity of molecular nitrogen (80-95 molecular %), and that it be heated to high stagnation temperature ($T_0 \geq 1500$ K [1, 2].

For many widespread types of fuel with C, H, O, N-elemental compositions these two requirements are frequently alternative. Thus, in the continuous CO_2-gas dynamic lasers which have set records with respect to power level and which operate on nitrogen-diluted products of combustion of carbon monoxide in the air [3, 4-6], the molecular nitrogen is present in the composition of the working medium in amounts close to optimal (85-90 molecular %), but the relatively low stagnation temperature (1100-1500 K) attainable in this case limits the efficiency of the laser and its energy possibilities. One of the methods of increasing the energy characteristics of the laser is connected with preliminary heating of the nitrogen added to the composition of the combustion products. By heating the nitrogen to 800-1000 K, it is possible to increase the stagnation temperature in the gas dynamic laser on combustion of carbon monoxide to 2000-2200 K, and to achieve an increase in the maximum available vibrational output energy by 50% [4,5]. However, the use of additional heating elements in the support system of the gas dynamic lasers leads to complication of its structural design. Another direction on the path of increasing the stagnation temperature is selection of new high-enthalpy lasing compositions of the mixtures for the gas dynamic lasers and directional combination of already known combustible and oxidizing components of fuels. In the gas dynamic lasers operating on the combustion products of gas mixtures, the replacement of the oxygen by nitrous oxide N_2O permits a significant step to be taken in this direction. The theoretical analysis of the use of N_2O as the oxidizing agent in combination with CO and C_6H_6 is the subject of

references [7, 8]. Reference [9] reports stimulated emission in a gas dynamic laser with an explosion chamber in which detonation of the gas mixtures $CO-N_2O-He$ was realized. The experimental investigation of the mechanism of the formation of population inversion in the expanding products of combustion of $CO-H_2-N_2O$ mixtures diluted with nitrogen, argon or helium was carried out in [10, 11]. A number of experimental and theoretical results with respect to the use of high-temperature field components in gas dynamic lasers are presented in the survey [12].

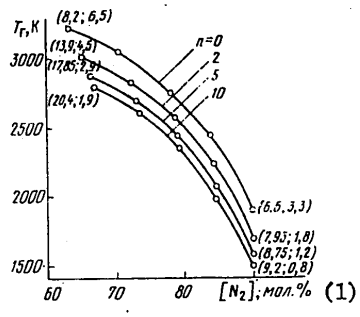

Adiabatic flame temperature of fuel mixtures $C_2H_2-nCO-(5+n)N_2O-mN_2$ as a function of the molecular nitrogen concentration in the combustion products; the equilibrium concentrations of carbon dioxide and water vapor are indicated, respectively.

Key:
1. molecular %

The application of acetylene (or benzene) as the basic fuel component instead of carbon monoxide in fuel combinations in which nitrous oxide is used as the oxidizing agent permits a noticeable increase in the total enthalpy of the laser mixtures. In turn, the joint use of acetylene and carbon monoxide offers the possibility of obtaining the required proportions between the carbon dioxide gas and water vapor molecules in the components of the combustion or explosion products. In this paper a study is made of the fuel combinations of the type $C2H2-pCO-(5+n)N_2O-mN_2$. The thermodynamic calculation of the values of the adiabatic flame temperature as a function of the nitrogen content in the combustion products with a given family of mixtures is presented in the figure. It is obvious that even for 90% concentrations of nitrogen in the combustion products temperatures of 1500-1900 K can be reached. A small reduction in the N_2 concentration to 85 molecular % permits the combustion temperature to be raised to 2000-2500 K. Let us note that the achievement of this successful combination -- high combustion temperature and high nitrogen concentration in the working medium -- makes it possible to use fuel versions of the type $C_2H_2-N_2O-N_2$ not only in the ordinary gas dynamic laser systems with preliminary mixing of the molecular components of the laser mixture, but also in hybrid systems in which the principle of selective thermal excitation of the working gas is used [13]. For such gas dynamic lasers it would be expedient to increase the ratio of the combustible to the oxidizing agent, that is, to use mixtures of $C_2H_2-3N_2O-mN_2$,

on combustion of which basically molecules of the exciting gas (N_2, CO) are formed with small addition of water vapor and hydrogen.

(1) Состав	(2) Топливная смесь	(3) $T_г$, K	(4) Основные компоненты продуктов сгорания, мол. % N_2	CO_2	H_2O	O_2	CO	NO	(5) $K_{0,m}$, $м^{-1}$	(6) $K_{0,т}$, $м^{-1}$	(7) W_m, Дж/г
1	$C_2H_2 - 1,5CO - 6,5N_2O - 20N_2$	2450	84,7	9,4	3,0	0,8	1,2	0,5	0,70	0,87	34,1
2	$C_2H_2 - 4CO - 8N_2O - 32N_2$	2150	85,1	10,7	2,0	—	2,1	—	0,92	0,86	33,5

Key:
1. Composition
2. Fuel mixture
3. T_g, K
4. Basic components of the combustion products, molecular %
5. K_0, m^{-1}
6. $K_{0,t}$, m^{-1}
7. W_m, joules/g

The two fuel versions presented in the table were tested in a gas dynamic laser operating in the quasi-steady-state mode by the ordinary system using the combustion products of gas mixtures [14, 15]. After initiation of the reaction by an igniter in the precombustion chamber 3 liters in volume, fast combustion of the fuel mixtures took place with characteristic time in the interval of 10^{-2} to 10^{-1} sec. The transition of the combustion to detonation was not observed.

The amplification coefficients K_0 were measured for the case of expansion of the combustion products through a plane, shaped nozzle with height of critical cross section of 0.03 cm, degree of expansion 50 and width 40 cm. The probing point of the active medium was at a distance of 5.3 cm from the critical cross section of the nozzle. The method of measuring K_0 and processing the experimental data is described in [14]. In the table the maximum values of the amplification ($K_{0,m}$) obtained in the experiments with the given mixtures are presented. These maximum values of $K_{0,m}$ correspond to stagnation parameters: $T_0 \approx 1600$-1700 K and $p \approx 10$-13 atm. The amplification coefficients which were recorded for higher values of the stagnation parameter ($T \approx 2000$ K, $p \approx 20$ atm) differed from the ones presented in the table by a total of 10%. The partial optimization of the nozzle parameters which consisted in increasing the degree of expansion to 75 and contraction of the height of the critical cross section to 0.02 cm promoted the fact that for composition 2 K_0 was measured stably at a level of 1 m^{-1} in the stagnation temperature range of 1800-2000 K. In the last columns of the table, the theoretical values of the amplification $K_{0,т}$ and the maximum available vibrational energy output obtained using the calculation method discussed in [16, 17] are presented for comparison.

The presented results experimentally confirmed the possibility of achieving high values of $K_0(\geq 1\ m^{-1})$ for stagnation temperatures of $\sim$2000 K in gas dynamic lasers using combustion products, and they also indicate the expediency of further selection of the high-enthalpy fuel components with high nitrogen content and searching for optimal versions of their use in the CO_2-gas dynamic lasers.

The author is grateful to S. V. Kulikov for assistance in performing the calculations and to G. B. Manelis and A. P. Genich for useful discussion.

BIBLIOGRAPHY

1. Konyukhov, V. K. KVANTOVAYA ELEKTRONIKA [Quantum Electronis], No 4, 1977, p 1014.

2. Konyukhov, V. K. TRUDY FIAN [Works of the Physics Institute of the USSR Academy of Sciences], No 113, 1979, p 50.

3. Klass, P. AVIATION WEEK, Vol 97, No 8, 1972, p 32.

4. Lundell, J. H.; Otten, L. J.: Dickey, R. R. AIAA PAPER, No 75-177.

5. Launders, R. C.; Otten, L. J. AIAA PAPER, No 76-58.

6. Vagin, Yu. S. TRUDY FIAN, No 113, 1979, p 115.

7. Pallay, B. G.; Zovko, C. T. AIAA PAPER, No 73-1233.

8. Anderson, J. D. ACTA ASTRONAUT, No 2, 1975, p 911.

9. Bokhon, Yu. A.; Davletchin, I. I.; Marchenko, V. M., et al. KRATKIYE SOOBSHCHENIYA PO FIZIKE, FIAN [Brief Reports of Physics, Physics Institute of the USSR Academy of Sciences], No 11, 1972, p 52.

10. Kudryavtsev, N. N. Author's review of candidate's dissertation, MFTI, 1977.

11. Kudryavtsev, N. N.; Novikov, S. S.; Svetlichnyy, I. B. FIZIKA GORENIYA I VZRYVA [Combustion and Explosion Physics], No 3, 1979, p 93.

12. Cassady, P. E.; Pindroh, A. L.; Newton, J. E. AIAA J., No 17, 1979, p 845.

13. Kroshko, V. N.; Soloukhin, R. I. DAN SSSR [Reports of the USSR Academy of Sciences], No 211, 1973, p 829.

14. Yevtyukhin, N. V.; Genich, A. P.; Yudanov, A. A.; Manelis, G. B. KVANTOVAYA ELEKTRONIKA, No 5, 1978, p 1013.

15. Yevtyukhin, N. V.; Genich, A. P.; Manelis, G. B. FIZIKA GORENIYA I VZRYVA, No 4, 1978, p 36.

16. Genich, A. P.; Yevtyukhin, N. V.; Kulikov, S. V.; Manelis, G. B.; Solov'yeva, M. Ye. PMTF [Applied Mathematics and Technical Physics], No 1, 1979, p 34.

17. Genich, A. P.; Kulikov, S. V.; Manelis, G. B. PMTF, No 4, 1979, p 11.

10845
CSO: 1862

UDC 539.1

KINETIC PROCESSES IN GASES, AND THE MOLECULAR LASER

Moscow KINETICHESKIYE PROTSESSY V GAZAKH I MOLEKULYARNYYE LAZERY in Russian 1980 (signed to press 28 Jul 80) pp 2-11

[Annotation, preface, introduction and table of contents from book "Kinetic Processes in Gases, and the Molecular Laser", by Boris Fedorovich Gordiyets, Aleksey Iosifovich Osipov and Leonid Aleksandrovich Shelepin, Izdatel'stvo "Nauka", 3450 copies, 512 pages]

[Text] The book is devoted to the theory of kinetic processes in gases and low-temperature plasma, and to an analysis of physical processes in molecular lasers based on this theory. Chapters 1-8 examine basic problems of the theory of relaxation processes in gases, including translational, rotational, vibrational and electronic kinetics of molecules. Considerable attention is given to vibrational kinetics (including vibrational relaxation of anharmonic oscillators), the kinetics of thermal dissociation and laser chemistry. Advances in the kinetics of coherent processes are systematically presented. Chapters 9-13 examine in detail the theory of kinetic processes in molecular lasers based on vibrational-rotational transitions (electric discharge, chemical, gasdynamic), as well as in lasers based on electronic transitions of molecules.

The book is intended for scientists and for graduate and undergraduate students of physics and chemical kinetics, quantum electronics, molecular physics, and also in a variety of related fields such as physics of the atmosphere, plasma physics, and physical gasdynamics. Figures 77, tables 11, references 1316.

Preface

This book deals with the theory of kinetic phenomena in molecular gases and low-temperature plasma, and with the analysis of physical processes in molecular lasers on the basis of this theory. The current stage of science and technology faces physical kinetics with the problem of studying systems far from equilibrium. Such states arise for example under the action of strong electric fields, hard electromagnetic and corpuscular radiation, powerful laser emission and the like. Elaboration of this class of problems has led in essence to the creation of a new field of physical kinetics -- physical kinetics of appreciably nonequilibrium systems.

The development of laser physics has stimulated laser research, and has itself been based on advances in the kinetics of appreciably nonequilibrium systems. The study

of the interaction of laser radiation with molecular gases and the analysis of physical processes in the active medium of molecular lasers (electric-discharge, gasdynamic, chemical, plasma) would not be possible today without consideration of advances in physicochemical kinetics. Moreover, the kinetics of molecular processes in lasers can be treated as part of physicochemical kinetics.

However, at present there is no monograph that takes a unified standpoint in the presentation of the kinetics of relaxation processes and specific mechanisms of the operation of molecular lasers. The authors of this book have attempted to fill this gap in the literature.

The contents of the book can be nominally divided into two parts. The first part (chapters 1-8) deals with major problems of the theory of relaxation processes in gases, including translational, rotational, vibrational and electronic kinetics of molecules. Considerable emphasis is given to the special fields of vibrational kinetics, the kinetics of thermal dissociation and laser chemistry. Advances in the kinetics of coherent processes are systematically presented for the first time in chapter 8. The second part of the book (chapters 9-13) is a detailed examination of the theory of kinetic processes in molecular lasers based on vibrational-rotational transitions (electric-discharge, chemical, gasdynamic), and also in lasers based on electronic transitions of molecules.

In writing the book, the authors did not have the purpose of analyzing experimental data. References to experimental research are cited only to illustrate general concepts or for the sake of completeness of the presentation. The monograph is arranged in such a way as to be of use to an extensive class of readers. It is intended first of all for persons specializing in physical and chemical kinetics, quantum electronics, molecular physics, and also in a variety of related fields such as physics of the atmosphere, plasma physics, physical gasdynamics and so on.

The work of the authors in writing the book was distributed as follows: chapters 1, 2, 3, 5 were written by A. I. Osipov; chapters 4, 6, 10, 12 were written by B. F. Gordiyets; chapters 7, 8, 9, 13 were written by L. A. Shelepin; chapter 11 was written by Yu. A. Kulagin and L. A. Shelepin.

The instigator of this work was Academician R. V. Khokhlov. He has been of great assistance and support, and the authors pay their respects to his memory. The authors also consider it their duty to thank Ye. V. Stupochenko, I. S. Lakoba, A. V. Masalov, S. A. Reshetnyak and S. I. Yakovlenko for discussing some problems, and also Sh. S. Mamedov for assisting in preparation of the manuscript.

Introduction

Physical kinetics is the basis for description of various irreversible processes, determining their time characteristics, ascertaining methods of action and finding ways to control these processes. At present the most highly developed division of physical kinetics is the kinetic theory of gaseous systems that are close to a state of thermodynamic equilibrium. In this area general methods have been developed for solving kinetic problems, which can be used for example in a detailed investigation of transport phenomena. Things are different in analysis of arbitrarily nonequilibrium systems, because in this case no unified general-purpose method

can be proposed like the Gibbs method or the method of thermodynamically irreversible processes.

At the same time, practical demands have led to the investigation of systems far from equilibrium. The progress of research in this field has had its own specific features. At first the problems of the theory of translational, rotational, vibrational and electronic relaxation were elaborated to a great degree independently of each other, as occasioned by research in shock wave physics, chemical kinetics and plasma physics. On this stage, the theory of kinetic processes in gases and plasma was not connected with the theory of gas lasers. But the initial approach to the problem of setting up a population inversion in the active media of lasers consisted in analyzing only two-level and three-level schemes assuming external pumping to an upper working level and emptying of a lower level. However, this scheme was limited for analyzing the operation of lasers, and it has now become obvious that a theory of lasers, like a theory of the action of laser radiation on gases, cannot be constructed without a detailed investigation of the kinetics of physical processes in the corresponding medium.

In gas lasers the active medium is a nonequilibrium gas with inverse population. Thus the study of physical processes in the active medium of lasers is a job for physical kinetics.

In constructing a kinetic theory of a nonequilibrium gas, the initial equations are the equations of balance for the populations of individual molecular states. In formulating and solving such equations, the main difficulty is that molecular collisions, like laser radiation lead, generally speaking, to excitation of all degrees of freedom -- translational, rotational, vibrational and electronic -- as well as to chemical conversions and ionization. One of the fundamental principles in analyzing such situations is the comparison of characteristic times of energy transfer in molecular systems (hierarchy of characteristic times). It is this approach that enables investigation of such complex systems as molecular gases, enabling isolation of the determining processes from those that play a secondary role or have been already completed in the given phenomenon. The existence of a hierarchy of characteristic times enables formulation within the framework of kinetic equations of a general procedure based on analysis of quasi-steady distributions of the populations formed in the relaxation process. These distributions are typical of multilevel systems with different relaxation times and permit description of the temporal evolution of the systems by using a small number of time-dependent parameters.

In most cases the approach indicated above ensures a satisfactory description of the evolution of the system. However, the restriction to the kinetics of populations alone frequently will not work for analyzing intensive and rapidly occurring processes. Under these conditions the particles no longer emerge by themselves, but rather act in concert, displaying properties that are not resident in an isolated particle. The cooperative properties of such states are described by the formalism of the density matrix, and their analysis is the topic of the so-called kinetics of coherent processes, that includes the kinetics of populations as a special case. Thus in studying stimulated emission of lasers in the general case, the electromagnetic field inside the laser cavity, and the active medium should be treated quantum mechanically on the basis of the density matrix, i. e. within the

framework of the kinetics of coherent processes. A similar approach must be used in studying the action of short-duration high-intensity laser emission on a molecular gas.

Thus at the present time there is a close interconnection between the kinetic theory of appreciably nonequilibrium systems and the theory of physical processes in molecular gas lasers. This book can be taken as a first experiment in the combined presentation of this class of questions from a unified standpoint.

Contents

[43-6610]
CSO: 1862

MOLECULAR PHYSICS

UDC 539.1

PROBABILITIES OF OPTICAL TRANSITIONS OF DIATOMIC MOLECULES

Moscow VEROYATNOSTI OPTICHESKIKH PEREKHODOV DVUKHATOMNYKH MOLEKUL in Russian 1980 (signed to press 2 Jun 80) pp 2-8

[Annotation, preface and table of contents from book "Probabilities of Optical Transitions of Diatomic Molecules", by Lyudmila Alekseyevna Kuznetsova, Nikolay Yegorovich Kuz'menko, Yuriy Yakovlevich Kuzyakov and Yuriy Aleksandrovich Plastinin, Izdatel'stvo "Nauka", 2600 copies, 319 pages]

[Text] The monograph represents the state of the art in experimental and theoretical research on the probabilities of optical transitions of diatomic molecules. Practical recommendations are given on the most reliable values of the strengths of electronic transitions, their dependences on r-centroids, oscillator strengths, lifetimes of electronically excited states, Franck-Condon factors and some other radiation characteristics for approximately 300 diatomic molecules. The absorption cross sections over a wide temperature range (from 500 to 12,000 K) are calculated for a large number of transitions of practically important molecules. This is the first Soviet publication of its kind. Figures 49, tables 23, references 1245.

Preface

Quantitative studies of the radiative and absorptive processes that take place in heated gases and plasma are impossible without a knowledge of such physical characteristics as the oscillator strengths of electronic transitions of atoms and molecules, the matrix elements of dipole moments, lifetimes of excited states, the Franck-Condon factors, absorption cross sections of free-free and free-bound transitions of electrons in a field of atoms and molecules, and also the spectral coefficients of absorption of individual components that depend on them and those of the entire gas medium (plasma).

In connection with the development of new high-velocity, high-temperature and high-pressure techniques and equipment, and also in connection with the growing demands of astrophysicists, spectroscopists, researchers in radiation and gas dynamics and in plasma diagnosis, the information enumerated above (and especially the probabilities of optical transitions) have now taken on first-rank importance. And this is apparently just the reason for the exponential explosion of publications on the probabilities of transitions that began in the mid sixties and has not yet abated. The number of publications is so great, that it is now nearly impossible to find one's way through the enormous volume of information strewn through numerous periodical publications without generalizing surveys, reference books or special monographs.

Detailed information on the probabilities of transitions and lifetimes of excited states for atoms are systematized in various well-known reference books and monographs [Ref. 1-3, 44, 225]; however, there are no analogous publications for diatomic molecules in either the Soviet or non-Soviet literature. The useful surveys of Soshnikov [Ref. 4], and of Orenberg and Antropov [Ref. 6] are now considerably out of date. A series of later works in the Soviet Union [Ref. 5, 105-107] and elsewhere [Ref. 7, 8] deals mainly with the components of highly heated air. Some generalizing works came out in subsequent years [Ref. 18-21, 49, 50, 188]; however, not one of them can pretend to completeness in systematization of data. The recommendations of Hefferlin et al. [Ref. 20] practically disregard the research of the last decade. The survey by Hsu and Smith [Ref. 21] considers data only for molecules that are of astrophysical interest. A two-volume reference work [Ref. 49, 50] offers detailed spectroscopic information on electronic spectra and molecular states of diatomic molecules; however, the data given there on the probabilities of electronic transitions is fragmentary and sporadic.

The most complete analysis of the results of experimental research on the probabilities of optical transitions of diatomic molecules was given in the surveys of Ref. 9 and 10, and it was the authors' experience in working for a number of years on systematizing transition probabilities that convinced us of the necessity of writing a monograph utilizing and generalizing the latest advances in experimental research and the results of the present-day theory of radiative transitions. The authors have tried insofar as possible to cover all research and to incorporate into the book the most important results published up to 1978 inclusive. The data available in the literature on the probabilities of molecular transitions are often contradictory not only because of difficulties in experimental determination, but also due to the lack of a unified viewpoint on a number of such theoretical ideas as the moment of an electronic transition and the normalization of Hanle-London factors. In this connection the problems of determining transition probabilities and lifetimes are considered in the book in their broad aspect both from the standpoint of the whole set of recommended values, and from the standpoint of theoretical notions of transition probabilities and methods of experimental determination.

The book consists of five chapters and numerous tables.

The first chapter is devoted to the characteristics of energy levels and an examination of the structure of vibronic-rotational spectra of diatomic molecules. The authors considered it advisable to give a condensed presentation of the major results of the quantum mechanical consideration of the structure of diatomic molecules. This information is necessary for a clear understanding of the problems involved in calculating the positions of energy levels and the matrix elements of transitions. Using selection rules in conjunction with the given formulas, the reader has the opportunity of calculating the position of spectral lines in the vibronic-rotational spectrum independently without resort to additional specialized literature. A more detailed exposition of the problems treated in the first chapter can be found in a number of monographs [Ref. 12, 15, 25, 26, 32].

The second chapter deals with the theory of intensities of vibronic-rotational spectra of diatomic molecules, analyzes major theoretical concepts on optical transition probabilities, assumes a unified definition of the moment of an electronic transition, and the resultant definition of a universal rule of sums for the

Hanle-London factors for spin-allowed and spin-forbidden electronic transitions. Since there are no reliable methods at present for calculating the probabilities of electronic transitions, these quantities are experimentally determined, using mainly two methods: the method of measuring intensities in spectra, and the method of measuring lifetimes of vibrationally excited states. The chapter discusses the limits of applicability of these two methods, their advantages and disadvantages, and the degree of reliability of the results. An examination is also made of the feasibility of using the r-centroid approximation to interpret intensities in the spectra of diatomic molecules.

The third chapter is devoted to analysis of the state of the art in methods of calculating Franck-Condon factors, and to a systematic exposition of some major techniques that are most widely used in computational practice. Each method is explained up to the level of a rigorous algorithm that is readily translatable to computer language.

Largest in volume is the fourth chapter, since it is here that all factual material is presented on the absolute and relative probabilities of electronic transitions and Franck-Condon factors published in the literature up to 1978 inclusive. Based on criteria developed for practical utilization, recommendations are made on the most reliable values of the strengths of electronic transitions and their dependences on internuclear distance, as well as oscillator strengths, lifetimes of electronically excited states and Franck-Condon factors.

The fifth chapter examines questions of emission and absorption of isolated lines, and gives the results of determination of the optical characteristics of molecules over a wide spectral band based on a general statistical approach to solution of the problem of transmission of radiation in an aggregate of a large number of molecular lines. Original results of the authors are given on calculation of optical characteristics (molecular absorption cross sections and parameters of line density) over a wide temperature range.

The authors hope that the proposed book will make data on transition probabilities accessible to a broad class of specialists working in the area of astrophysics, quantum electronics, plasma chemistry, radiation gasdynamics, plasma diagnosis, quantitative spectral analysis, and will also be of use to graduate and undergraduate students majoring in the corresponding fields. The authors have directed their efforts toward making this monograph convenient for use as a handbook as well. It is for this reason that all the factual material that is discussed and recommended has been systematized in tabular form.

Chapter 1 was written by Yu. Ya. Kuzyakov, chapter 2 by L. A. Kuznetsova, chapter 3 by N. Ye. Kuz'menko, chapter 4 by N. Ye. Kuz'menko and L. A. Kuznetsova, and chapter 5 by Yu. A. Plastinin, although the entire text was repeatedly discussed by all the authors and frequently revised jointly.

The authors were continuously aware of the assistance and support of Rem Viktorovich Khokhlov throughout work on the book.

The authors are sincerely grateful to A. P. Monyakin for direct and active participation in preparing materials used in chapter 4, and also for constructive discussions of a number of sections of other chapters.

The authors sincerely thank G. G. Baula and A. D. Smirnov who did a large series of calculations, the results of which were used in preparing chapters 5 and 4 respectively, and also V. A. Zhizhikina for assistance in putting the manuscript into shape.

Contents

[52-6610]
6610
CSO: 1862

NUCLEAR PHYSICS

APPROXIMATE COMPRESSION THEORY AND DIMENSIONLESS RELATIONS FOR THIN-SHELL TARGETS

Moscow PRIBLIZHENNAYA TEORIYA SZHATIYA I SOOTNOSHENIYA PODOBIYA DLYA TONKIKH OBOLOCHECHNYKH MISHENEY in Russian 1980 (signed to press 19 Dec 79) pp 1-35

[Preprint FIAN-30, "Approximate Compression Theory and Dimensionless Relations for Thin-Shell Targets" by Yu. V. Afanas'yev, Ye. G. Gamaliy, S. Yu. Gus'kov and V. B. Rozanov, Laser Plasma Laboratory, Physics Institute imeni P. N. Lebedev, USSR Academy of Sciences, 100 copies, 35 pages]

[Text] An analytical solution is found for the problem of vaporization and compression of a thin shell in the approximation that steady-state flow in the "corona" adjusts to shell motion with zero lag. The solution implies that the dynamic characteristics of the shell (coefficient of transformation of laser energy to kinetic energy, relative unvaporized mass and velocity of compression) are the same for targets characterized by the same value of the parameter $\alpha = \frac{R_0}{\Delta R_0} \cdot \frac{\rho_{0J}}{\rho_0}$ (ΔR_0, R_0, ρ_0 are the initial thickness, radius and density of the shell, ρ_{0J} is the characteristic density at the sonic point of the corona). These solutions can be used to get dimensionless relations both for compression, and for hydrodynamic instability on the outer boundary of the shell, and to determine the maximum attainable aspect ratio.

The processes of laser heating, evaporation and compression of spherical laser targets have been investigated by numerical simulation on a computer for the most complete description of them [1, 2]. Theoretically, this approach permits consideration of numerous physical processes in the target, detailed description of the properties of the substance and the processes of the interaction of radiation with the substance and, at the same time, it offers quantitative solution of the problem. However, with this approach it is difficult to establish the general laws of the phenomenon and find dimensionless ratios with variation of the scales of the basic parameters. Therefore in a number of papers efforts have been made to solve a simpler problem for determination of a series of mean values (such as temperature and density at the time of maximum compression, and so on) or integral characteristics (the proportion of absorbed energy, hydrodynamic transfer constant, and so on).

In references [1] and [4] estimates were made of the maximum temperatures and density of the gas in targets compressed under hydrodynamic (ablation) conditions. However, in [1] the processes in the "corona" were essentially not investigated when deriving the formula for the degree of compression. In [4] the "corona" was considered isothermal, which is far from reality. A number of papers [3, 6] were devoted to estimates of the density and temperature of the gas during compression under conditions of an "exploding" shell with instantaneous release of energy per unit mass. Let us note that in all the indicated papers the conditions of additional adiabatic compression of the passage of shock waves, equality of the shell and gas pressures and the law of conservation of the energy at the time of collapse of the shell were used to evaluate the degree of gas compression.

In the present paper the compression of a thin ($\Delta R_0 \ll R_0$) shell is investigated under the assumption that the stationary "corona" adjusts to the moving shell "infinitely quickly." In this case the dynamics of the shell are determined by one dimensionless parameter α which depends on the parameters of the target, the laser and the compression conditions. Thus, the dynamic characteristics of the shell -- the laser-to-kinetic energy conversion factor, the relative evaporated mass, compression rate -- turn out to be identical for targets characterized by the same value of the parameter $\alpha=(R_0/\Delta R_0)(\rho_{0J}/\rho_0)$ (here R_0, ΔR_0, ρ_0 are the initial radius, thickness and density of the shell, ρ_{0J} is the characteristic density at the sonic point (the Jouguet corona point). Then under the assumption that the indicated dynamic characteristics do not change for the gas-filled shell (for $\mu_{gas} \ll \mu_{shell}$) the maximum temperature and density of the compressed gas are determined. In addition, it turns out to be possible to define dimensions relations for the development of long-wave disturbances in a thin target.

1. Evaporation and Flight Dynamics of a Thin Shell

Let us consider the processes of flight and evaporation of a thin spherical shell accelerated toward the center under the effect of the jet propulsion of "corona" vapor, which has been formed as a result of the absorption of laser emission near the critical density. If the heating time of the "corona" by means of thermal conductivity $\tau_y \sim (R_{cr}-R_0)^2(\kappa_0 T_{cr}^{5/2}\rho_{cr}(z/M_i))^{-1}$ is much less than the characteristic variation times of the laser pulse τ_{pulse} $E \cdot \dot{E}^{-1}$ and the hydrodynamic time τ_{hydr}

$$\tau_y \ll \tau_{pulse} \sim \tau_{hydr} \tag{1}$$

the flow in the "corona" can be described by a quasistationary approximation [7]. The target is compressed under the effect of pressure applied to the evaporation boundary. Hereafter, we shall consider that the radii of the outer surface of the target R_0 coincide at the evaporation surface.

Let us obtain the equations of motion and evaporation of a shell in the following approximation. Let us divide a shell with initial mass M_0 into two regions separated by the evaporation boundary R_{evap} into the unevaporated part with variable mass M in which the velocity u does not vary with respect to the mass coordinate, and the "corona," the plasma flux in which will be assumed to be steady-state. The distribution of the plasma parameters in the shell is illustrated schematically in Figure 1. The total impulse of the shell will be written in the form

$$J_{total}=4\pi\cdot\int_0^\infty \rho v r^2 dr = J_{evap} - Mu;\quad J_{evap}=4\pi\int_{R_{evap}}^\infty \rho v r^2 dr \tag{2}$$

Differentiating (2) with respect to time and using the equation of Euler and the equation of continuity in spherical coordinates we obtain

$$\frac{dMu}{dt}=4\pi R^2_{evap}\left[p+\rho v\left(v-\frac{dR_{evap}}{dt}\right)\right]-8\pi\cdot\int_0^{R_{evap}} prdr \tag{3}$$

Analogously, for variation of the mass we have, assuming that $\rho\to 0$ for $r\to\infty$

$$\frac{dM}{dt}=-4\pi R^2_{evap}\rho\left[v-\frac{dR_{evap}}{dt}\right] \tag{4}$$

Then we propose, according to [8], that the evaporation boundary is a hydrodynamic discontinuity at which all the conservation laws are satisfied and, in addition, the Jouguet condition is satisfied at this boundary: the evaporation boundary velocity with respect to the expanding corona is equal to the speed of sound.

Assuming that $u>0$ and considering that $-dR_{evap}/dt=u+D$, we obtain the mass conservation law and the Jouguet condition at the evaporation boundary

$$\rho_0 D=\rho(v+u+D)$$
$$u+v+D=c \tag{5}$$

Considering (3), (4), (5), the equations of motion and evaporation of a spherical shell are written in the form (for $u+v>D$)

$$M\frac{du}{dt}=4\pi R^2_{evap}(p+\rho c^2)-8\pi\int_0^{R_{evap}} p\cdot r\cdot dr \tag{6}$$
$$\frac{dM}{dt}=-4\pi R^2_{evap}\cdot\rho\cdot c$$

Here p, ρ, c are the pressure, density and speed of sound at the evaporation boundary, respectively. Now let us express the plasma parameters at the evaporation boundary in terms of the values at the Jouguet point (sonic point),[1] assuming that the flow is steady-state. Then

$$p+\rho c^2 \simeq 2\rho_{Jouguet} v^2_{Jouguet} R^2_{Jouguet}/R^2_{evap} \tag{7}$$

$$\rho c = \rho_{Jouguet} \cdot v_J \cdot R^2_{Jouguet}/R^2_{evap}$$

for a thin ($\Delta R \ll R_{evap}$) shell, inasmuch as when deriving (7) the term

$$8\pi \int_0^{R_{evap}} p \cdot r \cdot dr \simeq 8\pi R^2_{evap} \cdot \Delta R/R_{evap} \cdot \bar{p} .$$

Finally, the equations of motion of a thin spherical shell can be written in the following form

$$M \frac{du}{dt} = 4\pi \cdot 2\rho_J \cdot v^2_J \cdot R^2_J \tag{8}$$

$$\frac{dM}{dt} = -4\pi R^2_J \cdot \rho_J \cdot v_J .$$

The energy flux density at the sonic point is

$$q_J = \rho_J c_J \left(\varepsilon_J + \frac{p_J}{\rho_J} + \frac{c^2_J}{2}\right) = \frac{3\gamma - 1}{2(\gamma - 1)} \rho_J c^3_J = a \rho_J c^3_J . \tag{9}$$

The characteristics of the "corona" in the approximation used depend only on one parameter [7]

$$\gamma_0 = \frac{\kappa_0^{3/4} \dot{E}_\pi}{4\pi \rho_k^{3/4} \cdot R^{11/4}} \left(\frac{M_i}{z}\right)^{21/8} \tag{10}$$

Here κ_0 is the coefficient of electronic thermal conductivity, ($\kappa = \kappa_0 \cdot T_0^{5/2}$), $\dot{E}_\pi$ is the absorbed power of the laser (erg/sec), ρ_k is the critical density, R is the target radius, M_i, z are the mass and the charge of the "corona" ions.

Depending on the value of γ_0, various heating, evaporation and steady-state "corona" flow are realized, and, accordingly, different functional dependence of ρ_J, c_J, R_J on the target and laser pulse parameters. Let us consider two cases: constant power $\dot{E}_\pi = \text{const}$ and constant flux at the critical surface $q_0 = \dot{E}_\pi / 4\pi R^2_M = \text{const}$. Then the plasma parameters at the Jouguet point can be written in the following form [7]:

$$\underline{q_0 = \text{const} \quad \gamma_0 \ll \gamma^*}$$

$$\rho_J = \rho_k, \; c_J = (q_0/a\rho_k)^{1/3} = \text{const}, \; R_J = R_k \tag{11}$$

---

[1] At this point the hydrodynamic velocity of the plasma and the speed of sound coincide.

$\dot{E}_\pi$=const, $\gamma_0 \ll \gamma^*$

$$\rho_J = \rho_k,\ c_J = c_{0J}(R/R_0)^{-2/3};\ c_{0J} = \left(\frac{\dot{E}_\pi}{4\pi R_0^2\, a\rho_k}\right)^{1/3},\ R_J = R_k \tag{12}$$

$\dot{E}_\pi$ = const, $\gamma_0 \gg \gamma^*$

$$\rho_J = \rho_{0J}(R/R_0)^{-11/7},\ c_J = c_{0J}(R/R_0)^{-1/7},\ R_J = 1.2R$$

$$\rho_{0J} = \frac{0.17}{(4\pi)^{4/7}} \frac{\dot{E}_\pi^{4/7} \cdot \kappa_0^{3/7}}{p_0^{11/7}} \left(\frac{M_i}{z}\right)^{3/2};\ c_{0J} = 0.748\left(\frac{\dot{E}_\pi}{\kappa_0 R_0}\right)^{1/7}\left(\frac{z}{M_i}\right)^{1/2} \tag{13}$$

Let us note that for constant flux at the critical density it is not possible to construct a stationary solution for $\gamma_0 \gg \gamma^*$ inasmuch as γ_0 and q_0 must be constant simultaneously, which is impossible. Therefore this case will not be considered hereafter.

As follows from (11) and (13) the density and speed of sound at the Jouguet point are either constants or step functions of the radius, and the scaling factors are a combination of the initial data of the problem. Considering (11) and (12, 13), equations (8) are conveniently written in dimensionless variables

$$\mu = \frac{M}{M_0},\ v = \frac{u}{c_{0J}},\ x = \frac{R}{R_0}$$

and converted to the variable

$$dt = \frac{R_0}{c_{0J}} \cdot \frac{dx}{v},$$

Then the evaporation and flight dynamics of a thin spherical shell are described by the universal system of equations (for $0 \leq x \leq 1$)

$$\mu v \frac{dv}{dx} = -2\alpha \cdot x^{2-(2\beta+\sigma)} \tag{14}$$

$$v \frac{du}{dx} = \alpha \cdot x^{2-(\sigma+\beta)}$$

with the initial conditions

$$v(1) = 0 \tag{15}$$

$$\mu(1) = 1.$$

Above, we denoted $\rho_J = \rho_{0J} \cdot x^{-\sigma}$; $c_J = c_{0J} \cdot x^{-\beta}$,

where σ and β assume the following values

$$q_0 = \text{const},\ \gamma_0 \ll \gamma^*,\ \sigma = \beta = 0 \tag{16}$$

$$\dot{E}_\pi = \text{const} \begin{cases} \gamma_0 << \gamma^*, \ \sigma=0, \ \beta=2/3 \\ \gamma_0 >> \gamma^*, \ \sigma=11/7, \ \beta=1/7 \end{cases}$$

The solutions of system (14) depend on the unique dimensionless parameter

$$\alpha = \nu \frac{4\pi R_0^3 \rho_{0J}}{M_0} = \nu \frac{R_0}{\Delta R_0} \frac{\rho_{0J}}{\rho_0} \tag{17}$$

Here ΔR_0, R_0, M_0, ρ_0 are the initial thickness, radius, mass and density of the target, respectively; ρ_{0J} is the characteristic density at the Jouguet point defined by (11)-(13), ν is the numerical coefficient which varies within the limits of $1 \leq \nu \leq 1.44$ in accordance with the shift of the Jouguet point from the target surface ($\gamma_0 << \gamma^*$, $R_J \sim R_0$) to the maximum distance $R_J = 1.2\ R_0$ ($\gamma_0 >> \gamma^*$). For $\gamma_0 << \gamma^*$ and given characteristics of the laser and the target substance (ρ_k, ρ_0) the variation of α is determined by the value of the aspect ratio $R_0/\Delta R_0$, and it does not depend on the coefficient of thermal conductivity. The dependence on κ naturally arises on going to the thermal conducting conditions of evaporation ($\gamma_0 >> \gamma^*$).

An important dynamic characteristic of the laser-target system is the conversion factor of the absorbed power to the kinetic energy of the unevaporated part of the shell

$$\eta = \frac{Mu^2}{2\int \dot{E}_\pi dt} = \frac{M_0 \cdot c_{0J}^3}{2R_0} \frac{\mu v^2}{\int \dot{E}_\pi \frac{dx}{v}} \tag{18}$$

For $\dot{E}_\pi = \text{const}$ (18) can be written in the form

$$\eta = \frac{1}{2\pi a \nu \alpha} \cdot \frac{\dot{E}_J}{\dot{E}_\pi} \cdot \frac{\mu v^2}{\int \frac{dx}{v}} \tag{19}$$

Here it is designated that $\dot{E}_J = 4\pi R_{0J}^2 \cdot a \rho_{0J} c_{0J}^3 = 4\pi R_{0J}^2 q_J$.

As is known [7], the value of $\dot{E}_J/\dot{E}_\pi = \phi(\gamma_0)$ and it varies within the limits

$$\dot{E}_J/\dot{E}_\pi = \begin{cases} 1 & \gamma_0 << \gamma^* \\ <0.3 & \gamma_0 >> \gamma^* \end{cases} \tag{20}$$

For $\gamma_0 \to \infty$, $\phi(\gamma_0)$ decreases logarithmically. Thus, in the general case the conversion factor is a function of x, α, γ_0.

The analysis of system (14) indicates that for $x \lesssim 1$, $dv/dx < 0$, and finally, $d\mu/dx > 0$ and $\left.\frac{d\mu}{dx}\right|_{x \to 1} \to \infty$. Near $x \geq 0$, the velocity is finite, $\left.\frac{dv}{dx}\right|_{x \to 0} \to 0$, $\left.\frac{d\mu}{dx}\right|_{x \to 0} \to 0$,

$v(x)$ is a monotonically increasing function, and $\mu(x)$ is monotonically decreasing with a decrease in x. With an increase in α, the final value of velocity $v(0)=v_k$ increases by a power law, and the final unevaporated mass $\mu(0)=\mu_k$ approaches zero exponentially. Dividing the second equation of (14) by the first, it is possible to obtain the following relation for the relative evaporated mass

$$\mu = \exp\{-1/2 \cdot \int_1^x x^\beta dv\}. \tag{21}$$

Combining the same equations, we obtain expressions for the derivatives of the kinetic energy of the unevaporated part of the shell

$$\frac{d}{dx}\cdot\frac{\mu v^2}{2} = 2\alpha x^{2-(2\beta+\sigma)}[vx^\beta - 4] \tag{22}$$

and the transformation coefficient

$$\frac{d\eta}{dx} = (2a\mu v)^{-1}\frac{\dot{E}_J}{\dot{E}_\pi}\left[\int\frac{dx}{v}\right]^{-1}\{\alpha\cdot x^{2-(2\beta+\sigma)}(vx^\beta-4) - \frac{\mu v}{\int\frac{dx}{v}}\}. \tag{23}$$

From the last two expressions it follows that the kinetic energy and the transformation coefficient for α less than some α_{lim} reach the maximum for x=o. When $\alpha>\alpha_{lim}$ the maximum is reached at 0 x 1, where with an increase in the point shifts towards the initial position of the shell x_{max} 1.

Initially we obtain the solutions for $\gamma 0 \ll \gamma *$. In the case q_0=const it is easy to obtain exact solutions of the systems analogously to how this was done for the two-dimensional case [8]

$$\mu = e^{-v/2} \tag{24}$$

$$1 + \alpha/6\ (x^3-1) = e^{v/2}(\frac{v}{2}+1)$$

$$\eta = \frac{2}{a}\cdot\frac{\mu \ell n^2 \mu}{1-\mu}$$

The relative unevaporated mass as a function of x for different α and also its value at the time x=0 as a function of are presented in Figure 2. Thus, for the given conditions $\alpha_{lim} \approx 3$, which corresponds to μ_k=0.2. For α=6 the shell evaporates entirely before the time of collapse. The maximum transformation coefficient is 0.41 in accordance with the solution for plane geometry [8]. The maximum transformation coefficient and its value at the time of collapse for x=0 is presented in Figure 3 as a function of the parameter α. In order to illustrate the relations obtained in the specific example, the correspondence between α and $R_0/\Delta R_0$ is presented in the same figure for a neodymium laser and glass shell ($\rho_k 3.3.10^{-3}$, ρ_0=2.5 gcm^{-3}, z=10). It is obvious that the maximum transformation coefficient is reached at $R_0/\Delta R_0 \geq 10^3$, which is inadmissible in practice as a result of the restrictions connected with hydrodynamic instability. In the region of reasonable values of the aspect $R_0/\Delta R_0 \sim 10^2$, the transfer constant is appreciably lower and reaches $\eta \lesssim 0.1$.

For $\dot{E}_\pi$=const when $\gamma_0 \ll \gamma^*$ the approximate solutions can be written in the form

$$v = v_k(1-x^{5/3})^{1/2}, \quad v_k = (12/3\alpha)^{1/2} \tag{25}$$

$$\mu = \exp\{-F(x)\alpha^{1/2}\}, \text{ where } F(x)=0.645\int_1^x \frac{x^{4/3}dx}{(1-x^{5/3})^{1/2}}$$

$$\eta = 0.35\alpha^{1/2}(1-x^{5/3})^{1/2}\exp\{-F(x)\alpha^{1/2}\}$$

The qualitative relations for the dependence of the indicated values on x and α are close to the ones investigated above for the case of q_0=const (see Figures 3, 4). However, the maximum transformation coefficient is reached at $\alpha \approx 2.2$ and it is $\eta_{max} \approx 0.2$. It is significant to note that in the region $\alpha \lesssim 0.2$ corresponding, in practice, to the interesting values of the aspect ratio $R_0/\Delta R_0 \sim 10^2$, the functions $\eta_k(\alpha)$ for the conditions q_0=const and $\dot{E}_\pi$=const are also similar quantitatively. The compression time of the shell calculated using the solutions of (25)

$$t \simeq \frac{R_0}{c_{0J}} \left(\frac{12}{5}\alpha\right)^{-1/2} \arccos x \tag{26}$$

agrees with the results of the numerical experiments and the experimentally measured compression times of the glass shells [9].

Analogously to (25) it is easy to obtain approximate solutions for the case $\dot{E}_\pi$=const, $\gamma_0 \gg \gamma^*$.

$$v \simeq v_k(1-x^{8/7})^{1/2}, \quad v_k = (7/2\alpha)^{1/2} \tag{27}$$

$$\mu = \exp\{-0.81\alpha^{1/2}(1-x^{9/7})^{1/2}\}$$

$$\eta = \frac{\phi(\gamma_0)}{\nu} 0.542(1-x^{8/7})^{1/2}\alpha^{1/2}\mu$$

These solutions give the same qualitative behavior of all the variables as (24) and (25). However, the maximum transfer constant under the conditions of large γ_0 is $\phi(\gamma_0)/\nu \lesssim 0.208$ of the corresponding value under conditions 0 *. The difference in the transformation coefficient is basically related to the factor $\phi(\gamma_0)/\nu$ characterizing the proportion of the absorbed energy reaching the Jouguet surface (or the evaporation boundary).

The coefficient of transformation of absorbed energy to kinetic energy η_k and the relative unevaporated mass of the shell μ_k at the time of collapse are dimensionless integral characteristics of the compression process. Namely, these parameters serve as the basic efficiency indexes of the laser target system determining the magnitude of the maximum temperature and degree of compression of the substance. Using (27), these parameters can be written in the form

$$\mu_k = \exp\{-0.81\alpha^{1/2}\} \tag{28}$$

$$\eta_k = \frac{1.63\phi(\gamma_0)}{a\cdot\nu}\cdot\alpha^{1/2}\mu_k, \quad a=\frac{3\gamma-1}{2(\gamma-1)}$$

Here γ is the adiabatic exponent, $\phi(\gamma_0)$ obtained by numerical integration of the equations of the steady-state "corona" is presented in [14]. Thus, η_k and μ_k are functions of two dimensionless parameters γ_0 and α. Under the given evaporation conditions (selected γ_0) the dependence on α is controlling and the strongest. Let us note that expressions (28) are approximately correct in the entire range of variation of α and γ_0 and can be used to select the optimal laser-target system with respect to the value of η_k or as dimensionless relations in going from one scale of laser and target parameters to another for any given value of η_k. Thus, under the assumption that the evaporation and acceleration of the shell are determined by the pressure at the Jouguet point, the shell characteristics ΔR_0, R_0, ρ_0 (or M_0), $\varkappa_0$, M_1/z and the laser characteristics $\dot{E}_\pi$, ρ_k can be combined in two parameters c_{0J} and α which completely define the stated problem. Here the relative unevaporated mass of the shell $\mu=M/M_0$, and its velocity $v=u/c_{0J}$ are, in practice, universal functions with respect to the radius $x=R/R_0$ in the entire range of variation of γ_0, and they depend on the single dimensionless parameter $\alpha=(R_0/\Delta R_0)(\rho_{0J}/\rho_0)$. The coefficient of transformation of laser energy to kinetic energy of the unevaporated part of the shell, which is the index of efficiency of the laser-target system, has a maximum at $\alpha>1$ equal to 0.2 to 0.4 depending on the heating conditions of the target ($\dot{E}_\pi$=const or q_0=const). Finally, it is possible to point out that the dynamics of shells characterized by identical α are described by the same dimensionless solutions. Physically, the comparison of α for different shells indicates, in particular, the equality of the final unevaporated relative mass at the time of collapse and the transfer constant. The presented solutions can be used for comparison of different numerical and physical experiments and for constructing dimensionless relations using the parameter α.

Let us note that approximate dimensionless relations were obtained in references [11] using a formal analysis of the equations of hydrodynamics, thermal conductivity and absorption of laser radiation for the case of target compression by a peaked pulse and a decelerating absorption coefficient. It is possible to demonstrate that these dimensionless relation [11] can also be obtained under the condition of conservation of the relative evaporated mass for a defined evaporated law.

Thus, the optimal shell targets with respect to the value of the transfer constant are characterized by the parameter $\alpha\gtrsim1$. Let us demonstrate the practical recommendations that this condition can lead to. For example, let us consider a glass shell (ρ_0=2.5 gcm^{-3}, ρ_k=3.33·10^{-3}). Then for the case of small γ_0 ($\rho_k\sim\rho_J$) from the condition $\alpha=(R_0/\Delta R_0)(\rho_k/\rho_0)\sim2$, we have $R_0/\Delta R_0\approx10^3$. Consequently, for the hydrodynamic evaporation conditions (low fluxes, thermal conductivity insignificant), extraordinarily thin shells, the use of which is in practice impossible as a result of the restrictions imposed by the requirements of hydrodynamic stability, lead to the maximum transfer constant.

It is easy to see that there is another way of reaching the maximum transfer constant for the given value of the aspect ratio of the shell and for low laser radiation fluxes when $\rho_{0J} \sim \rho_{cr}$. In this case increasing α to a value corresponding to η_{max} is possible by increasing ρ_{cr}, that is, decreasing the wave length of the heating laser. The physical meaning of this effect is clear — the energy is brought closer to the evaporation boundary. The effect from shortening the wave length can be highly significant. Thus, the conversion from λ_{Nd}=1 micron to the 4th harmonic of the Nd-laser for the above-investigated case of a glass shell leads to the fact that the maximum hydrodynamic efficiency can be reached at $R_0/\Delta R_0 \simeq 1$ [sic]$\simeq 10^2$. The use of the short-wave lasers can make it advantageous to use shells with low aspect ratio.

Inasmuch as the only way to increase the hydrodynamic efficiency for the given aspect ratio consists in increasing ρ_{0J}/ρ_0, the latter can be increased either by lowering the density of the ablator or using ablators with high thermal conductivity, since $\rho_{0J} \sim \kappa_0^{3/8}$ (for $\gamma_0 \gg \gamma^*$). In this case the evaporated part of the shell is advantageously made of material with low z, since $\kappa_0 \sim (z+4)^{-1}$.

2. Calculation of the Gas Density and the Temperature at the Time of Maximum Compression for a Thin Gas-Filled Shell Compressed Under Hydrodynamic Conditions

Consideration of the finite thickness of the shell, its heating by shock waves, hard electrons and compression and also the gas counter pressure lead to a change in nature of motion of the shell. However, as comparison with the numerical calculations indicates, these factors have a weak influence on the final value of the transfer constant and the evaporative mass which are close to the values at the time of collapse already after the shell-gas interface travels a distance of $\sim(1/2)R_0$, where the gas counterpressure is not felt in the motion of the shell. This fact permits the above-obtained results to be used to estimate the maximum densities and temperatures of the compressed gas.

We shall consider compression of the gas-filled shell under hydrodynamic (ablation) conditions for relatively low laser radiation fluxes $q_\ell \simeq 10^{14}$ watts/cm^2, where the entropy introduced into the shell and the gas is basically determined by the shock waves, and the effect of heating by hard electrons is low. For simplicity let us assume that the equations of state of the shell and the gas are ideal gases with different adiabatic exponents. Let the pressure after the front of the first powerful shock wave passing over the shell be equal to the pressure at the sonic point $P_{0s}=P_{0J}$ for the initial value of the radius R_0 and absorbed power E_π. Then the state of the shell after passage of the first wave will be characterized by the following values ("s" is the index referring to the shell characteristics)

$$P_{0s} = P_{0J}, \quad \rho_s = \frac{\gamma_s+1}{\gamma_s-1}\rho_{0s} \tag{29}$$

the entropy

$$\sigma = (P_{0s}/\rho_s^{\gamma_s}).$$

The state of the gas after passage of the shock wave through it can be easily calculated from the decay of the discontinuity at the shell-gas interface

by the known procedure of [12] ("g" is the index distinguishing the gas characteristics),

$$P_g = \frac{2\gamma_s(\gamma_g+1)}{(\gamma_s-1)^2}\,\rho_{0g}\frac{P_{0s}}{\rho_{0s}}\cdot\left[1-\left(\frac{P_g}{P_{0s}}\right)\frac{\gamma_s-1}{2\gamma_s}\right]^2 \tag{30}$$

If $\rho_{0g}/\rho_{0s}\ll 1$, then the speed of the interface is maximal

$$u\simeq\frac{2}{\gamma_s-1}c_{0s},\quad c_{0s}=\gamma_s\frac{P_s}{\rho_{0s}} \tag{31}$$

and the pressure and density of the gas behind the wave are described by the relations

$$\rho_g=\frac{\gamma_g+1}{\gamma_g-1}\rho_{0g} \tag{32}$$

$$P_g\simeq\frac{2\gamma_s(\gamma_g+1)}{(\gamma_s-1)^2}\cdot\frac{\rho_{0g}}{\rho_{0s}}\cdot P_{0s}.$$

The subsequent compression and increase in the entropy of the gas takes place in the shock wave reflected from the center of symmetry. We have estimated the state of the gas behind the reflected wave (the index "Γ"), using the two-dimensional solution of reflection of the shock wave from a rigid barrier [13] under the assumption that the reflected wave is powerful ($p_g u^2 \gg p_{0g}$). Then

$$P_\Gamma=\frac{3\gamma_g-1}{\gamma_g-1}\cdot p_g;$$

$$\rho_{\Gamma g}/\rho_g=\gamma_g/(\gamma_g-1), \tag{33}$$

The increase in entropy even in a very powerful wave is finite [13]

$$\frac{\sigma_\Gamma}{\sigma_g}=\frac{3\gamma_g-1}{\gamma_g-1}\left(\frac{\gamma_g-1}{\gamma_g}\right)^{\gamma_g} \tag{34}$$

thus, for $\gamma_g=5/3$, $\sigma_\Gamma/\sigma_g=1.3$. Assuming that further reflections of the wave do not lead to a noticeable change in entropy, we shall consider the further compression of the gas to be adiabatic. Using (32) and (33), it is possible to obtain the gas characteristics before the stage of complete adiabatic compression, expressed in terms of the initial data

$$\rho_{\Gamma g}=\frac{\gamma_g(\gamma_g+1)\cdot\rho_{0g}}{(\gamma_g-1)^2} \tag{35}$$

$$P_{\Gamma g} = \frac{2\gamma_s(\gamma_g+1)(3\gamma_g-1)}{(\gamma_s-1)^2(\gamma_g-1)} \frac{\rho_{0g}}{\rho_{0s}} p_{0s}$$

Then the maximum gas density is ("m" is the index distinguishing the values at the time of maximum compression)

$$\rho_{mg} = \rho_{\Gamma g}\left(\frac{p_m}{p_{\Gamma g}}\right)^{1/\gamma_3} \tag{36}$$

Substituting (35) in (36) we finally obtain

$$\rho_{mg} = \frac{\gamma_g(\gamma_g+1)}{(\gamma_g-1)^2}\left[\frac{(\gamma_g-1)(\gamma_s-1)^2}{2(3\gamma_g-1)(\gamma_g+1)\gamma_s}\right]^{1/\gamma_g} \rho_{0g}\left(\frac{\rho_{0s}}{\rho_{0g}}\right)^{1/\gamma_g}\left(\frac{p_m}{p_{0s}}\right)^{1/\gamma_g} \tag{37}$$

or for $\gamma_g=5/3$

$$\rho_{mg} = 125\left[\frac{(\gamma_s-1)^2}{\gamma_s}\right]^{3/5} \rho_{0g}\left(\frac{\rho_{0s}}{\rho_{0g}}\right)^{3/5}\left(\frac{p_m}{p_{0s}}\right)^{3/5} \tag{38}$$

An estimate of the maximum mean density of the shell can be made assuming that the entropy in it is introduced only by the first shock wave. The effect of the thermal conductivity and the preliminary heating will be neglected. Then

$$\rho_{ms} = \frac{\gamma_s+1}{\gamma_s-1} \rho_{0s}\left(\frac{p_m}{p_{0s}}\right)^{1/\lambda_s} \tag{39}$$

Let us remember that $p_{0s}\simeq\rho_{0J}c^2_{0J}$ is the pressure at the sonic point of the "corona" (Jouguet point) calculated for the initial target parameters. The equation for determining the maximum pressure p_m will be obtained, assuming that at the time of maximum compression of the gas the target pressure is constant, that is,

$$p_m = p_{mg} = p_{ms} \tag{40}$$

and we shall use the energy conservation law

$$\eta_k E_\pi = E_s + E_g = p_m\left[\frac{M_k}{(\gamma_s-1)\rho_{ms}} + \frac{M_g}{(\gamma_g-1)\rho_{mg}}\right] \tag{41}$$

Here η_k, M_k are the coefficient of transformation of absorbed energy and the unevaporated mass of the shell calculated in section 1 of this paper

$$\eta_k \sim \alpha^{1/2}\cdot e^{-\alpha^{1/2}}, \quad M_0 = M_{0s}\cdot e^{-\alpha^{1/2}}, \quad \alpha = \frac{4\pi R^3{}_0\rho_{0J}}{M_{0s}}$$

Equation (41) is the algebraic equation for determining p_m with coefficients that depend only on the initial data of the problem. It is convenient to write (41) for the variable p_m/p_{0s}, that is, the ratio of the maximum pressure to the pressure in the "corona" (the Jouguet point). In addition, we shall consider the laser pulse with duration no less than the compression time, that is, $\tau_\ell \geq t_k$

Then $E_\pi = \dot{E}_\pi \cdot t_k$, and

$t_k \simeq \frac{R_0}{c_{0J}} \cdot \alpha^{-1/2}$ (see section 1 (26)). Using the indicated expressions and also the fact that

$\rho_{0J} c_{0J}^3 \simeq \frac{E_\pi}{4\pi R_0^2}$, equation (41) can be reduced to the form ($\gamma_g = 5/3$)

$$\frac{p_m}{p_{0s}} = \frac{A_1 (p_m/p_{0s})^{3/5}}{1 + A_2 (p_m/p_{0s})^{3/5 - 1/\gamma_s}} \tag{42}$$

where

$$A_1 = 6\left[\frac{(\gamma_s - 1)^2}{\gamma_s}\right]^{3/5} e^{-\alpha 1/2} (\rho_{0s}/\rho_{0g})^{3/5} \tag{43}$$

$$A_2 = \frac{0.416 \cdot A_1}{\gamma_s + 1} \cdot \frac{\Delta R_0}{R_0}$$

Equation (42) can easily be solved numerically for various values of the parameters A_1 and A_2 and at the same time it is possible to define the maximum densities of the shell ρ_{ms} and the gas ρ_{mg} for different evaporation conditions. Thus, the indicated values depend on ρ_{0s}/ρ_{0g}, γ_s, γ_g, $R_0/\Delta R_0$, α. The dependence on the absorbed power and thermal conductivity is manifested only under the conditions of $\gamma_0 >> \gamma^*$ ($\rho_{0J} \sim \dot{E}_\pi^{11/7} \chi_0^{3/7}$) and affects determination of the proportion of the unevaporated mass of the shell $M_k/M_{0s} = e^{-\alpha 1/2}$. It is simplest to find p_m/p_{0s} in the case of coinciding adiabatic exponents $\gamma_g = \gamma_s = 5/3$.

Then $p_m/p_{0s} = [\frac{A_1}{1+A_2}]^{5/2}$. Let us find the parameters of the gas and the shell in the final stage of compression for a gas-filled glass target similar to the one investigated in the experiment [9]:

$$\rho_{0s}/\rho_{0g} = \frac{2.5}{4.8 \cdot 10^{-3}} = 5.2 \cdot 10^2, \quad \frac{R_0}{\Delta R_0} = 35, \quad \rho_{0J} = \rho_k = 3.3 \cdot 10^3, \ g/cm^3$$

$$\alpha = 4.6 \cdot 10^{-2}$$

Hence, for $\gamma_g = \gamma_s = 5/3$ we have $A_1 = 92.5$; $A_2 = 0.413$ and $p_m/p_{0s} = 1.38 \cdot 10^4$,

$\delta_{mg} = \rho_{mg}/\rho_{0g} = 7.5 \cdot 10^3$, $\delta_{ms} = 1.2 \cdot 10^3$.

The results of the numerical solution of equation (42) for certain values of the parameters A_1 and A_2 are presented in Figure 5. Using these data, it is possible to obtain the compression parameters of the target, the initial characteristics of which are presented above, for the case $\gamma_3=3$. In this case ($A_1=2.4\cdot10^2$, $A_2=1.09$), we have $p_m/p_{0s}=2.5\cdot10^3$; $\delta_{mg}=7\cdot10^3$; $\delta_{ms}=27$. Thus, increasing the effective adiabatic exponent by comparison with 5/3, that is, actually consideration of the contribution of the elastic pressure to the equation of state of the shell, leads to a significant decrease in pressure and maximum density of the shell. The presented data agree qualitatively with the results of the numerical calculations.

From the energy conservation law it is easy to obtain estimates from above for the degree of compression of the gas. Thus, the upper bound

$$\delta_{mg}^{2/3} < 1.9\,\frac{(\gamma_s-1)^2}{\gamma_s}\cdot\frac{R_0}{\Delta R_0}\cdot\frac{M_{0s}}{M_g}\,e^{-\alpha^{1/2}} \tag{44}$$

differs from the previously presented one [1] by the numerical coefficients and more exact calculation of the evaporated mass.

The complete solution for an increase in pressure on compression p_m/p_{0s} as a function of the combined parameters A_1 and A_2 (Figure 5) permits isolation of the dependence on the ratio of the initial densities ρ_{0s}/ρ_{0g} and the aspect ratio $R_0/\Delta R_0$ under the assumption that the proportion of unevaporated mass of the shell $e^{-\alpha^{1/2}}$ is given. Under this assumption it is possible to construct p_m/p_{0s} as a function of the aspect ratio $R_0/\Delta R_0$ for different values of the density ratio ρ_{0s}/ρ_{0g} (Figure 6) and the analogous curves for the maximum degree of compression of the gas $\delta_{mg}=\rho_{mg}/\rho_{0g}$ (Figure 7). From the last figure it is obvious that the function $\delta_{mg}(R_0/\Delta R_0)$ is weaker than follows from the upper bound of (44).

The maximum gas temperature can easily be obtained from the energy conservation law (41)

$$T_{mg} = \frac{(\gamma_g-1)\eta_k E_\pi}{\frac{zk}{m_i} M_g\left[1+\frac{\gamma_g-1}{\gamma_s-1}\frac{M_k}{m_g}\frac{\rho_{mg}}{\rho_{ms}}\right]} \tag{45}$$

The last expression jointly with (37), (39) and (42), defines the dependence of the temperature on the initial target and laser parameters. Using the formulas obtained above for the transfer constant the compression time and the speed of sound in the "corona" it is easy to obtain the maximum temperature as a function of the laser and the target parameters. Under the conditions $\tau_k \lesssim \tau_{laser}$ we have

$$T_m \sim \begin{cases} \dot{E}_\pi^{2/3} R_0^{5/3} \cdot \rho_k^{1/3} M_g^{-1} e^{-\alpha^{1/2}}, & \gamma_0 \ll \gamma^* \\ \dot{E}_\pi^{6/7} R_0^{8/7} \chi_0^{1/7} M_g^{-1} \left(\frac{m_i}{z}\right)^{1/2} e^{-\alpha^{1/2}}; & \gamma_0 \gg \gamma^* \end{cases} \tag{46}$$

Hence, it follows that T_m depends strongly on the absorbed power, and this dependence increases under high flux conditions. The dependence on the thermal conductivity shows up only when $\gamma_0 >> \gamma^*$, and it is weak. Using (45), it is possible to estimate the maximum temperature of deuterium gas compression in a glass shell for the initial parameters given above, and $\dot{E}_\pi = 10^{17}$ ergs/sec, $R_0 = 7 \cdot 10^{-3}$ cm. In this case $T_m \approx 0.6$ kev. Let us note that in the given case the formulas (45) and (46) give the dependence on the initial parameters qualitatively (and for introduction of the numerical coefficients also quantitatively) coinciding with the results of the numerical calculations. Let us emphasize that, in our opinion, the purpose of the above-described approximate theory consists not in replacing the numerical calculation, but in obtaining pure qualitative relations which facilitate the search for the optimal target and permit classification of the results of the numerical and physical experiments.

Let us show how it is possible to use the obtained formulas to select the target leading to the given value of some of the parameters in the final stage of compression. Let the duration and the average power of the laser $\dot{E}_\pi$ be given. We shall find the target of the simplest structure in the form of a single-layer gas-filled shell. Theoretically the optimization is a little more complicated to carry out also for the two-layer shell consisting of an ablator with mass M_a and the nonevaporating part of the shell M_{shell}. In this case the mass of the ablator is selected from the condition that it evaporates completely at the time of maximum compression, that is,

$$M_k = (M_{shell} + M_a) \cdot e^{-\alpha^{1/2}}.$$

When selecting the composition of the single-layer shell which must simultaneously execute the functions of the ablator and the compressing spherical piston, it is necessary to consider that the imposed requirements are contradictory. From the point of view of maximum transfer constant it is advantageous to have a light heat-conducting layer as the evaporated layer (ρ_{0J}/ρ_{0s} is large). For the compressing shell, on the contrary, the gas compression is higher, the greater ρ_{0s}/ρ_{0g}. We shall consider that the initial density ρ_{0s} and the shell material have been selected. It is necessary to determine the radius R_0 and the thickness of the shell ΔR_0 and also the initial density of the gas ρ_{0g} (D_2 or DT). Inasmuch as for a value of the aspect ratio corresponding to the maximum transfer constant it is difficult to satisfy the requirements of symmetric compression, the real value of $R_0/\Delta R_0$ is determined from the arguments of hydrodynamic stability. Let us set $(R_0/\Delta R_0)_{max} \approx 10^2$. Then (for $\gamma_0 << \gamma^*$) the parameter α will be defined

$$\alpha = 10^2 \, \rho_k/\rho_{0s}$$

and at the same time the value of the transfer constant η_k and M_k will be defined. The equation for determining the shell radius will be obtained from the requirement that the duration of the laser pulse be equal to the compression time

$$\tau_\ell = \frac{R_0}{c_{0J}} \cdot \alpha^{-1/2} \rightarrow R_0^{5/3} = \tau_\ell \alpha^{1/2} \frac{4\pi a \rho_k}{\dot{E}_\pi}^{1/3}$$

The missing equation for determining the initial gas density can be obtained by requiring that in the final stage of compression either a defined value of the gas density ρ_{mg}, the inertial confinement parameter $\rho_{mg} R_m$ or the temperature T_m is to be reached.

Thus, for example, for a laser pulse ($\dot{E}_{\pi}=10^{17}$ ergs/cm^3; $\tau_{laser}=2\cdot10^{-9}$ sec) and a glass shell ($\rho_{0s}=2.5$ g/cm^3, $\rho_k=3.3\cdot10^{-3}$ g/cm^3) with the aspect ratio $R_0/\Delta R_0=10^2$ the condition $\tau_{\ell}=\tau_k$ leads to $R_0=1.63\cdot10^{-2}$ cm. Then, in order to obtain the given value of the inertial confinement parameter $\rho_{mg}R_m=\rho_{0s}R_0$, we find that the initial gas density was to be $\rho_{0g}=3.4\cdot10^{-3}$ g/cm^3, and on reaching $T_{mg}=1$ kev it is necessary that $\rho_{0g}\leq5.6\cdot10^{-4}$ g/cm^3.

On the basis of the obtained formulas it is also possible to estimate the target and laser parameters for reaching the physical threshold of thermonuclear reaction. This threshold is determined by the values of the inertial confinement parameter $\rho R\approx0.6$ gcm^{-2} and $T_i=10$ kev. Let us define the laser pulse power and duration, the mass of the DT-mixture for the simplest target consisting of the DT-ice layer and ablator, assuming that $R_0/\Delta R_0=10^2$, and the duration of the laser pulse and the collapse time coincide $\tau_{laser}=\tau_k$. Using the indicated conditions and assuming that $\alpha=0.5$ ($\eta_k=0.14$), we find that

$$R_0=0.1216 \text{ ohm}; \quad \tau_k=\tau_{laser}=6.7\cdot10^{-9} \text{ sec}$$

$$M_{DT}=2.26\cdot10^{-5} \text{ g}; \quad \dot{E}_{\pi}=2.4\cdot10^{13} \text{ watts}; \quad E_{\pi}=1.6\cdot10^{5} \text{ joules}.$$

For calculation of these parameters we assumed that the ablator consists of Be (z=4, A=9), and its mass is comparable to the mass of the DT-mixture. Thus, in order to reach the breakeven condition in the simplest target, a laser energy on the level of hundreds of kilojoules is required.

3. Dimensionless Relations in the Case of Hydrodynamic Instability

Using the above-obtained solutions (25, 27), let us estimate the rate of development of hydrodynamic disturbances at the evaporation boundary. We shall consider the linear stage of development of disturbances, that is, $\Delta k\ll1$ (Δ is the amplitude, k is the wave number of the disturbance), and we shall consider that the disturbance wave length is appreciably greater than the characteristic density gradient $k\ll\nabla\ell n\rho$. Then for estimation of the growth rate of the disturbance it is possible to use the classical Taylor result [10] considering the variation of the acceleration with time

$$\Delta = \Delta_0 \exp\left\{\int_0^t \left(k\frac{du}{dt}\right)^{1/2}dt\right\}. \tag{47}$$

Considering (27), this expression is easily reduced to the form

$$\Delta = \Delta_0 \exp\left\{\left(\frac{kR_0}{2}\right)^{1/2}\int_1^0 \left[-\frac{d\ell n f^2(x)}{dx}\right]^{1/2}dx\right\} \tag{48}$$

where $f(x)=1-x^{8/7}$, $x=R/R_0$. Thus, for any point of the shell ($\Delta R_0\ll R_0$) in the linear approximation the relative amplitude at the time of collapse (x=0) is a universal function of the number of the spherical harmonic of the disturbance

$$n = k\cdot R_0 = \frac{2\pi R_0}{\lambda}.$$

From these conditions it is possible to draw the conclusion that the results of investigating the stability for small target dimensions and laser energy

can be carried over to large targets, using the indicated dimensionless relations.

Hence, it is possible to obtain the initial amplitude of the disturbance as a function of the wave length and aspect ratio if we require that in the maximum compression phase the final disturbance amplitude Δ_k does not exceed 0.1 R_k (R_k is the radius of the shell in the compressed state). Since

$$R_k = \left(\frac{3\,\Delta R_0 R_0^2}{\delta}\right)^{1/3} = 3^{1/3}\cdot R_0\left(\frac{R_0}{\Delta R_0}\right)^{-5/6} \qquad (49)$$

and $\int_1^0 \left[-\frac{d\ell n f^2(x)}{dx}\right]^{1/2} dx \simeq 2$ for $f=1-x^{8/7}$, using (48) and (49) it is easy to find that the condition $\Delta_k(x=0)=0.1\cdot R_k$ can be satisfied if the initial relative amplitude of the disturbance satisfies the expression

$$\frac{\Delta_0}{\Delta R_0} = 0.144\left(\frac{R_0}{\Delta R_0}\right)^{1/6}\cdot e^{-(2kR_0)^{1/2}} \qquad (50)$$

Thus, for example, for $n=kR_0=10$ ($k\cdot\Delta R_0=10^{-1}$) and $R_0/\Delta R_0=10^2$, we have $\Delta_0/\Delta R_0\simeq 4\cdot 10^{-3}$, $\Delta_k/\Delta_0=87$, which agrees satisfactorily with the results of the numerical calculations of [15]. From the above-presented results it follows that for achievement of the symmetric compression of the shells with the aspect ratio $R_0/\Delta R_0=10^2$ the initial amplitude of the low-frequency disturbances must be $\Delta_0/\Delta R_0\leq 10^{-9}$. On going over to a larger aspect ratio $R_0/\Delta R_0=10^3$ the requirement on the magnitude of the amplitude of the low-frequency disturbances increases by ~10 times.

BIBLIOGRAPHY

1. Afanas'yev, Yu. V.; Basov, N. G.; Volosevich, P. P.; Gamaliy, Ye. G.; Krokhin, O. N.; Kurdyumov, S. P.; Levanov, Ye. I.; Rozanov, V. B.; Samarskiy, A. A.; Tikhonov, A. N. PIS'MA V ZHETF [Letters to the Journal of Experimental and Theoretical Physics], No 21, 1975, p 150.

2. Nuckolls, J.; Wood, L.; Thiessen, A.; Zimmerman, G. NATURE, No 239, 1972, p 139.

3. Nuckolls, J. LASER FUSION ANNUAL REPORT LLL, 1976.

4. Brueckner, K. A. NUCL. FUSION, 16, No 3, 1976, p 387.

5. Kidder, R. E. NUCL. FUSION, 14, No 53, 1974, p 707.

6. Ahlborn, B.;Key, M. H. RUTH. LAB REPORT, RL-79-033, 1979; Storm, E. K.; Larsen, J. T.; Nuckolls, J. M.; Ahlstrom, H. G.; Manes, K. R. VCRL Report, 79788, 1977.

7. Afanas'yev, Yu. V.; Gamaliy, Ye. G.; Krokhin, O. N.; Rozanov, V. B. ZHETF [Journal of Experimental and Theoretical Physics], Vol 71, No 2(8), 1976, p 594.

8. Afans'yev, Yu. V.; Gamaliy, Ye. G.; Krokhin, O. N.; Rozanov, V. B. IPM [Institute of Mechanics Problems], No 39, 1975, p 453.

9. Basov, N. G.; Volosevich, P. P.; Gamaliy, Ye. G.; Gus'kov, S. Yu.; Zakharenkov, Yu. A.; Krokhin, O. N.; Rozanov, V. B.; Sklizkov, G. V.; Shikanov, A. S. PIS'MA V ZHETF, No 28, 1978, p 135.

10. Taylor, G. PROC. ROY. SOC., Ser. A, No 201, 1950, p 192.

11. Volosevich, P. P.; Degtyarev, L. M.; Levanov, Ye. I.; Kurdyumov, S. P.; Popov, Yu. P.; Samarskiy, A. A.; Favorskiy, A. P. FIZIKA PLAZMY [Plasma Physics], Vol 2, No 6, 1976, p 883.

12. Zel'dovich, Ya. B.; Rayzer, Yu. P. FIZIKA UDARNYKH VOLN I VYSOKOTEMPERATURNYKH GIDRODINAMICHESKIKH YAVLENIY [Physics of Shock Waves and High-Temperature Hydrodynamic Phenomena], Moscow, Nauka, 1963.

13. Stanyukovich, K. P. NEUSTANOVSHIYESYA DVIZHENIYA SPLOSHNOY SREDY [Nonsteady Motion of a Continuous Medium], Moscow, Nauka, 1971.

14. Gamaliy, Ye. G.; Rozanov, V. B.; Tyurina, N. N.; Tishkin, V. F.; Samarskiy, A. A.; Favorskiy, A. P. PREPRINT IPM [Preprint of the Institute of Mechanics Problems], No 117, 1978.

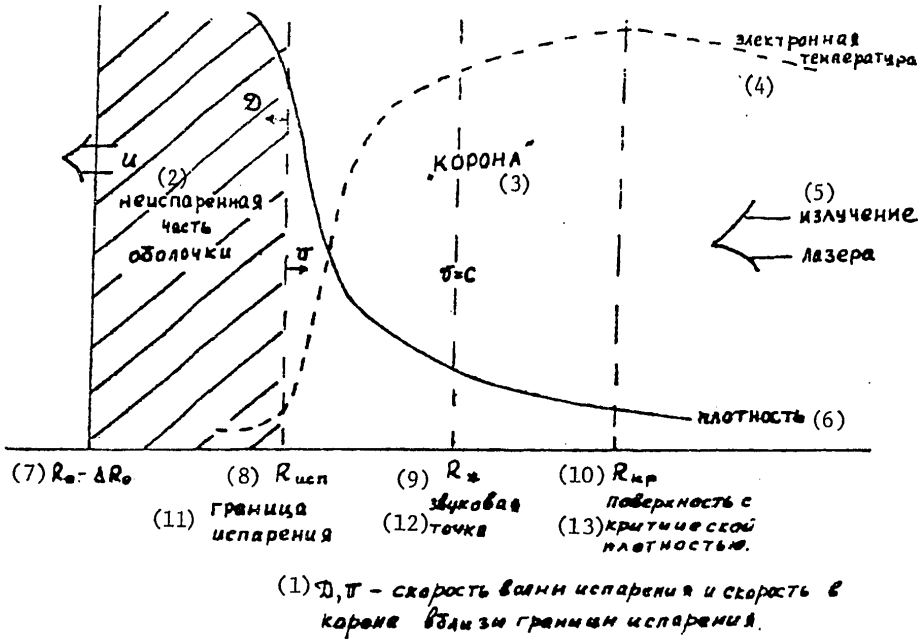

Figure 1. Plasma parameter distribution in a shell under the effect of laser radiation

Key:

1. D, π -- evaporation wave velocity and the velocity in the corona near the evaporation boundary
2. Unevaporated part of the shell
3. "Corona"
4. Electron temperature
5. Laser radiation
6. Density
7. $R_0-\Delta R_0$
8. R_{evap}
9. R_J
10. R_{cr}
11. Evaporation boundary
12. Sonic point
13. Surface with critical density

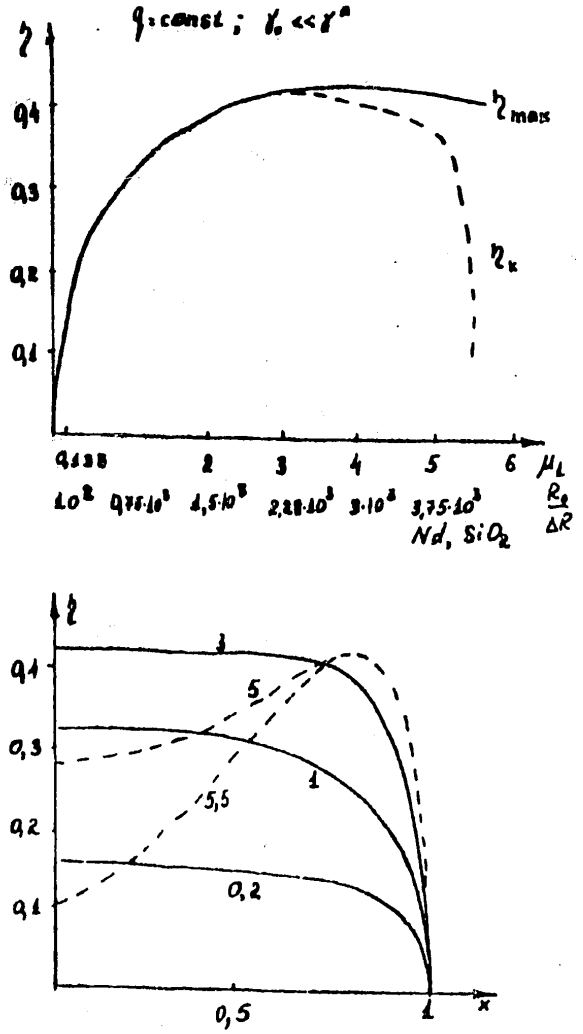

Figure 2. Hydrodynamic efficiency for the case q=const, $\gamma_0 << \gamma^*$

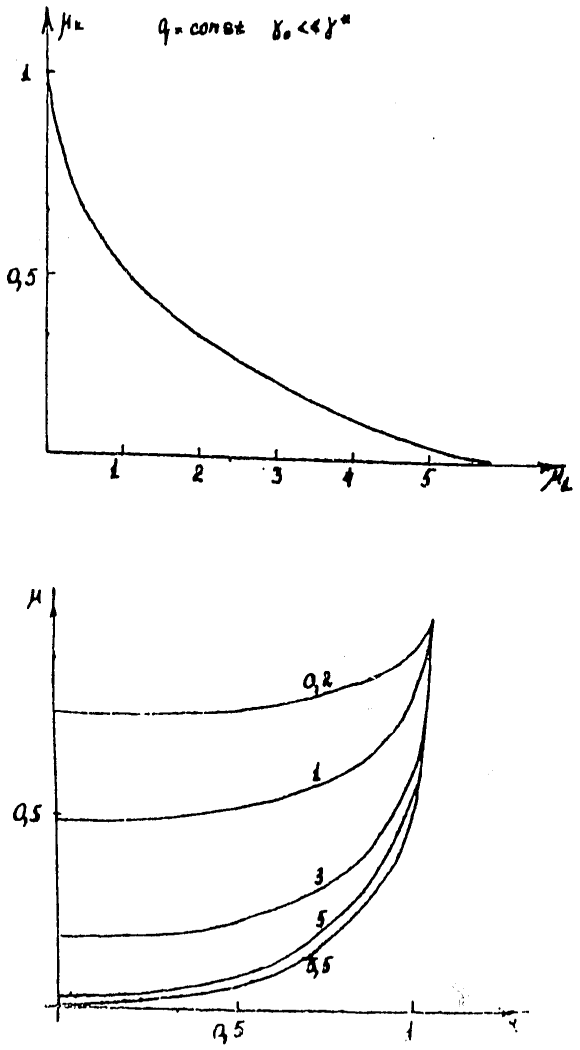

Figure 3. Relative evaporated mass for the case q=const; $\gamma_0 << \gamma^*$

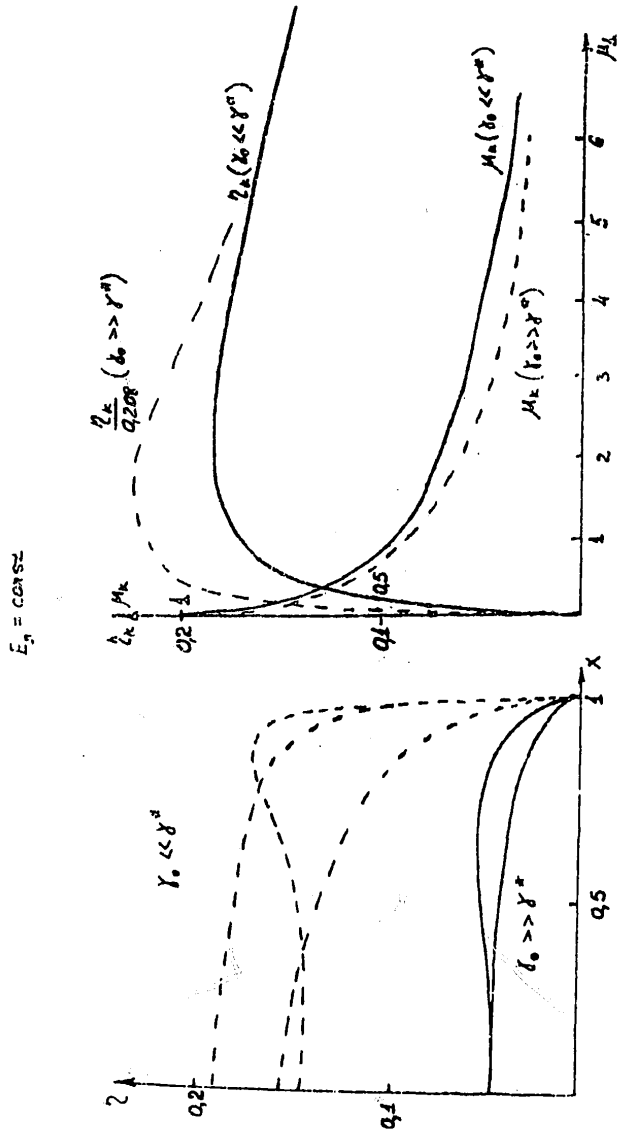

Figure 4. Relative evaporated mass and hydrodynamic efficiency for the case $\dot{E}_n$=const

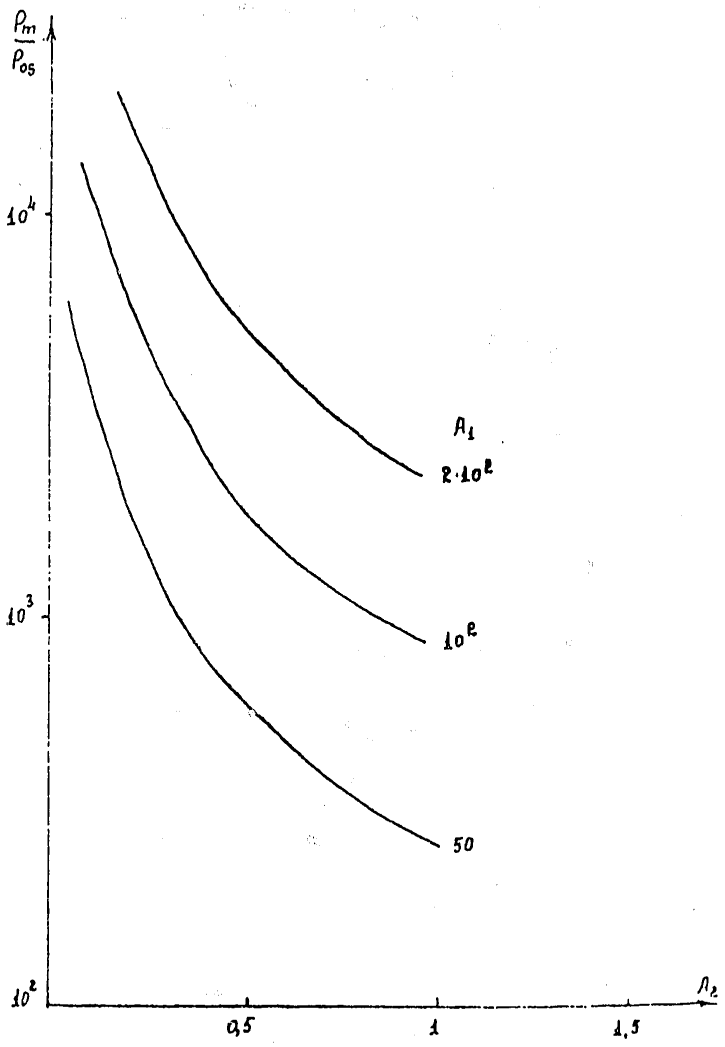

Figure 5. Ratio of maximum pressure in the gas to the pressure in the "corona" p_m/p_{0s} as a function of the coefficients A_1 and A_2

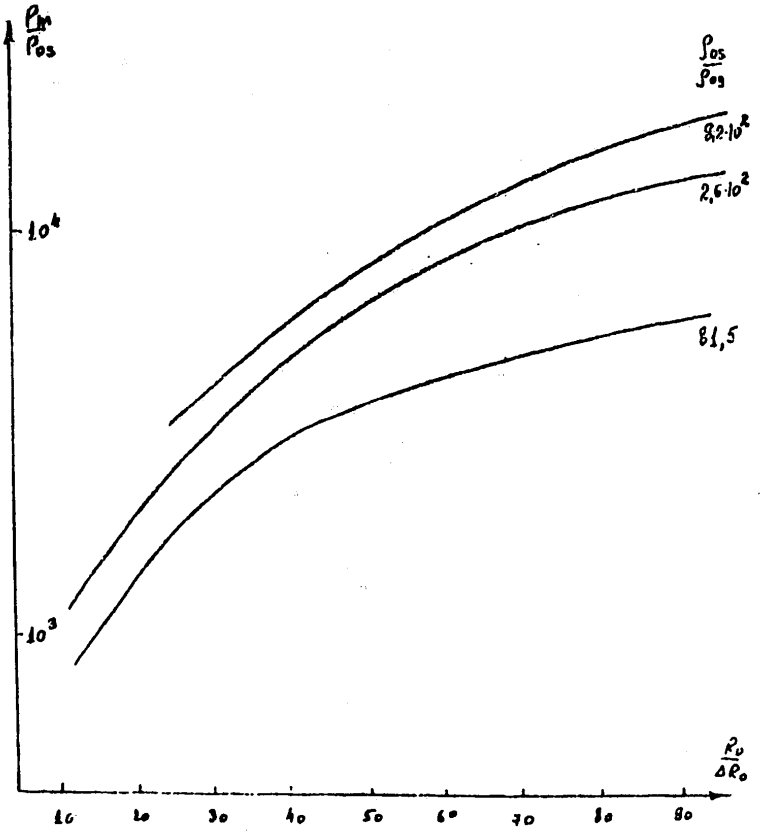

Figure 6. p_m/p_{0s} as a function of $R_0/\Delta R_0$ for different ρ_{0s}/ρ_{0g}

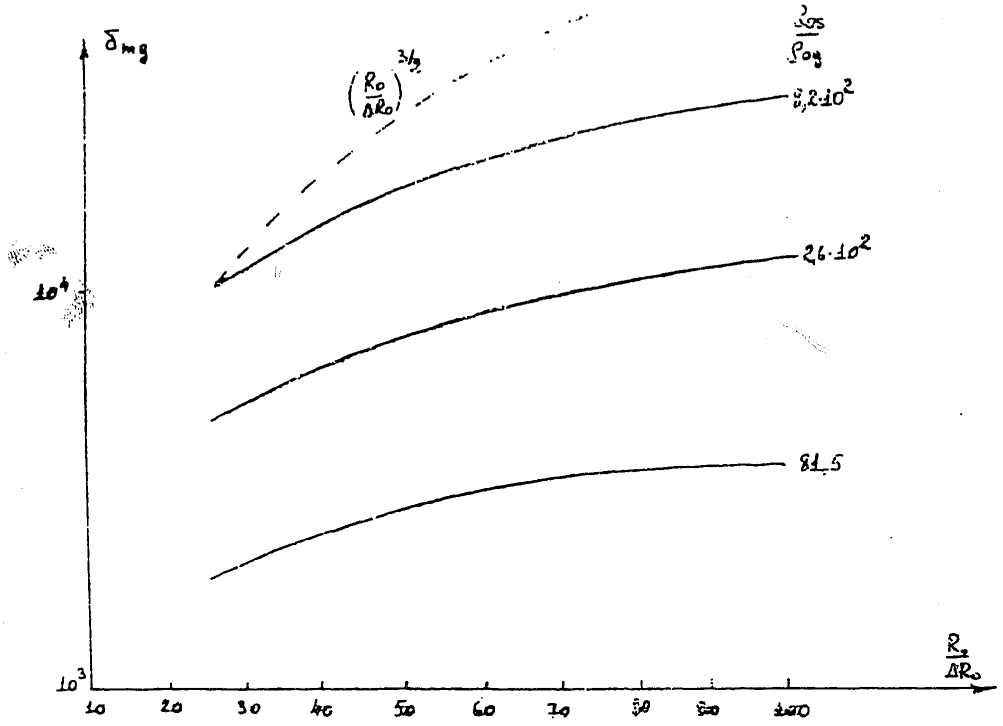

Figure 7. $\delta_{mg}=\rho_{mg}/\rho_{0g}$ as a function of $R_0/\Delta R_0$ for different ρ_{0s}/ρ_{0g}

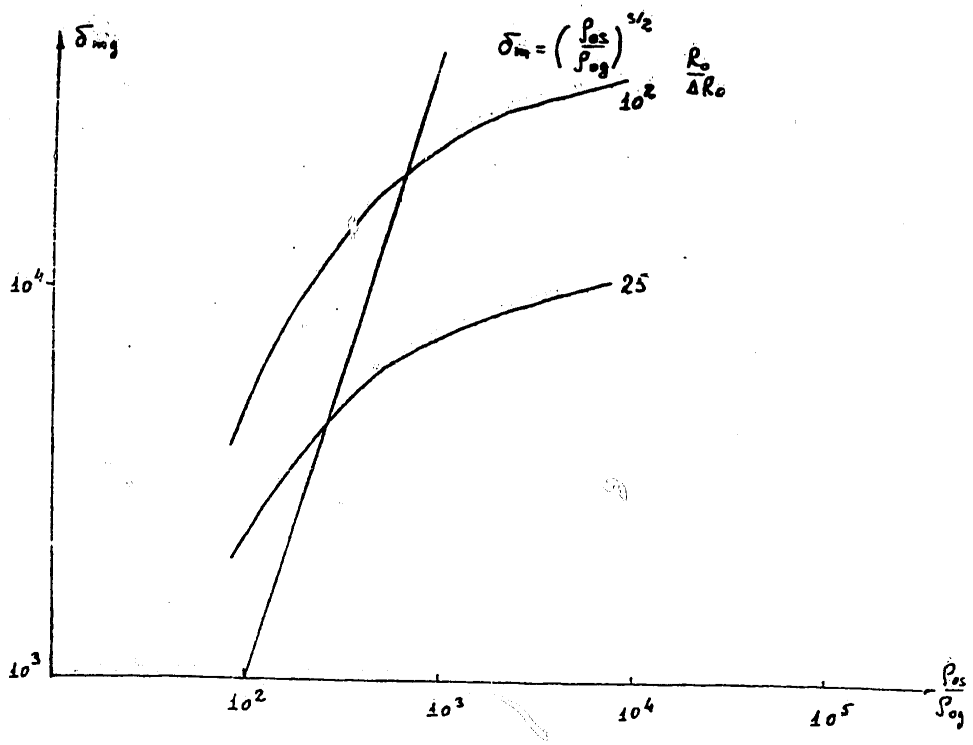

Figure 8. $\delta_{mg}=f(\rho_{0s}/\rho_{0g})$ for different $R_0/\Delta R_0$

[8144/0581-C-10845]

10845
CSO: 8144/0581-C

CALCULATING THE COMPRESSION OF DT-GAS GLASS SHELL TARGETS CONSIDERING CO_2-LASER RADIATION REFRACTION AND RESONANCE ABSORPTION

Moscow RASCHET SZHATIYA STEKLYANNYKH OBOLOCHECHNYKH MISHENEY S DT-GAZOM S UCHETOM REFRAKTSII I REZONANSNOGO POGLOSHCHENIYA IZLUCHENIYA CO_2-LAZERA in Russian 1979 (signed to press 23 Jan 79) pp 1-14

[Paper by Yu. V. Afanas'yev, P. P. Volosevich, Ye. G. Gamaliy, N. N. Demchenko, O. N. Krokhin and V. B. Rozanov, preprint No 77 of the Order of Lenin Physics Institute imeni P. N. Lebedev, 100 copies, 14 pages]

[Text] 1. Introduction

In this paper a numerical analysis is made of the laser compression of a thermonuclear target--a thin glass shell filled with DT-gas--under conditions corresponding to the experiments at the Los Alamos Laboratory (United States) [1] performed on a dual-beam CO_2-laser. The calculations were made by the "Rapid" (FIAN) program [2] and the "Luch" (IPM-FIAN) program [3]. The indicated physicomathematical programs as applied to the present calculations permit investigation of the process of collapse of the given target both in the model of laser ablation of the shell considering the processes of laser radiation refraction and absorption, electron and ion thermal conductivity and under the conditions of developed hydrodynamics ("Rapid") and in the model of heating and subsequent collapse of the target under the effect of epithermal electrons generated by a powerful laser field in the target "corona" near the critical point ($\rho = \rho_{cr}$) adopted in [1]. A comparison of the calculations performed by the indicated models and also the results of the numerical analysis by the American "LASNEX" program [4] permit the controlling mechanisms of the investigated process to be distinguished.

2. Experimental Setup

In the experiments of [1] two diametrically opposite laser beams with a total energy of $E_{total} = 380$ joules were focused on a target with an initial radius $R_0 = 105$ microns, an initial thickness of the outer glass shell (SiO_2) $\Delta R_0 = 1.4$ microns, filled with DT-gas with an initial density of $\rho_{0DT} = 2.09 \cdot 10^{-4}$ g/cm^3 to $2 \cdot 10^{-3}$. The total duration of the laser pulse was $\tau_0 = 2.92$ nanoseconds, the steepness of the leading edge $\Delta\tau_0 = 0.17$ nanosecond, the peak power $(dE/dt)_{max} = 2.6 \cdot 10^{11}$ watts.

Focusing system: $2\alpha = 26$ cm, $F = 52$ cm, $FL = 3 \cdot 10^{-2}$ cm (see Figure 1).

3. Calculation by the "Rapid" Program

a) Statement of the Problem

The "Rapid" program uses successive integration of the equations of one-dimensional, spherically symmetric hydrodynamics with electronic thermal conductivity jointly with the Maxwell equations for the incident radiation. The calculation is performed for the case of an arbitrary laser beam arriving at the target and experiencing absorption and refraction processes in the "corona," that is, in the region $\rho \lesssim \rho_{cr}$. Here phenomena of anomalous absorption and linear transformation are taken into account. The energy release connected with absorption of all of the beams hitting the target is averaged with respect to angles. The given approximation retains one-dimensional motion, which greatly simplifies the problem by comparison with the complete three-dimensional problem of disintegration of a target irradiated by a finite number of beams.

Formally, an elemental area $dS_0(\xi, \phi) = \xi d\xi d\phi$ connected with a defined "beam" characterized by the radiation flux $dq_0 = I(\xi)dS_0$ is isolated in the plane of the focusing lens (see Figure 1), where $I(\xi)$ is the intensity in the laser beam. The distribution of the energy released from this flux with respect to the radius in the "corona" is calculated. In addition, the electric field vector is broken down into components in the plane of incidence and perpendicular to it, and the energy release is integrated over the angle ϕ, that is, the two-dimensional problem is considered for the incident radiation: one dimension is taken along the beam with the corresponding wave problem in the vicinity of the reflection point, and the other, along ξ, that is, the laser beam is broken down into a set of concentric elemental areas $2\pi\xi d\xi$. As follows from the statement of the problem, in the case of a linearly polarized laser beam the differential portion of the lost radiation is

$$\delta(\xi, \phi) = [dq_{lost}/dq_0(\xi, \phi)] = \delta(\xi, 0) \cos^2 \phi + \delta[\xi, (\pi/\lambda)] \sin^2 \phi \qquad (1)$$

From (1) it is easy to obtain the expression for the instantaneous proportion of the absorbed energy

$$q_{abs}/q_0 = 1 - \left(\int_0^{\xi_0} [\delta(\xi, 0) + \delta(\xi, [\pi/2])]/2\ I[\xi]\xi d\xi\right)/\int_0^{\xi_0} I(\xi)\xi d\xi \qquad (2)$$

where ξ_0 corresponds to the edge rays.

Here, the part of the absorbed energy determined by the resonance absorption effect is

$$q^*/q_0 = \left(\int_0^{\xi_0} [\delta(\xi, [\pi/2]) - \delta(\xi, 0)]/2\ I(\xi)\xi d\xi\right)/\int_0^{\xi_0} I(\xi)\xi d\xi \qquad (3)$$

b) Calculation Results

Figure 2 shows the time diagrams of the incident radiation absorption and refraction processes, that is, the functions $\Delta_0(t) = q_{abs}(t)/q_0(t)$ and $\Delta^*(t) = q^*(t)/q_0(t)$. The total proportion of the absorbed energy is $E_{abs}/E_0 = 0.188$, and the contribution of the resonance absorption $E^*/E_0 = 0.136$.

Figure 3 shows the families of differential losses $\delta(\xi, \phi)$ for the investigated case at the time 1.2 nanoseconds and for the case of the Nd-laser [2]. The dip of the curve $\delta(\xi, 0)$ in the latter case corresponds to a decrease in losses as a result of resonance absorption of the rays of the central part of the beam. In the case of a long wavelength (CO_2-laser) the resonance absorption is the controlling process, and it is most strongly expressed for the peripheral rays. Let us note that this result can be obtained only within the framework of a strict wave problem and is connected with significant penetration of the longitudinal component of the field into the region of critical density for rays with optimal angle of incidence. In the investigated case of the CO_2-laser (λ = 10 microns) the edge rays satisfy the optimal relation, but, for example, for the Nd-laser [2, 5] the rays of a small central part of the beam are incident in the optimal region, and the resonance absorption effect is insignificant. Of course, the indicated effect depends on the radiation focusing system.

Figure 4 illustrates the spatial distribution of the specific energy release (averaged in each case over the angles). The maximum energy release comes at the critical point ($\rho = \rho_{cr}$), which obviously is connected with the resonance absorption effect. It must be noted that in the case where the resonance absorption is small, the maximum energy release as a result of the refraction phenomenon comes at the point with $\rho < \rho_{cr}$.

Figure 5 shows the time diagrams of the hydrodynamic efficiency $-\eta = E_{kin}/E_0(t)$ (E_{kin} is the kinetic energy of the collapsed, unevaporated part of the shell) averaged over the radius of the parameters of the DT-region $T_{iDT}(t)$, $\overline{\rho}_{DT}(t)$ and the Rt-diagram of the DT-glass interface. The time of collapse of the shell (the collapse time) is t_k = 1.45 nanoseconds, the maximum (with respect to time) values of the density and temperature of the DT-gas are $\overline{\rho}_{DT}^{max} = 3.6$ g/cm^3, $\overline{T}_{DT}^{max} = 0.77$ kev.

4. Calculation in the Approximation of Epithermal Electrons

In the given model it is proposed that the absorbed radiation is completely transformed to fast electron fluxes, as a result of which, during the laser pulse uniform heating of the target substance with respect to mass is realized, that is, the specific heat release $W(\text{watts/cm}^3) = Q(t) \cdot \rho$ where $Q(t) = 9.25 \cdot 10^{16}$ watts/g $\cdot$ $f(t)$, the function $f(t)$ simulates the shape of the laser pulse ($f(t) = 1$ at the maximum incident power),

$$\int_0^{\tau_0} Q(t)M_0 dt = 0.15 \int_0^{\tau_0} q_0(t)dt$$

which corresponds to 15 percent absorption of the incident radiation adopted in [1], M_0 is the total mass of the target.

In the indicated approximation calculations were performed by the uniform hydrodynamic program with electron thermal conductivity (the "Luch" program with the module related to the incident radiation disconnected). The basic results are presented in Table 1.

Table 1

t_k, nanoseconds	R_{DT-SiO_2}, microns	$\overline{T}_{eDT}$, kev	$\overline{T}_{iDT}$, kev	$\overline{\rho}_{DT}$, g/cm^3	E_{abs}, joules	N
0.418	17.2	1.0	3.16	$4.5 \cdot 10^{-2}$	12.6	$9 \cdot 10^7$

In Table 1 all of the values are presented for maximum compression ("collapse"), E_{abs} is the energy absorbed at the indicated time, N is the neutron yield.

5. Discussion of the Results

Table 2 contains the results of calculations of the given target by the "Rapid" {1}, "Luch" {2} and "LASNEX" {3} programs.

Table 2

	t_k, nanoseconds	R_{DT-SiO_2}, microns	$\overline{T}_{iDT}$, kev	$\overline{T}_{eDT}$, kev	$\overline{\rho}_{DT}$, g/cm^3	$\frac{E_{abs}}{E_{epi}}$	ρ_{0DT}, g/cm^3
{1}	1.450	8.63	0.77	0.77	3.68	0.188	$2.09 \cdot 10^{-3}$
{2}	0.418	17.20	3.16	1.00	$4.50 \cdot 10^{-2}$	0.150	$2.09 \cdot 10^{-4}$
{3}	0.530	20.90	1.34	--	$2.65 \cdot 10^{-2}$	0.150	$2.09 \cdot 10^{-4}$

As follows from Table 2, consideration of the incident radiation refraction and absorption processes by the "Rapid" program agrees satisfactorily with the experimental figure ~0.15 obtained in [1]. As has already been pointed out, the resonance absorption effect makes a significant contribution to the absorption. Noticeable divergence in the collapse time and in the final parameters of the DT-mixture obtained in the calculations of {1} and the calculations of {2, 3} is obviously connected with the above-indicated difference of the physical models. Thus, for example, in case {2} and {3} the defining role is played by heating of the compressed DT-mixture by epithermal electrons. The large difference in final temperatures of the DT-gas in the calculations of {2} and {3} and, consequently, also in the hydrodynamic efficiency in the epithermal electron model does not seem to be clear at the present time. Nevertheless, the presented results indicate the extremely high sensitivity of the process of laser compression of shell targets of the investigated type with respect to the mechanism of laser radiation energy conversion.

BIBLIOGRAPHY

1. D. V. Giovanelli, G. N. McCall, T. H. Tan, LA-UR-77-1703; G. H. McCall--private communication.

2. Yu. V. Afanas'yev, Ye. G. Gamaliy, N. N. Demchenko, O. N. Krokhin, V. B. Rozanov, ZhETF [JOURNAL OF EXPERIMENTAL AND THEORETICAL PHYSICS], 1979 (in print).

3. Yu. V. Afanas'yev, N. G. Basov, P. P. Volosevich, Ye. G. Gamaliy, O. N. Krokhin, S. P. Kurshchomov, Ye. I. Levanov, V. B. Rozanov, A. A. Samarskiy, A. N. Tikhnov, "Doklad na II-y konferentsii po fizike plazmy i upravlyayemomu termoyadernomu sintezu" [Report at the 2d Conference on Plasma Physics and Controlled Nuclear Fusion], Tokyo, 1974.

4. Charles W. Cranfill, LA-6827-MS, 1977.

5. N. G. Basov, A. A. Yerokhin, Yu. A. Zakarenkov, N. N. Zorev, A. A. Kologrivov, O. N. Krokhin, A. A. Rupasov, G. V. Sklyazkov, A. S. Shikanov, PIS'MA V ZhETF, No 26, 1977, p 581.

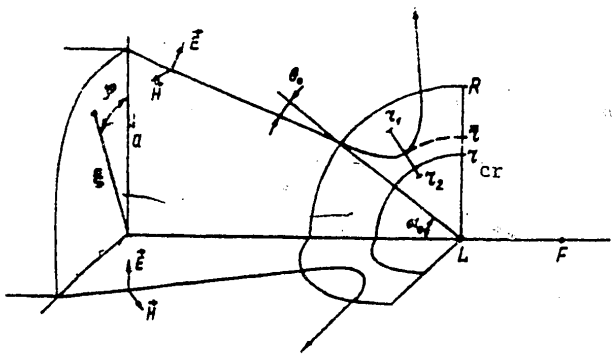

Figure 1. Geometry of the beam path in the calculations by the "Rapid" program.

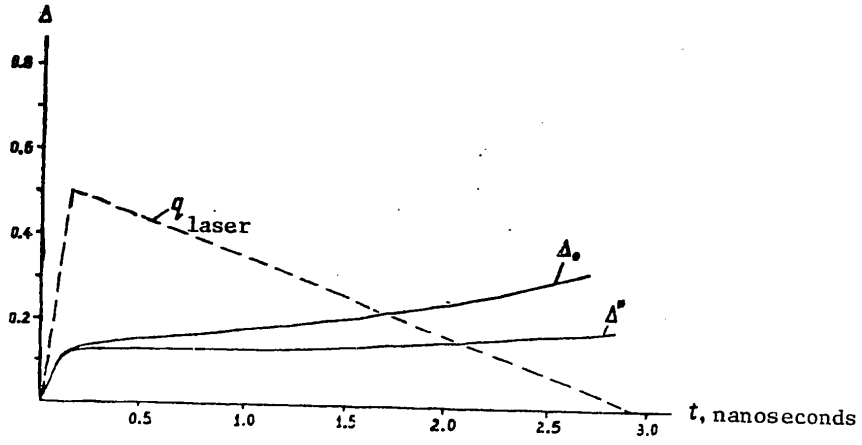

Figure 2. Time diagrams of the process of a contribution of radiation energy to the target "corona" (the dotted line gives the time shape of the laser pulse).

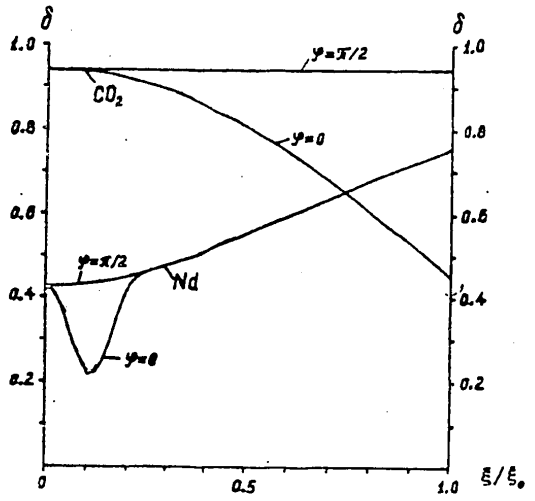

Figure 3. Family of differential losses in the case of CO_2- and Nd-lasers.

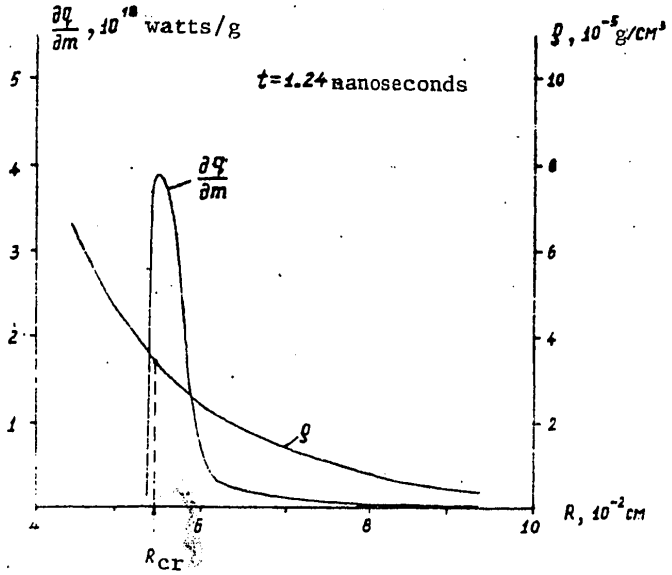

Figure 4. Spatial density distribution and specific energy release in the "corona."

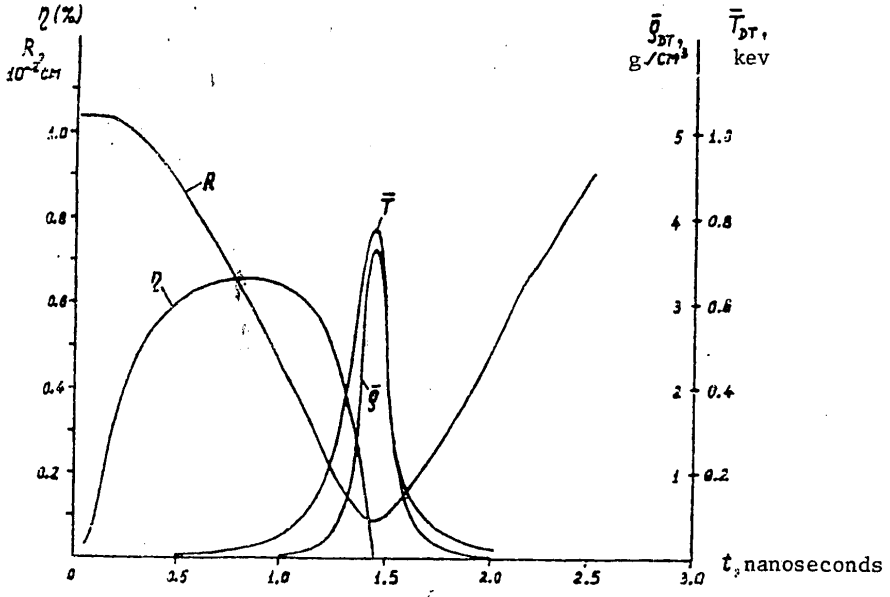

Figure 5. Time diagrams of the average parameters of DT-gas, Rt-diagram of the gas-glass interface, time behavior of the hydrodynamic efficiency.

[8144/0581-B-10845]

10845
CSO: 8144/0581-B

UDC 532.51+533.95

SINGULAR SELF-SIMILAR CONDITIONS OF LASER COMPRESSION OF MATTER TO SUPERHIGH DENSITIES

Novosibirsk ZHURNAL PRIKLADNOY MEKHANIKI I TEKHNICHESKOY FIZIKI in Russian No 4, 1980 pp 20-24

[Article by S. I. Anisimov and N. A. Inogamov, Chernogolovka; submitted 19 Jul 79]

[Text] The approach proposed in [1, 2] to laser initiation of thermonuclear reactions is based on the special conditions of laser-driven compression of matter to densities on the order of 10^3-10^4 from the initial solid state. The optimal choice of the shape of the laser pulse and the target parameters based on numerical calculations presents significant difficulties. As the guiding idea in the calculations usually the requirement of adiabatic compression of the dense nucleus of the target is used; the arguments of dimensionality then make it possible to establish an asymptotic law of increase with time of the mechanical power expended on compression [3]: $E_M \sim |t|^{-2}$ (here and hereafter we are talking about spherical compression of matter with the adiabatic exponent $\gamma = 5/3$; the time is reckoned from the collapse time). The partial self-similar solution corresponding to this law is indicated in [4, 5]. The following problems remained unresolved: 1. Does the self-similar solution of [4, 5] correspond to the unique optimal compression conditions, and are flows close to self-similar realized during numerical simulation? 2. How is the shape of the laser pulse related to the dependence of the mechanical power on time? In this paper it is demonstrated that the solution of [4, 5] is ambiguous in the indicated sense, and two new families of self-similar solutions of the equations of gas dynamics have been constructed which describe the compression of simple shells and solid homogeneous laser targets. The constructed solutions are singular; the corresponding values of the self-similarity index lie inside an interval of admissible values. For construction of the solutions it is necessary to proceed to the scale-invariant representation of the hydrodynamic variables. For the inverse procedure of calculating the physical variables, the characteristic parameters of the medium are necessary: the specific entropy in the case of shells and the initial plasma density in the case of continuous targets. The constructed solutions describe the process of unlimited energy concentration on approaching the collapse time; in a real experiment the total energy, of course, is limited and determines the maximum degree of compression. By comparison with the numerical calculations it has been demonstrated that with proper choice of the parameters the self-similar solutions found give a quantitative description of the compression dynamics of the dense nucleus of the target under conditions analogous to the ones studied earlier by numerical methods in

[1, 2]. It has been discovered that for shells with degrees of compression of interest in practice, the law of the power variation can differ noticeably from asymptotic. Let us note that the investigated solutions are suitable for description of nonisentropic compression conditions under which the initial disturbance is a convergent shock wave. This is significant inasmuch as in the experiment it is not possible to avoid the formation of the initial shock wave and corresponding heating of the central part of the target.

The analysis of the numerical calculations [6] shows that in the case of thin shells laser and mechanical powers essentially depend on the time differently. This difference is almost entirely connected with ablation of the material leading to a decrease in mass of the dense nucleus.

As is known, in laser targets there are two regions with sharply differing properties: the hot corona in which the light is absorbed, and a recoil impulse is created, and the dense nucleus which is compressed under the effect of the recoil impulse. In the nucleus the thermal flux is negligibly small, and the electron and ion temperatures are equal. Therefore the compression of the nucleus can be described by the system of equations of gas dynamics. The latter has a class of partial solutions which depend on the variable $\xi = ar/(-t)^{\delta}$. With respect to the meaning of the problem of compression to superhigh densities, the singular solutions describing the cumulation of the entire mass of the substance at the center of symmetry at some point in time $t = 0$ are of interest.

First let us consider collapse of the shell. After switching on a laser pulse with initial power $\dot{E}_0$, a shock wave arises in the shell which communicates a specific entropy to the substance $\Delta S = c_v \ln \mu$, $\mu \simeq 0.02\, \rho_0^{1/3}\dot{E}_0^{2/3}p_0^{-1}R_0^{-4/3}$ (ρ_0 is the initial density). For thin shells the entropy distribution with respect to mass is uniform. Further compression takes place with constant entropy, and the final state of compression depends on the magnitude of the entropy. The system of equations of gas dynamics is conventionally reduced [7] to one ordinary differential equation, the variables in which are dimensionless flow velocity and speed of sound related to the corresponding dimensional variables by the expressions $v(r, t) = (r\delta/t)\phi(\xi)$, $c(r, t) = -(r\delta/t)\psi(\xi)$. The desired singular solution corresponds to the integral curve in the plane (ϕ, ψ) joining the singularity $Q(1, 0)$ which corresponds to the boundary with the cavity and the singularity $R(1/2\delta, 1/2\sqrt{3}\delta)$. Actually, for the simplest singular solution $v = r/2t$, $c = -r/2\sqrt{3}t$ the power law $\dot{E}_M = 4\pi R_n p_n v_n \sim |t|^{-2}$ (the subscript n denotes the parameters of some fixed Lagrange particle belonging to the dense nucleus). For singular conditions with the asymptotic form $\dot{E}_M \sim |t|^{-2}$ for $t \to 0$ it is necessary that $\phi(\xi_n(t)) \to 1/2\delta$, $\psi(\xi_n(t)) \to 1/2\sqrt{3}\delta$. These integral curves exist under the condition that the self-similarity index δ satisfies the inequalities $1/2 \leq \delta \leq (\sqrt{3} + 1)/2\sqrt{3} \simeq 0.7887$. For $\delta = 0.5$ the desired solution is given by a segment of a straight line $\phi = 1$, the temperature distribution follows from the formula $\psi^2 = (\xi^2 - 1)/3\xi^2$, and the velocity distribution is linear with respect to the radius. This special case was investigated in [4]. For $\delta < 0.5$ the integral curve all lies in the region $\phi > 1$. Here the required asymptotic behavior is not achieved for $t \to 0$. For $\delta > 0.7887$ the integral curve intersects the doubling line of the solutions S, the equation of which $\psi = 1 - \phi$ (for more details on the straight line S, see [7]). Actually, the curve emerges from the saddle Q along the separatrix $\phi = 1 - (9/5)([2\delta - 1]/[1 - \delta])\psi^2 + O(\psi^3)$, but here $(2\sqrt{3}\delta)^{-1} < 1 - (2\delta)^{-1}$. Finally, if $\delta < 0.7887$, we

have $(2\sqrt{3\delta})^{-1} > 1 - (2\delta)^{-1}$. Here the point R is the node. It is possible to demonstrate that in the bunch of curves emerging from R there is always one that is incident in Q.

In order to find the desired integral curve numerical integration is necessary. However, a simple approximate solution which gives the following formulas for the density profile has sufficient accuracy:

$$\rho(r, t) \simeq \begin{cases} 0.25(-[r/\sqrt{\mu}t])^3[\delta(1-\delta)\ln\xi]^{3/2}, & \xi < 1.4, \\ 0.011(-[r/\sqrt{\mu}t])^3, & \xi > 2, \end{cases}$$

where $\xi = r/r_0(t)$; $r_0(t)$ is the inside radius of the shell. The accuracy of the formulas is no less than 10 percent. Figure 1 shows the trajectory of a Lagrange particle 0.18 M_0 and the variation in density of the particle with time, and the self-similar solution found (curves 2, 3, $\delta = 0.77$ and 0.53, respectively) is compared with the numerical calculation (curve 1) of the compression of the shell performed for a uniform two-temperature hydrodynamic model considering the absorption of light and the transport processes with restriction with respect to flow [6] (DT mixture target, $M_0 = 0.2$ micrograms, thickness 10 microns, $\dot{E}_0 = 3 \cdot 10^9$ watts). The calculation was performed for a laser pulse of the type $\dot{E}_1(t) - \dot{E}_0(t_0/|t|)^m$ with the parameters $t_0 = 1.2$ nanoseconds, m = 1.3 and an energy of 200 joules. It is obvious that the motion of the dense part of the target is well described by the self-similar solution.

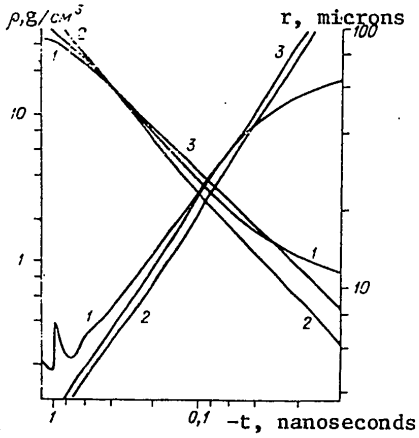

Figure 1

Let us note that for degrees of compression that are of interest in practice ~10^3-10^4, the movement of the shell still differs significantly from asymptotic, corresponding to infinite compression, and the power expended on compression does not depend on time by an exponential law. If we take the usually used exponential approximation for the power, the exponent always turns out to be less than the

asymptotic value. The magnitude of the exponent depends, of course, on the shell parameters and the degree of compression so that the above-presented approximate expression for the laser power is not universal.

Now let us consider the singular conditions of compression of continuous targets. The assumption of self-similarity of the movement again allows the problem to be reduced to the integration of an ordinary differential equation [7, 8]. The desired integral curve joins the singularity $M(3/4, \sqrt{5}/4)$, corresponding to a powerful shock wave to the singularity $N(1/2\delta, \sqrt{(5/3)([2\delta - 1]/[4\delta + 1])}/2\delta)$. The approximation to the latter corresponds to emergence at the asymptotic form $\dot{E}_M \sim |t|^{-2}$. The physically proper solution exists for all values of δ satisfying the inequalities $1/2 \leq \delta < A(\gamma)$. The upper edge of the spectrum is determined from the condition that the points M and N are on the same side of the doubling line S; here N is the node. Let us note that $A(\gamma) \leq \delta_g(\gamma)$, where $\delta_g(\gamma)$ is the exponent corresponding to the Landau-Guderley converging shock wave [8, 9], $A(5/3) = \delta_g(5/3) = 0.688$. When $\delta < 1/2$ the point N leaves the physical area $p > 0$, $\psi > 0$. Let us also note (this comment also pertains to the case of a shell target) that above the obtained edge of the continuous spectrum of δ there can theoretically be discrete values of the exponent δ giving proper solutions of the problem which correspond to the integral curves intersecting S at the singularity. This problem requires special study.

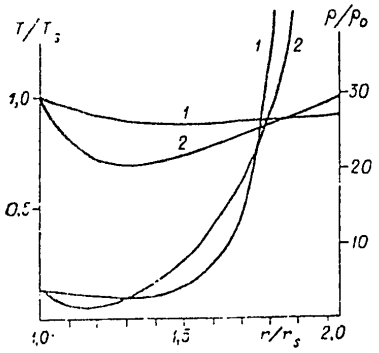

Figure 2

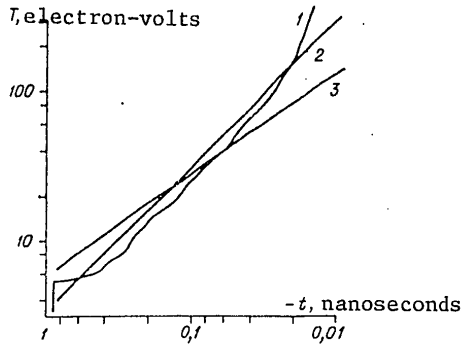

Figure 3

The solution was constructed as follows. The shock wave behind the front of which the temperature $T \approx 0.1(M_i/k)(\delta R_0/t_0)^2(|t|/t_0)^{2(\delta-1)}$ converges to the center of the target, where M_i is the ion mass; k is the Boltzmann constant; R_0 is the initial target radius; t_0 is the pulse duration. The spatial temperature and density profile in the continuous target are shown in Figure 2 (1--$\delta = 0.527$, 2--$\delta = 0.667$). Under the conditions with a shock wave, the temperature in the disturbed region depends weakly on the coordinate. Figure 3 shows a comparison of the mean temperature of the compressed substance calculated numerically (curve 1), with the temperature behind the front of the self-similar shock wave for $\delta = 0.527$ and 0.667 (curves 2 and 3, respectively). The results pertain to a continuous target, $M_0 = 0.2$ micrograms, $R_0 = 66$ microns, $t_0 = 0.87$ nanosecond, $m = 2$, $E = 200$ joules. The results agree well.

Thus, the described self-similar solutions give a proper quantitative description of the compression and heating of the dense regions of the laser targets and they can be used for optimizing the conditions of laser compression of a plasma and estimation of the conditions of laser-initiation of thermonuclear fusion.

The authors express their appreciation to M. F. Ivanov for his assistance in the numerical calculations.

BIBLIOGRAPHY

1. Nuckolls, J., Wood, L., Thiessen, G., Zimmerman, G., "Laser Compression of Matter to Superhigh Densities: Thermonuclear (CTR) Applications," NATURE, Vol 139, No 2, 1972.

2. Clark, J. S., Fisher, H. N., Mason, R. J., "Laser-Driven Implosion of Spherical DT Targets to Thermonuclear Burn Conditions," PHYS. REV. LETT., Vol 30, No 2, 1973.

3. Prokhorov, A. M., Anisimov, S. I., Pashinin, P. P., "Laser Thermonuclear Fusion," UFN [PROGRESS IN THE PHYSICAL SCIENCES], Vol 119, No 3, 1976.

4. Kidder, R. E., "Laser-Drive Compression of Hollow Shells: Power Requirements and Stability Limitations," NUCL. FUSION, Vol 16, No 1, 1976.

5. Anisimov, S. I., "Hydrogen Transition to the Metallic State in a Laser Pulse-Initiated Compression Wave," letters in ZhETF [JOURNAL OF EXPERIMENTAL AND THEORETICAL PHYSICS], Vol 16, No 10, 1972.

6. Anisimov, S. I., Ivanov, M. F., Inogamov, N. A., Pashinin, P. P., Prokhorov, A. M., "Numerical Simulation of the Processes of Laser Compression and Heating of Simple Shell Targets," FIZ. PLAZMY [PLASMA PHYSICS], Vol 3, No 4, 1977.

7. Sedov, L. I., "Metody podobiya i razmernosti v mekhanike" [Similarity and Dimensionality Methods in Mechanics], Moscow, Nauka, 1966.

8. Brushlinskiy, K. V., Kazhdan, Ya. M., "Self-Similar Solutions of Some Problems of Gas Dynamics," UMN [PROGRESS IN THE MATHEMATICAL SCIENCES], Vol 18, No 1, 1963.

9. Zel'dovich, Ya. B., Rayzer, Yu. P., "Fizika udarnykh voln i vysokotemperaturnykh gidrodinamicheskikh yavleniy" [Physics of Shock Waves and High-Temperature Hydrodynamic Phenomena], Moscow, Nauka, 1966.

[8144/0581-A-10845]

10845
CSO: 8144/0581-A

PROBLEM OF LASER-INITIATED THERMONUCLEAR FUSION

Novosibirsk PROBLEMY SOVREMENNOY OPTIKI I SPEKTROSKOPII: O PROBLEME LAZERNOGO TERMOYADERNOGO SINTEZA in Russian 1979 (signed to press 5 Dec 79) pp 1-23

[Preprint No 15, "On the Problem of Laser-Initiated Thermonuclear Fusion", by Aleksandr Markovich Rubenchik, from "Problems of Modern Optics and Spectroscopy", an inter-institute seminar under the joint auspices of Novosibirsk State University and the Siberian Branch of the USSR Academy of Sciences, under the leadership of USSR Academy of Sciences Corresponding Member S. G. Rautian, published by the Institute of Automation and Electrometry, 200 copies, 23 pages]

[Text] Annotation

A description is presented of the modern state of the art with regard to the problem of laser-initiated thermonuclear fusion (LTF). Basic requirements on the parameters of the laser emission and targets, their dependence on the absorption and compression processes are presented. A study is made of the basic physical problems of LTF (compression stability, anomalous absorptions and thermal conductivity). The results of the latest experiments and prospects for future research are discussed.

In spite of the intensive research conducted in various countries for more than 20 years, the problem of controlled thermonuclear fusion still is quite far from achieving practical results. However, inasmuch as mankind would altogether receive in practice an inexhaustible source of energy, the research front is continuing to be expanded. Recently, along with more thorough studies and development of the traditional system for steady confinement, new systems have appeared, including the laser thermonuclear fusion system.

Below, we shall investigate the basic problems which arise when attempting to initiate thermonuclear reactions by powerful pulses of laser radiation.

Energy Relations of Laser Driven Fusion. Usually the following reaction is considered as the source of energy for controlled thermonuclear fusion (CTF) [1]

$$D + T \to He^4 + n.$$

Here the neutron removes a large part of the energy (14.1 Mev); 3.5 Mev remains for the α-particle. As a result of the long path of the neutrons, the use of their energy is complicated and usually only the energy of the α-particle is used in the calculation.[1] This reaction proceeds only at very high temperature, and therefore for a positive power yield it is necessary that the energy obtained as a result of the reaction exceed the expenditures on creating the hot plasma.

In a hot plasma with deuterium and tritium concentrations of n_0 and n_T, respectively, the energy released per unit volume in the time τ will be

$$n_0 n_T \langle \sigma v \rangle E \tau. \qquad (1)$$

Here E is the energy released as a result of the reaction, E=3.5 Mev; σ is its cross section, and the brackets denote the averaging with respect to Maxwell distribution.

Considering $n_0=n_T=n/2$ and introducing the efficiency of the plasma heating systems η, we find that for a positive energy yield it is necessary that the following condition be satisfied:

$$n\tau \geq 2T/(\eta \langle \sigma v \rangle E). \qquad (2)$$

The righthand side of (2) is equal to ~(10^{14}/ [sic]) cm^{-3}/sec at T~10 kev, and it increases rapidly with a decrease in temperature [1].

When investigating stationary systems with magnetic thermal insulation (for example, the Tokamak devices) the research goal is to achieve the Lawson criterion ($n\tau \sim 10^{14}$). This is justified by the fact that the efficiency of the electrical engineering systems used is quite high.[2] As will be demonstrated

---

[1] We shall not discuss the "hybrid" CTF systems in which the appearing neutrons are used [2].

[2] Nevertheless, the increase in confinement time as a result of low efficiency is significant when selecting the auxiliary heating source in the tokamaks [2].

below, the problem of the efficiency of heating the plasma with LTF is more significant yet.

The idea of using microexplosion to obtain thermonuclear energy (inertial confinement) arose a long time ago. However, as is obvious from (2), with a decrease in the reaction time, the density of the reacting deuterium-tritium mass must increase, which leads to the necessity for a high energy concentration to "initiate" the reaction. Therefore the studies of the use of thermonuclear microblasts developed only after the creation of powerful laser systems and also powerful electron and ion beams.

For an exploding deuterium-tritium particle the reaction time is equal with respect to order of magnitude to the hydrodynamic disintegration time r_0/c_s (r_0 is the particle radius, c_s is the speed of sound). Instead of (2) we now have

$$nr_0 \geq 2Tc_s/(\eta\langle\sigma v\rangle E). \tag{3}$$

The righthand side of (3) has a smooth minimum at T~20 kev [3]. Here the analog of the Lawson criterion for inertial fusion assumes the form

$$nr_0 > 2\cdot 10^{22}/\eta cm^{-2} = \frac{(nr_0)_L}{\eta}. \tag{4}$$

Considering nr_0 equal to its minimum value, we find the energy required to initiate the reaction with a positive yield:

$$E_{thr} = \frac{4}{3}\frac{\pi r_0^3 nT}{\eta} = 10 \text{ megajoules } \left(\frac{n_s}{n}\right)^2 \frac{1}{\eta^4}, \tag{5}$$

where n_s is the density of solid hydrogen.

It is obvious that even for η~1 and $n \sim n_s$, the required energies greatly exceed the technological possibilities of today, especially if we consider how it follows from (4) that this energy must be expended in a time on the order of 10^{-9} sec. Therefore, immediately after N. G. Basov and O. N. Krokhin [4] proposed the idea of LTF, obtaining thermonuclear energy appeared to be not too realistic.

Significant advancements in the field of inertial fusion occurred in 1972 when it was proposed in reference [5] that a laser pulse be used not only for heating, but also for compression of the target. In the first numerical calculations performed in [5], the possibility of compression by a specially selected pulse to densities of $n \sim 10^4 n_s$ was demonstrated, where only a small part of the total expended energy is necessary for compression.

Let us consider the process of compression of a spherical D-T-droplet in more detail. If we begin to compress the droplet too rapidly, the shock wave will penetrate deeply into it after which, as is known, the density increases by only a few times. Reaching the center of the target, it heats it up, preventing further compression. Therefore it is necessary to compress the droplet

adiabatically so that its boundary travels at the speed of sound. Here, all of the disturbances reach the center simultaneously, compressing the cold substance. Let us discover what the shape of the laser radiation pulse must be in this case.

As was already mentioned above, the displacement rate of the boundary must be

$$\frac{dR}{dt} \approx c_s.$$

Let us consider adiabatic compression of an ideal gas: $p \sim \rho^{5/3}$. Then $c_s \sim p^{1/3}$. Relating ρ and R by the condition of conservation of mass for $\rho R^3 = \text{const}$, we find that the drop radius $R \sim (t-t_0)$. The supplied power must vary according to the law

$$P \sim p \cdot 4\pi R^2 R \sim (t-t_0)^{-2}. \qquad (6)$$

Thus, in practice all of the energy is contributed at the final moment of compression.

The above-described tempting compression system obviously is unrealistic. The fact is that in addition to the very rigid requirement on the time profile of the pulse, the target irradiation must be highly symmetric. Correspondingly, the symmetry of the target must be very high. Later, however, it was demonstrated that if the deuterium-tritium nucleus is surrounded with shells of different thickness and density it is possible to organize the hydrodynamic process so that a high degree of compression is reached with a sufficiently arbitrary shape of the pulse.[6]. Here the requirements on the symmetry of the target and irradiation remain very high. This problem will be discussed in more detail below.

From formula (5) it is obvious that E_{thr} depends quite appreciably on the heating efficiency η. The efficiency η is the product of the laser efficiency η_l times the efficiency of absorption of light by the plasma corona ε_a and the efficiency of the absorbed energy transfer to the compressed nucleus ε_n:

$$\eta = \eta_l \varepsilon_a \varepsilon_n.$$

At this time the problem of the so-called scientific demonstration of the realizability of LTF, that is, obtaining more energy than the laser radiation energy, is being discussed. Being interested in this energy, we set $\eta_l = 1$. The absorption efficiency will be discussed below; as a rule, it exceeds 0.3. In order to define ε_n, let us consider how the drop compression takes place.

For compression of a substance to densities that exceed the solid state density by four orders, it is necessary that the pressure $p \sim 10^{12}$ atmospheres. This pressure, of course, cannot be created by laser emission alone, although in modern experiments with fluxes of $p \sim 10^{17}$ watts/cm^2, the light pressure reaches 10^8 atmospheres.

The increase in temperature caused by absorption leads to evaporation of the substance into the rarefied medium (see Figure 1) (ablation). The flow of substance from the ablation surface carries away the momentum, and as a result of the recoil effect the substance compresses. As a result of this "rocket" mechanism, the required pressure is reached.

The movement of the surface of the drop can be described analogously to the movement of a rocket [7], and simple estimates can be made based on the model of an accelerating flat layer. It turns out that the ratio of the kinetic energy of the accelerating layer to the absorbed energy is maximal for evaporation of 80% of the substance and it is approximately 8%. The computer calculation of spherical compression gives a similar result for ε_n: $0.05<\varepsilon_n<0.1$. Substituting the degree of compression 10^4, $\varepsilon_a \sim 0.3$ and $\varepsilon_n \sim 0.1$ in (5), we obtain $E_{thr} \sim 10^5$ joules.

It would appear that this estimate is not too reliable. We have taken the largest value of ε_n. A decrease in the degree of compression and so on can lead to an increase in E_{thr}. However, there is a favorable circumstance not taken into account above: the α-particles scattered in the substance also heat it and cause thermonuclear reaction, that is, the energy contribution of the external source. The ratio of the size of the compressed drop to the path length of the α-particle at the given temperature is proportional to nr, and the "capture" of the α-particles begins at values nr which exceed $(nr)_L$ by approximately 20 times.

The values of the efficiency that we selected for the estimates indicate that the self-heating of the droplet has already been noted, which permits the hope of correctness of the obtained estimate (of course, if compression to superhigh density is achieved). Actually, approximately the same value was obtained as a result of a cycle of numerical calculations.

The energy balance calculations considering self-acceleration are highly complicated and are not described by simple estimates. The numerical calculations demonstrate that if the laser energy exceeds E_{thr} the energy release increases, but only to some limit. The gain G -- the ratio of the energy released as a result of the reaction to the laser energy -- is an important parameter for LTF.

It turns out that the maximum gain for energy of 10^5 to 10^6 joules for multilayer optimal targets does not exceed G~200 to 100 [6, 8-10].

Basic Physical Problems of LTF. As was mentioned above, the basic theoretical results for LTF were obtained by machine calculations. The primary indeterminacy here is connected with a number of purely physical problems, the explanation of which still does not exist at the present time. Let us discuss the main ones of them. Figure 1 shows the diagram of laser compression of a target.

As is known, the electromagnetic radiation cannot penetrate into the region where the wave frequency is greater than the plasma frequency ω_p: $\omega_p^2 = ne^2/m$. The magnitude of the crtical density $n_c = \frac{m\omega^2}{4\pi ne^2}$ is 10^2 cm^{-3} for neodymium lasers, and for CO_2-lasers it drops to 10^{19} cm^{-3}. The energy absorbed in the quite rarefied plasma corona leads to heating of still denser layers of the target. The heat flux, reaching the ablation surface, leads to evaporation of the substance and acceleration of the target shell. In the described picture it is possible to isolate three problems.

1) What part of the incident laser radiation is absorbed in the corona?

2) What are the heat transfer mechanisms to the ablation surface? To the evaporation surface?

3) Is the symmetric compression stable?

Let us begin the discussion of these problems with the last.

Rayleigh-Taylor Instabilities of Shells. As was noted above, it is considered that the thermonuclear target will have a complex shell structure. The use of heavy shells permits accumulation of the energy of the laser pulse, significantly lowering the requirements on its shape. In addition, a heavy shell slows down dispersal of the "burning" mixture and leads to an increase in the burnup of fuel.

However, for such targets the problem of stability stands out especially sharply. Let us consider a shell moving with acceleration. It is obvious that for such ($p \sim 10^{12}$ atmospheres) pressures it can be considered as a liquid. The greatest danger is presented by the instabilities of the Rayleigh-Taylor type. Their picture can be represented as follows. The acceleration of the shell is equivalent to the introduction of an effective gravitational force directed opposite to its movement. Here the denser ("heavy") liquid (the shell) turns out to be above the light one and, naturally, is unstable. The analogous instability arises when the accelerated shell begins to brake, compressing the dense nucleus of the target.

It is known that the dispersion law of surface waves in the water $\omega=\sqrt{gk}$. If we vary the direction of the gravitational force, we obtain an instability with the increment $\gamma \sim \sqrt{gk}$. In itself the fact of instability may not lead to catastrophic consequences. It is necessary that the instability not develop during the compression time. Therefore it is possible to control it by decreasing the initial amplitude of the asymmetric disturbances, that is, using targets with minimum deviations from spherical symmetry[1] and achieving uniformity of irradiation of the target, and so on.

It is considered that after taking such "precautionary measures" the long wave disturbances (comparable with respect to scale to the target size) are not terrible [11].

The fastest growing short wave modes are stabilized by the thermal conductivity, the finite width of the ablation zone, and so on. Therefore in practice the 10th to the 15th harmonics turned out to be the most dangerous [12].

The studies of collapse of a shell of zero thickness demonstrated that it always ruptures during implosion [13]. On the other hand, it is clear that a sufficiently thick shell does not rupture. However, a great deal of energy goes to acceleration of the heavy shell which does not participate in the reaction,

---

[1] At the present time it is possible to make targets with radius $R \sim 10^{-2}$ cm and $\Delta R/R$ which do not exceed a few percentages for a shell thickness of several microns.

and increasing its thickness leads to a reduction in the target gains. The complexity of optimization of the shell thickness consists in the fact that the already ruptured turbulized shell can still compress the nucleus quite well. The final explanation obviously can only be obtained by experimentation. However, experimental studies in this field have only just begun [14].

Anomalous Thermal Conductivity. As was noted above, the energy of laser emission is absorbed far from the ablation zone and is transported to it as a result of thermal conductivity. It is clear that the variation of the thermal conductivity is felt essentially in the compression efficiency.

It turns out that when describing laser heating it is impossible to use the usual expression for thermal conductivity in a plasma. The temperatures arising in a corona are so large that the length of free path will become comparable to the characteristic scales of the corona. For consideration of this fact the expression for the heat flux is used in hydrodynamic calculations in the following form:

$$q^{-1} = q_T^{-1} + q_{max}^{-1}$$

Here $q_T = -\chi(T)\nabla T$, $q_{max} = \alpha n T v_T$ (nTv is the maximum heat flux transported by the free electrons, and the constant α must obviously be close to unity). However, there are two effects which greatly increase the thermal conductivity. Firstly, for such large heat fluxes the plasma becomes unstable with respect to the excitation of ion-sound vibrations [15]. The dispersion in the vibrations leads to a significant decrease in the heat fluxes.

Another mechanism greatly decreasing the thermal conductivity is spontaneous generation of the magnetic field. In the fields with intensity on the order of a megagauss, the Larmor electron radius becomes less than the characteristic dimensions of the temperature gradients and, consequently, the thermal conductivity decreases sharply. There are several mechanisms of the generation of magnetic fields (see the survey [16]). A large part of them are connected with the occurrence of a current caused by nonparallelness of the density and temperature gradients. From the equations of magnetic hydrodynamics it is easy to obtain an estimate for the field

$$H \sim \frac{c}{en}[\nabla n \nabla T]\tau$$

(τ is the laser pulse duration).

The temperature gradients can occur as a result of the limited nature of the focal point, nonuniformity of the illumination and absorption. They can also appear spontaneously as a result of the development of instabilities. Simple estimates indicate that these mechanisms completely insure generation of megagauss fields.

Experimentally, fields of H~1 megagauss were detected on irradiation of plane targets [17]. The magnetic field was measured by the Faraday rotation of a probe beam. The experiments performed later [18] confirmed the results of [17], but on irradiation of spherical targets no noticeable magnetic field was detected. Thus, the absence of a clear picture of the occurring magnetic fields does not permit reliable estimation of the magnitude of the heat flux.

Experimentally, the presence of an anomalous thermal conductivity was confirmed recently by direct experiments [19]. The target was irradiated by a laser pulse which has two intensity peaks in the cross section. Correspondingly, during heating two regions with increased temperature arose. The distance between them was such that during the time of the pulse the classical thermal conductivity would have to lead to equalization of the temperatures. However, X-ray measurements demonstrated the existence of two sharply expressed heating regions. How is the anomalous thermal conductivity taken into account in the numerical calculations? This is done by selecting the numerical factor α in the formula. A comparison of the experimental data with the results of the numerical calculation gives $10^{-2}<\alpha<10^{-1}$ [20].

Absorption of Laser Radiation. The problem of absorption of laser radiation obviously is the most complex and unexplained. At the same time, as we see, the high efficiency of the absorption is entirely necessary for successful development of the LTF program. The simplest absorption mechanism is collision damping of the electromagnetic wave during the propagation process. From the expression for the dielectric constant of a plasma $\varepsilon=1-\frac{\omega_p^2}{\omega(\omega+i\nu_{ei})}$ it is easy to find that the collisions lead to a decrease in the radiation energy with the decrement $\nu=\nu_{ei}\frac{\omega_p^2}{\omega^2}$ where ν_{ei} is the electron-ion collision frequency: $\nu_{ei}\sim\frac{2\cdot10^{-5}zn}{T^{3/2}}$; n is the plasma density in cm^{-3}; z is the ion charge, and the temperature is measured in electron volts.

In the quasiclassical approximation the spatial attenuation of the radiation energy ε is described by the equation

$$\frac{d}{dx}\nu_{\lim}\varepsilon=-\nu\varepsilon$$

from which the ratio of the reflected and incident wave intensities is

$$R=e^{-k_0};\ k_0=2\int_{-\infty}^{x}\frac{\omega_p(x)\nu_{ei}(x)\,dx}{c\omega^2\sqrt{1-\omega_p^2/\omega^2}}. \qquad (8)$$

It is obvious that the basic contribution to the integral (8) is made by the region near the reflection point x_0. Expanding $\omega_p(x)$, $\nu_{ei}(x)$ near $n=n_c$, we obtain $k_0\sim2\nu_{ei}L/c$. Here $L=(\frac{d\ln n}{dx})^{-1}$, and the values of ν_{ei} and L are taken at the reflection point. The characteristic temperature of the corona T~1 kev, and for the dimension L it is possible to write the estimate $L\lesssim c_s\tau$, where τ is the pulse duration. The existing laser systems for CTF can be divided into two groups: systems with pulse duration on the order of several nanoseconds and characteristic energy flux densities p~10^{-15} to 10^{14} watts/cm^2 and systems with pulse duration on the order of several tens of picoseconds and fluxes of 10^{16} to 10^{17} watts/cm^2. Here the energy expended on the target is of approximately the same order.

For picosecond pulses we find that L does not exceed several microns. Calculating k_0, we find that the collision damping is negligibly small and cannot explain the experimentally observed absorption even for neodymium lasers. For nanosecond pulses the absorption is quite large, especially for targets with large z, but nevertheless it cannot explain the entire set of observed phenomena. For CO_2 lasers the collision attenuation is small even in this case. Thus, we arrive at the conclusion of the existence of strong additional absorption mechanisms.

All of these mechanisms have a collective nature. The energy of the electromagnetic wave is transmitted in one way or the other to the plasma waves which then give up their energy to the particles. The nonlinear effect which has primarily begun to be discussed in the literature has led to absorption, and on the contrary, to intense reflection. This is stimulated Mandelstam-Brillouin scattering (SMBS). This process can be represented as decay of the electromagnetic wave ω_t into sonic and electromagnetic oscillations:

$$\omega_t \rightarrow \omega_t + \omega.$$

It is obvious that here only a small (on the order of c_s/c) portion of the energy remains in the plasma and the rest is reflected. It is easy to see that for fluxes of $p \sim 10^{12}$ watts/cm^2 the threshold of this process is passed, and at the beginning of the 1970's, accordingly, fear for the future fate of the LTF was stated. However, the first experiments allayed these fears, and later, as it then appeared, the absence of SMBS was theoretically explained. It turned out that the SMBS is extraordinarily sensitive to plasma nonuniformity, and it is responsible for disruption of the instability [21, 22]. Inasmuch as the plasma profiles in the corona were not too well known, this explanation satisfied everyone. However, recently experiments have appeared in which, analyzing the scattered radiation spectrum, it was possible to demonstrate the existence of SMBS [12, 23]. With an increase in the radiation intensity the SMBS level remained low.

Obviously, the smallness of the SMBS is explained by the following fact. The process takes place in a highly rarefied plasma where under ordinary experimental conditions $E^2 > 8\pi nT$. Let the scattering of a significant part of laser radiation have occurred. As a result, the electric field pressure gradient arises. The ponderomotive forces lead to deformation of the density profile and an increase in the gradients leading to interruption of the scattering. Inasmuch as this process occurs with sonic velocities, time modulation of the SMBS is observed.

Let us now proceed to a discussion of the processes leading to absorption of light. If we move from the rarefied plasma region, then we first of all encounter the region where the decay of the electromagnetic wave into two Langmuir waves is possible:

$$\omega_t \rightarrow 2\omega_e.$$

This is the region of densities $n \sim n_c/4$. Then near n_c the following process can develop:

$$\omega_t \to \omega_e + \omega_s$$

$$2\omega_t \to 2\omega_e.$$

For energy fluxes that are typical of laser experiments the instability increments exceed the sonic frequency. At such intensities it is impossible to talk about the vibrations as about a gas of weakly interacting quasiparticles. The plasma turbulence that arises is not described by any regular method; therefore it is necessary to limit ourselves to different types of not too reliable estimates and also the results of machine calculations. Here the matter is significantly facilitated by the fact that the characteristic wave lengths of the plasma turbulence are two orders less than the wave length of the neodymium laser. Therefore we can break down the problem, first calculating the energy absorption in the uniform plasma with given pumping and thus determining the damping of the electromagnetic wave in equation (7) after which we can discover the contribution of the indicated processes to the light absorption. It turns out that the excitation of the plasma turbulence is a significant absorption mechanism for long pulses of a neodymium laser and insignificant for short pulses. Experimental confirmation of the existence of plasma turbulence near n_c and $n_c/4$ is the radiation on the harmonics 2ω and $(3/2)\omega$ appearing as a result of merging of the plasma waves (see [12, 14]). For short pulses and for experiments with CO_2-lasers where $E^2 \geqslant 8\pi nT$ the laser radiation pressure forms a density discontinuity encompassing the point n_c (Figure 2). For such sharp profiles the effect of "resonance absorption" becomes significant.

In a nonuniform medium the electromagnetic wave cannot remain purely transverse. If we select the z-axis along the direction of the nonuniformity, from the equation $\mathrm{div}\vec{D}=0$ we obtain $\mathrm{div}\vec{E}=-\frac{d\varepsilon}{\varepsilon dz}E_z$. It is obvious that in the presence of the electric field component along the nonuniformity (p is the polarization wave) separation of the charges $4\pi\delta\rho=\mathrm{div}\vec{E}$ takes place, that is, plasma vibrations occur. The generation of the plasma vibrations is especially powerful for $\varepsilon=0$. However, the p-polarized wave is reflected from the small values of the density at the point where $\varepsilon=\sin^2\theta$ (θ is the angle of incidence), and the electromagnetic field penetrates the region of critical density only by tunneling. It is clear that on a sharp profile this penetration is facilitated, and the transformation of the electromagnetic wave to a plasma wave is especially strong.

Usually the indicated effect explains the polarization dependence of the reflection coefficients.

Let us briefly enumerate several more absorption mechanisms. In Figure 2 we see the results of the numerical simulation of the interaction of the laser emission with a plasma. It is obvious that on the density discontinuity in the region $n \sim n_c$, intense surface vibrations are excited which absorb the energy and create the possibility of converting the electromagnetic wave to a plasma wave.

Another cause of conversion is intense ion-sound turbulence which is always near the critical surface.

The intensities of the electromagnetic waves near the critical density surface are so great that small modulation of the intensity is sufficient for reversal of the wave, capture of the electrons, and so on. Self-focusing of the radiation can lead to such results.

Of course, it is extraordinarily difficult to disentangle this entire knot, for all of the nonlinear processes are linked together. In addition, they are essentially determined by plasma hydrodynamics, the course of which, in turn, is caused by absorption, heat transport to the ablation surface, and so on, that is, it is necessary to solve the problem selfconsistently. Nevertheless, the results of the numerical experiments indicate that the above-enumerated mechanisms are insufficient to explain the observed absorption.

What are the experimental results of studying the absorption of light?

In spite of the fact that these experiments are the simplest in LTF and they are performed in many laboratories of different countries, it has only recently been possible to overcome the disparity in the results. The fact is that it is easy to measure the light reflected into a lens aperture. However, it turned out that a significant part of the radiation is scattered diffusely, where the proportion of the back-reflected light decreases with an increase in intensity. One of the reasons for this consists in the fact that the critical density surface is unstable (see Figure 2) and the scattering on the "riffled" surface also leads to this result. Therefore, for determination of the absorption efficiency it is necessary to measure all of the scattered radiation which is very complicated.

The experiments performed at the present time in various laboratories with measurement of the total reflection indicate that for short pulses where the light pressure is comparable to or exceeds the thermal pressure, with normal incidence approximately 40% of the incident light is absorbed independently of the intensity, the wave length and the target material [25]. The situation is more complex with long pulses. Up to now experiments performed here in the various laboratories give different results with approximately coinciding parameters [26, 12]. Obviously this is connected with dependence on the fine structure of the pulse, thermal conductivity in the target, and so on. For example, the experiments described in [26] demonstrated the strong dependence of the reflection on the presence of a weak forerunner. Nevertheless the absorption coefficients are higher than for short pulses in this case, and they can reach 80%.[1] It is possible to ask the following question: "From the pragmatic point of view why are we analyzing complex absorption mechanisms? Indeed, at the present time the absorption coefficients are being measured for energy fluxes and pulse durations in a wide range of parameters of interest for future reactors."

However, it turns out that it is even necessary to study this from the pragmatic point of view. The fact is that, as a rule, a significant part of the energy absorbed as a result of collective mechanisms is transmitted to fast particles. Strong plasma turbulence is an ensemble of oscillations deeply spatially modulated,

[1] All of the presented results pertain to flat targets; on spherical targets the absorption is somewhat lower as a result of refraction, and so on.

consisting of a set of pockets from which the electric field locked in them has forced the plasma. The size of the pockets can be so small and the field so large that an electron passing through them takes on significant energy in a time on the order of an oscillation period ω_p^{-1}. Stochastic acceleration in various pockets leads to drawing out the tails of the distribution function -- an effect which is quite obvious during numerical simulation. These fast electrons are a serious threat to LTF, for, reaching the target nucleus, they heat it and prevent compression. Therefore I should like to find conditions under which the generation of the fast electrons will be minimized as much as possible.

Experimental Results and Experimental Setups. At the present time different countries have a significant number of devices with pulse energy from hundreds of joules to a kilojoule. In the experiment performed on these devices, much varied physical data is obtained, from which the most valuable appears to be the detailed study of absorption with parameters corresponding to the large devices of the future.

A number of experiments have also been performed with respect to compression of glass microspheres with gaseous D-T-mixture. The compression conditions of these shells have been distinguished significantly from the above-described adiabatic compression. This is connected with the low energy of the beams in the existing devices. The performed experiments are well described by the so-called model of the "exploding piston" [6, 7]. A thin glass shell (thickness on the order of a few microns, radius 100 microns) is irradiated by a pulse with a duration of several tens of picoseconds. As a result, the shell is quickly heated to a temperature of ~1 kev and then "implodes." Part of the shell, flying to the center, compresses the D-T-gas and heats it. It is clear that in this case it is impossible to achieve high compression, but, with a fairly low energy investment, it is possible to obtain a high temperature at the center and, consequently, high neutron yield. In the experiments performed at Livermore, $\rho r \sim 3 \cdot 10^{-4}$ g/cm^{-2} and a neutron yield of $\sim 10^9$ were reached. Here the D-T-gas was compressed from a density of 0.001 to a density exceeding the solid deuterium density by 2-3 times [27]. Let us note that such values of ρr are approximately two orders less than required by the Lawson criterion $(\rho r)_L$, and they correspond to $n\tau \sim 10^{12}$ for steady confinement.

Still larger values of ρr and compression of D-T to densities exceeding the density of solid D-T by several times were obtained in experiments at the Physics Institute of the USSR Academy of Sciences [4].

In the experiments performed in Osaka, the targets with deuterium were compressed to a density at the center of $\rho \sim 1$ g/cm^3 and $\rho r \sim 10^{-3}$ g/cm^2, and the neutron yield was $\sim 10^7$ [12].

Another significant result of these experiments is comparison of the experimental results (x-radiation, neutron yield) with the results of the machine simulation. The importance of this is clear if we remember that all of the estimates of the outlook for laser fusion await numerical calculations.

It is necessary to note the development of experimental methods (see survey 28), for it is necessary to perform measurements with resolution of tens of picoseconds and several microns. Without discussing this, let us only note experiments from [29] in which, transilluminating the plasma with the fourth harmonic of a neodymium laser, it was possible to establish a density profile near $n \sim n_c$ with resolution of 1 micron.

Recently several devices have been put into operation or modified with an energy per pulse of 10^4 joules. These are the CO_2-laser system in Los Alamos and the neodymium glass devices: "Shiva" in Livermore, UMI-35 and "Del'fin" in Moscow, and "Omega" at Rochester University [12].

The first experiments have begun on the "Shiva," the results of which were reported at the 12th European Conference on the Interaction of Laser Radiation with Matter (Moscow, December 1978).

On compression of the glass shells, a neutron yield of $\sim 10^{11}$ and an ion temperature of T~6 kev were obtained. Apparently, experiments with compound targets have already started.[1]

Strong compression which exceeds the solid state density by 2 or 3 orders and also "significant combustion," in particular, on the "Shiva" to 10^{15} neutrons per shot are counted on with the devices of this generation.

Let us note that inasmuch as it is possible to pass limited power through the amplifying stages, the buildup of the energy yield leads to an increase in the number of output channels. They are synchronized with accuracy to picoseconds; adjustment after each firing, and so on constitute a complex technical problem. Therefore the successful operation of the 20-channel "Shiva" demonstrates that these problems can be solved.

Conclusion. The above-described devices and experiments are needed to check the physical principles of LTF. Their actual realizability imposes additional requirements on laser systems. Their efficiency is the most significant one.

Let us estimate the efficiency of laser systems η_ℓ required for positive energy yield. As has already been noted above, in numerical experiments it is possible to obtain gains G greater than 100 to 200. The energy contributed to the target is $E\eta_\ell$, where E is the energy input from an outside circuit. The energy yield is $E\eta_\ell G\eta_{e\ell}$, where $\eta_{e\ell}$ is the efficiency of conversion of the released energy to electric power (usually it is assumed to be 0.4 in the estimates). Hence, it is obvious that for positive energy yield for targets with G~100 the laser efficiency must exceed 2.5 percent.

---

[1] In recent experiments on the "Shiva" compression to densities of $\rho \sim 30$ g/cm^2, that is, $n \sim 150\ n_s$, was obtained.

Consequently, the neodymium glass lasers are entirely unsuitable for LTF with positive yield. The CO_2 lasers have appropriate efficiency (η_ℓ>2% for nanosecond pulses), but the absorption of such long-wave radiation obviously leads to generation of accelerated electrons, heating of the center of the target. As a result, it is difficult to achieve significant compression.

The use of lasers with a wave length on the order of 0.5 microns appears to be optimal. On the one hand, the wave length is quite small so that on absorption of nanosecond pulses the basic mechanism would be collision damping, and the generation of fast electrons would not be so dangerous. On the other hand, for such wave lengths it is possible to use ordinary optical systems.

Recently laser complexes have been developed which operate in this frequency band. They include the excimer laser pumped by an electron beam. This laser serves as a selective pump for group VI element (oxygen) lasers operating in the required frequency range. For completed facilities the total obtained efficiency of the system exceeds the efficiency of the carbon dioxide lasers [30].

From what has been discussed above it is obvious that it is possible to count on the realizability of LTF only when obtaining a gain close to maximum obtained in the numerical experiments. The lack of determinacy in understanding the physics of light absorption and compression creates the fear of unattainability of these results in real experiments.

Therefore experiments on devices with an energy of ~10^4 joules, the achievement of high degrees of compression on them and the results of experiments with "thermonuclear" targets appear to be very important.

It is necessary to emphasize also that the physics of LTF, in addition to the practical aspects, includes the study of quite unique phenomena. The interaction of laser radiation creating a pressure of 10^8 atmospheres with matter, the generation of megagauss magnetic fields, plasma turbulence excited by anomalously strong electromagnetic fields, and so on are more and more attracting the attention of the researchers.

BIBLIOGRAPHY

1. Artsimovich, A. A. UPRAVLYAYEMYYE TERMOYADERNYYE REAKTSII [Controlled Thermonuclear Reactions], Moscow, Fizmatgiz, 1963.

2. DOKLADY VSESOYUZNOGO SOVESHCHANIYA PO INZHENERNYM PROBLEMAM UPRAVLYAYEMOGO TERMOYADERNOGO SINTEZA [Reports of the All-Union Conference on Engineering Problems of Controlled Thermonuclear Fusion], T.I.L., izd. NIIEFA, 1975, Atomizdat, 1976.

3. Johnson, R.; Hall, R. J. APPL. PHYS., Vol 42, 1971, p 1035.

4. Basov, N. G.; Krokhin, O. N. ZHETF [Journal of Experimental and Theoretical Physics], Vol 46, 1964, p 171.

5. Nuckols, J., et al. NATURE, Vol 239, 1972, p 199; Nuckols, J., et al. in the book: PROBLEMY UPRAVLYAYEMOGO TERMOYADERNOGO SINTEZA [Problems of Controlled Thermonuclear Fusion], Moscow, Atomizdat, 1976.

6. Nuckols, et al. LAWRENCE LIVERMORE LAB. LASER FUSION PROGRAM ANNUAL REP. (Rep. UCRL-50021), 1976.

7. Brakner, K.; Dzhoriya, S. UPRAVLYAYEMYY LAZERNYY SINTEZ [Controlled Laser Fusion], Moscow, Atomizdat, 1977.

8. Basov, N. G., et al. 5th INTERN. CONFERENCE OF PLASMA PHYS. AND CONTROLLED NUCLEAR FUSION, Tokyo, 1974.

9. Mason, R. T.; Morse, R. L. LOS ALAMOS SCI. LAB. REPORT (LA-5789 MS), 1974.

10. Anisimov, S. I., et al. PIS'MA V ZHETF [Letters to the Journal of Experimental and Theoretical Physics], Vol 22, 1975, p 343.

11. Prokhorov, A. M.; Anisimov, S. I.; Pashinin, P. N. UFN [Progress in the Physical Sciences], Vol 119, 1976, p 401.

12. TEZISY DOKLADOV XII YEVROPEYSKOY KONFERENTSII PO VZAIMODEYSTVIYU LAZERNOGO IZLUCHENIYA S VESHCHESTROM [Topics of Reports at the 12th European Conference on the Interaction of Laser Radiation with Matter], Moscow, 1978.

13. Anisimov, S. I.; Ivanov, M. M.; Ikogamov, N. A. DINAMIKA LAZERNOGO SZHATIYA I NAGREVANIYA PROSTYKH MISHENEY [Dynamics of Laser Compression and Heating of Simple Targets], Preprint of the Technical Physics Institute imeni Landau, Moscow, 1977.

14. Basov, N. G., et al. VZAIMODEYSTVIYE MOSHCHNOGO LAZERNOGO IZLUCHENIYA S PLAZMOY. ITOGI NAUKI I TEKHNIKI [Interaction of Powerful Laser Radiation with a Plasma. Results of Science and Engineering], Moscow, VINITI, 1978.

15. Forslund, P. J. GEOPHYS. RES., Vol 75, 1970, p 17.

16. Max, C.; Manheimer, W.; Thomson, J. PHYS. FLUIDS, Vol 21, 1978, p 128.

17. Stamper, T., et al. PHYS. REV. LETT., Vol 26, 1972, p 1012.

18. Raven, A., et al. PHYS. REV. LETT., Vol 41, 1978, p 554.

19. NRL MEMORANDUM REPORT, N 3890, 29 November 1978.

20. Melone, R. C., et al. PHYS. REV. LETT., Vol 34, 1975, p 721; Mead, W. C., et al. PHYS. REV. LETT., Vol 37, 1976, p 489; Young, F., et al. APPL. PHYS. LETT., Vol 30, 1977, p 45.

21. Silin, V. P. PARAMETRICHESKOYE VOZDEYSTVIYE IZLUCHENIYA BOL'SHOY MOSHCHNOSTI NA PLAZMU [Parametric Effect of High-Power Radiation on a Plasma], Moscow, Nauka, 1973.

22. Liu, C. S. ADVANCES IN PLASMA PHYS., Vol 5, ed. by A. Simon and W. Thompson, John Wiley and Sons, Inc., 1976.

23. Gorbunov, L. M., et al. PIS'MA V ZHETF, Vol 27, 1978, p 242.

24. Estabrook, K. PHYS. FLUIDS, Vol 19, 1976, p 1733.

25. Godwin, R. APPL. OPT., Vol 18, 1979, p 3555.

26. NRL MEMORANDUM REPORT, N 3684, N 29.12.1977.

27. Nishikawa, K. 7TH CONFERENCE ON PLASMA PHYS. AND CONTROLLED NUCLEAR FUSION RESEARCH, Innsbruck, 1978.

28. Atwood, D. IEEE J. OF QUANTUM ELECTRONICS, Vol QE-14, 1978, p 309.

29. Atwood, D., et al. PHYS. REV. LETT., Vol 40, 1978, p 184.

30. LAWRENCE LIVERMORE LAB. LASER FUSION PROGRAM (Annual Report), 1975.

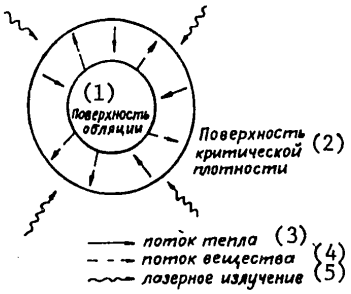

Figure 1. Laser heating system. The laser emission is absorbed in a plasma corona in the region of densities close to critical. The heat fluxes that arise, reaching the ablation surface, cause evaporation of the substance, creating a recoil pulse compressing the target.

Key:
1. Ablation surface
2. Critical density surface
3. Heat flux
4. Flow of substance
5. Laser radiation

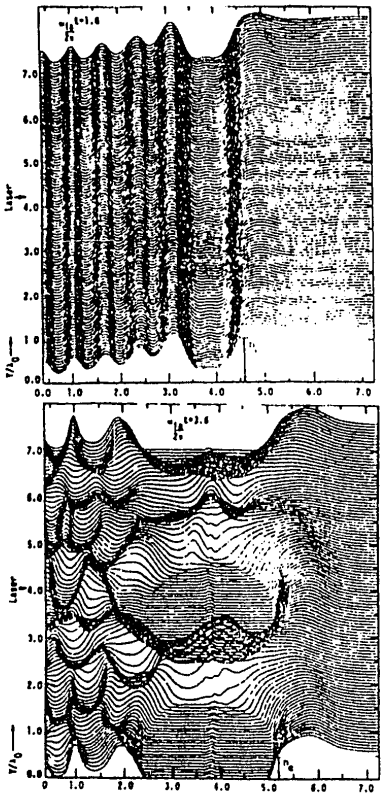

Figure 2. Results of machine simulation of interaction of a powerful electromagnetic wave with plasma $E^2 \geq 8\pi nT$ near the reflection point (taken from [24]). A plane electromagnetic wave is incident from the left. Two successive times are depicted: a -- the high-amplitude standing wave is obvious, the plasma profile is modulated under the effect of the ponderomotive forces; in the density region greater than critical, the electromagnetic wave damps; b -- the development of wave instability can be seen.

[8144/0581-D-10845]

10845
CSO: 8144/0581-D

EFFECT OF DRIFT INSTABILITY AND ITS STABILIZATION ON PLASMA TRANSFER IN A TOROIDAL STELLARATOR

Kiev VLIYANIYE DREYFOVOY NEUSTOYCHIVOSTI I YEYE STABILIZATSII NA PROTSESSY PERENOSA PLAZMY V TOROIDAL'NOM STELLARATORE in Russian 1979 (signed to press 17 Apr 79) pp 3-5, 37-38

[Introduction and conclusion from book "Effect of Instability and Its Stabilization on Plasma Transfer in a Toroidal Stellarator", by Aleksandr Yur'yevich Voloshko, Institut yadernykh issledovaniy, 180 copies, 40 pages]

[Text] Introduction

Drift instabilities of plasma have become during the past decade an object of close attention of investigators involved in the problem of controlled thermonuclear fusion. This was determined by the fact that in practically all experiments on toroidal confinement of plasma, abnormal heat and particle losses were observed [1-7] which significantly exceed the neoclassical values, in some cases by an order or more.

Drift fluctuations may make an appreciable contribution to energy losses from the plasma even if their relative level is very low [2, 4, 8-9].

Thermal conductivity at relatively low values of plasma density in tokamaks is in good agreement with the pseudo-classical formula proposed by L. A. Artsimovich to describe the experimental results obtained in the T-3 tokamak [11]:

$$\chi_{\perp pseud}^{e} \approx c^2 \rho_{\theta e}^2 \nu_{eff}.$$

Here c^2 is a constant value approximately equal to 10, $\rho_{\theta e}$ is the Larmor radius of the electron in a poloidal magnetic field, ν_{eff} is the effective frequency of electron collisions determined from measurements of the electric conductivity of the plasma: $\nu_{eff} = \omega_{pe}^2/4\pi\sigma$.

It was subsequently shown that the pseudo-classical law of losses is valid not only for tokamaks but in some cases for stellarators with current [2-7] and during confinement of a currentless plasma [10].

It follows directly from the pseudo-classical formula that heat losses through the electron channel decrease as T_e increases (as approximately $T_e^{-3/2}$) in the case of Coulomb conductivity of the plasma. In the general case the heat losses of the plasma in toroidal configuration are determined by the total effect due to thermal conductivity perpendicular to the magnetic field and due to particle diffusion [12], which increases with an increase of electron temperature (the "plateau" region).

The observed increased energy losses through the electron channel may be related to breakdown of magnetic surfaces (due to current flow in the plasma), to drift instabilities, to instabilities on trapped electrons and so on [13-17]. However, there is as yet no experimental proof of a direct relationship of abnormal electron thermal conductivity with the presence of one or another instabilities in the plasma.

With regard to charged particle confinement, measurement of the diffusion coefficient was also usually abnormal, although to a lesser degree in the extent of abnormality than for the coefficients of electron thermal conductivity. Detailed experimental investigations on stellarators (Uragan-1 [2], Uragan-2 [18], Kleo [5], W-PB [3], Heliotron-D [19] and so on) showed that turbulent diffusion is similar to neoclassical diffusion for the "plateau" by the nature of the dependence on plasma parameters, while it may differ from it by approximately an order in absolute value as a function of the ratio of the thermal electron velocity and the rate of current drift (see, for example [5, 20, 43]). These experimental results are in qualitative agreement with the results of [21] on the effect of drift instability in a plasma with current on particle diffusion.

As indicated by numerous theoretical [22-25] and experimental [survey 26] investigations, the negative effect of drift instabilities may be reduced considerably if the magnetic configuration has sufficient crossing of lines of force or a "magnetic well." Along with this, suppression of drift fluctuations can be achieved by increasing the ion viscosity due to increasing the collision frequency of ions with ions or of ions with neutral atoms [26]. Variation of the effective frequency of ion collisions during high-frequency heating of a plasma has a similar effect on the amplitude of drift instabilities [27-28, 47], due to which the use of ion viscosity to stabilize drift fluctuations may be promising in confinement of thermonuclear plasmas.

A decrease in the level of fluctuations can also be achieved by using feedback [29] or dynamic stabilization [29-30].

A knowledge of the type of fluctuations, their wave structure, mechanisms of oscillation and amplitude restriction is necessary for effective use of one or another method of stabilization.

This paper is a survey of complex experimental investigatios of low-frequency drift fluctuations of an SHF discharge plasma confined in the high-shear Saturn l=3 toroidal stellarator.

The method of creating the plasma, the diagnosis used and the plasma parameters are described in the first part of the paper.

The second part contains data of measuring the spatial and time characteristics of the low-frequency oscillations, their dependence on plasma parameters and the confining magnetic field. The measurements made it possible to determine the type of observed fluctuations and to indicate the mechanisms of their excitation.

The third part is devoted to experimental investigation of the mechanism of stabilization of drift-dissipative instability by shear and by the effect of the ion mass. It is specifically shown that the amplitude restriction of drift fluctuations is determined by Landau attenuation on ions with the presence of sufficiently high shear in the system.

Part 4 contains a qualitative theoretical consideration of the effect of electrons trapped in the potential well of the drift wave (resonance electrons [13, 28, 31, 32] and expressions of the coefficients of electron thermal conductivity are presented for the "plateau" region (on the plasma diffusion curve) and data of measuring the heat losses through the electron channel are also given. It is concluded from analysis of the functions that the observed pseudo-classical behavior of thermal conductivity is the consequence of a linear relationship between the values of $k_{||}v_{te}$ and ν_{eff} realized in the experiment.

Part 5 is devoted to study of the confinement of charged plasma particles as a function of plasma parameters and the parameters of the magnetic configuration: the particle losses correspond in both value and by functional dependence to neoclassical theory at high shear values.

Conclusions

Analysis of the experimental results presented in the given paper on investigation of currentless plasma confinement in the Saturn l=3 toroidal stellarator permits the following conclusions:

1. There are significant losses of charged particles perpendicular to the confining magnetic field ($\Gamma_{\sim} \propto \delta^2$) in an SHF discharge plasma, caused by drift-dissipative instability which develops due to the density gradient and curvature of the lines of force.

2. The level of the drift fluctuations and consequently of the turbulent plasma flows caused by them ($\delta \propto \theta^{-1.5}$, $\Gamma \propto \theta^{-3}$) can be reduced by increasing the shear. The stabilizing role of shear is manifested in a decrease of the dimensions of the localization region of drift fluctuations and by suppression of longitudinal modes with large numbers and phase velocities close to v_{ti}. Stabilization of these modes is determined by Landau attenuation on the ions.

3. The threshold value of shear ($\theta_{kr} \approx 0.05$) dependent on M_i was found, beginning with which strong suppression of the observed fluctuations is observed. The level of drift fluctuations is less, the higher the ion mass in the entire range of shear variation.

4. Energy losses through the electron channel are determined completely by drift-dissipative instability and are the result of interaction of resonance electrons with these fluctuations in the region of intermediate collision frequencies. The

observed pseudo-classical dependence of thermal conductivity is the result of the relationship between the values of ν_e and $k_{||}v_{te}$ realized in the experiment.

5. Turbulent plasmas in the case of small values of shear ($\theta < 0.05$) completely determine the charged particle losses from the confining space ($\alpha_n \propto \delta^{-2}$). The effect of drift instability on plasma losses decreases as shear increases and confinement is determined by neoclassical diffusion perpendicular to the confining magnetic field at shear values of $\theta \sim 0.1$.

6521
CSO: 1862

THERMODYNAMICS

HEAT AND CHARGE TRANSFER ON THE SURFACE OF METALS IN CHEMICALLY ACTIVE FLOWS

Riga PERENOS TEPLA I ZARYADA NA POVERKHNOSTI METALLOV V KHIMICHESKI AKTIVNYKH POTOKAKH in Russian 1980 (signed to press 31 Jan 80) pp 4-7, 245-246

[Annotation, foreword and table of contents from book "Heat and Charge Transfer on the Surface of Metals in Chemically Active Flows", by Viktor Konstantinovich Mel'nikov, Mayya Vilkhelmovna Zake and Viktor Nikolayevich Kovalev, Izdatel'stvo "Zinatne", 1000 copies, 247 pages]

[Text] The results of theoretical and experimental investigations of the processes of heat and electric charge transfer on the surface of titanium and zirconium during transient heating by high-temperature flows of chemically active gases are outlined in the monograph. The chemical kinetics of high-temperature oxidation and nitriding of metals in flows of an argon and oxygen and nitrogen mixture was investigated experimentally. Data are presented on the integral radiating capacity of metals for transient heating and chemical reaction modes. Electric charge transfer on the surface of chemically reacting metals was investigated and data were found on the effect of the electric field on transfer processes. A system of initial equations was analyzed, generalized dimensionless numbers for different kinetic laws were found and the main formulas for calculating a number of characteristics of heating modes of metals were derived. The experimental installation and method of measurements for complex investigation of the processes of heat and electric charge transfer on the surface of metals are described.

Foreword

Simultaneous heat and charge transfer on the surface of metals in chemically active gas flows is of important scientific and practical interest since transient processes with phase and chemical transformations of metals play a specific role in modern devices of high-temperature equipment and technology.

Similar processes occur in rocket technology [72, 141], during spontaneous combustion of metal particles [142, 162], during the use of briefly operating MHD generators [51] and in plasma-chemical technology of synthesizing inorganic compounds [112, 138]. In the latter case interaction of the particles is related to processes of charging and recharging by plasma ions and electrons [197]. Therefore, investigations of processes of heat and charge transfer during transient heating of metals in chemically active flows are an extremely timely problem for engineering practice.

Study of the processes of transfer on the surface of metals in chemically active flows has begun only during the past decade in our country and abroad. Investigations of Soviet thermophysicists, who are pioneers in this field of science, have acquired especially important significance. A large number of theoretical and experimental papers have now been published on the problem under consideration. In this regard study of transfer processes on the surface of metals in high-temperature chemically active media has assumed an independent direction.

Due to the importance of the problem, it has become necessary to systematically outline the theoretical and experimental investigations of the transfer processes and methods of diagnosing them.

Investigations of mass and enegy transfer in inert and chemically active flows of a low-temperature plasma with metal particles have been conducted for many years under the supervision of Academician Yu. A. Mikhaylov at the Institute of Physics of the Latvian SSR Academy of Sciences. One of the trends of this vast field of science is brought to the reader's attention in the proposed monograph. It is devoted to investigation of heat and charge transfer on the surface of metals during transient heating by chemically active flows of a low-temperature plasma. The given investigation is far from complete. However, the presented theoretical and experimental material will help further development of the theory of transient mass and energy transfer on the surface of metals in a low-temperature plasma. This should naturally precede investigations of the mechanisms of transfer since simultaneous mass and energy transfer may significantly affect individual components of the process.

The more widespread metals--titanium and zirconium--were taken as the object of investigations and oxygen and nitrogen were taken as the chemically active plasma.

The given paper is devoted to study of metals in flows of a weakly ionized plasma, i.e., a plasma with electron concentration of $n_i = 10^{10}-10^{12}$.

Concepts of the main processes--chemical kinetics, thermal radiation and charge transfer--are given in the monograph. The chemical kinetics of oxidation and nitriding of metals in low-temperature plasma flows was investigated experimentally. Moreover, data are presented in the paper on the integral radiation capacities of metals during heating and chemical reaction. The system of initial equations was analyzed and generalized criteria for different kinetic laws and also the main formulas were found to calculate a number of heat transfer characteristics. Data of investigations on charge transfer on the surface of a chemically reacting metal in the transient heating mode and also data on the effect of the electric field on the main processes are presented. Methods of diagnosis and experimental installations are described. The devices and installations developed by the authors permit one to expand the capabilities of experimental investigations of many transient thermal processes.

It should be noted that the list of the literature given at the end of the book does not claim to be complete. It contains sources, the data of which are presented by the authors in the monograph and also papers which contain a detailed bibliography.

The results of investigations carried out directly by the authors of the book and published during the past five years are outlined in greatest detail.

The authors hope that the results of investigations of heat and charge transfer on the surface of metals in chemically active plasma flows, presented in the monograph, will contribute to further development of the theory and practice of using a low-temperature plasma in various sectors of the national economy.

The authors would like to thank comrades A. G. Blokh and Ye. S. Ozerov for useful comments in discussion of the manuscript.

Contents

6521
CSO: 1862 END